ABSTRACT

ZAMBON, JOSEPH BRENDAN. An Examination of Tropical Cyclone Dynamics Utilizing the 3-Way Coupled Ocean Atmosphere Wave Sediment Transport (COAWST) Model. (Under the direction of Dr. Ruoying He).

Tropical Cyclones are fundamentally connected to the environment in which they exist. Currently most numerical models do not represent the interactions between the atmosphere, ocean, and wave environments. These environments are drastically modified by the existence of the tropical cyclone and therefore drastically modify the tropical cyclone as a continuous feedback mechanism. As a result, improvement of solutions provided by the individual numerical models representing the atmosphere, ocean, and waves is sought through coupling these models together.

In the first chapter, the dynamic feedback mechanisms are explored in depth through literature review of previous studies into the reaction of the ocean to tropical cyclones. Several analytical and numerical studies are researched in order to provide sufficient background into the problem, provide motivation into developing a coupled numerical model, and provide a base from which hypotheses for experimentation may be drawn.

In the second chapter, experiments will be based off of an atmospheric model tied to a simple 1-dimensional ocean model. Three different experiments are carried out, with the sea surface condition as the only variable between them. By including this simple configuration allowing ocean feedback, hypotheses regarding track, intensity, and sea surface temperature changes will tested.

In the third chapter, the Coupled Ocean Atmosphere Wave Sediment Transport (COAWST) model is introduced. An idealized tropical cyclone is placed into the model domain and the COAWST model is tested. Three experiments of increasing complexity are used in testing the coupling scheme and examining the dynamical differences in the model. The idealized tropical cyclone is used to test several hypotheses based on track, intensity, size, sea surface temperature change, and significant wave height. The COAWST model performs as expected and the initial proof of concept is successful.

In the fourth chapter, the COAWST model is tested with a realistic case, a hindcast simulation of Hurricane Ivan. The model is initialized within a spatial and temporal domain that was found to provide the best solution for a Hurricane Ivan hindcast using only the atmospheric model. Five experiments are carried out, with increasing complexity in resolving the ocean condition. Hypotheses for the realistic case are tested based on modeled track, intensity, size, sea surface temperature change, heat exchange, and significant wave height. The COAWST model demonstrates reasonable skill in the Hurricane Ivan hindcast, although additional improvement in the initial condition is desired.

The final chapter serves to review the discussions of the previous chapters and seeks to provide a platform for future research. The utility of coupled numerical modeling is reiterated and the success of the study highlighted. Likewise, significant improvement of the initial condition in the realistic hindcast will be sought in future research. In addition, several questions remain in improving and examining the coupled numerical solution of a tropical cyclone.

An Examination of Tropical Cyclone Dynamics Utilizing the 3-Way Coupled Ocean Atmosphere Wave Sediment Transport (COAWST) Model

by
Joseph Brendan Zambon

A thesis submitted to the Graduate Faculty of
North Carolina State University
in partial fulfillment of the
requirements for the degree of
Master of Science

Marine, Earth, and Atmospheric Sciences

Raleigh, North Carolina

2009

APPROVED BY:

Dr. Ruoying He Committee Chair	Dr. John Warner
Dr. Gary Lackmann	

BIOGRAPHY

Joe was born in Buffalo, NY on 26 August 1985 and attended high school at Canisius High School where he graduated in 2003. He developed an interest in meteorology at the age of six when a tornadic thunderstorm passed overhead in the summer of 1992. His mother, an avid librarian, nurtured his interest by providing a number of books on the subject. The destruction caused by Hurricane Andrew one day before his seventh birthday cemented his interest in the field.

Over the years his fascination in meteorology spread to a number of areas as his mother continued supplying him with books on a number of subjects related to earth science: from earthquakes to the atmosphere. Joe always came back to meteorology, especially during hurricane season when he would plot the locations of storms on his laminated hurricane-tracking chart, which still sits above his desk. Living in Buffalo, winter was always an active season. Joe began his young career providing Lake Effect Snow forecasts for his fellow schoolmates, advising them whether or not they should expect to be off from school the following day.

Joe continued his studies of the atmosphere at The State University of New York at Albany where he chose a major in Atmospheric Science and a minor in Mathematics and Statistics. Joe also nurtured his interest in computer science with a number of courses in the field, and worked for Information Technology Services with the University while attending classes. During his senior year, Joe attended a conference on Lake Effect Snow in Oswego, NY. Joe concluded his studies at Albany with a B.S. in Atmospheric Science, many interesting classes, and a little research under his belt.

Joe began his studies in the Department of Marine, Earth, and Atmospheric Sciences at The North Carolina State University in August 2007. He was fortunate enough to have his thesis advisor, Dr. Ruoying He, provide him with a topic that was as broad as his interests would allow. After initially beginning with a review of the related literature, Joe dived into the coupled model as Dr. John Warner and Dr. Ruoying He were developing it. Initially his research included development of an idealized tropical cyclone, and was then expanded to include hurricanes Isabel and Ivan.

During his Master's research, Joe was grateful to attend and present at a number of conferences and workshops. In his first year, Joe attended the February 2008 Weather Research and Forecasting model workshop at the National Center for Atmospheric Research in Boulder, CO. In his second year, Joe presented his initial research findings as a departmental seminar in September 2008, entitled "Investigating a 3-Way Coupled Model of a Landfalling Tropical Cyclone". Later that year, Joe presented "An Investigation of Coastal Ocean Response to Landfalling Hurricanes using the Coupled Ocean Atmosphere Wave Sediment Transport (COAWST) Model: Idealized Experiments" and "An Investigation of Coastal Ocean Response to Landfalling Hurricanes using the Coupled Ocean Atmosphere Wave Sediment Transport (COAWST) Model: Realistic Hindcast" at the December 2008 annual meeting of the American Geophysical Union in San Francisco, CA. Joe defended his Master's thesis in July 2009 and graduated in December 2009.

ACKNOWLEDGEMENTS

I would like to thank my advisory committee: Dr. Ruoying He, Dr. John Warner, and Dr. Gary Lackmann, for the opportunity to perform research in this exciting and rapidly expanding field of coupled modeling. I would especially like to thank Dr. Ruoying He for his helpfulness and patience in bringing me onboard with this extensive research project. It has been a very interesting and challenging road since the summer of 2007, looking back on it I cannot even begin to quantify the amount I have learned in my experience here at North Carolina State University.

I also wish to thank my friends here in Raleigh as well as the lifelong friends I have made in my life through this point. I would especially like to point out the assistance I have received from Kevin Hill. His contributions and guidance throughout the duration of this research have been invaluable.

These acknowledgements would not be complete without the mention of my brothers and sisters in the fire and rescue squads I have volunteered for over the years. The members of the McKownville Fire Department and Western Turnpike Rescue Squad in Albany, NY taught me the value of providing a critical service to the community, and how to manage my time effectively in doing so. Since relocating, the Swift Creek Fire Department in Cary, NC provided me with those same values and skills.

Lastly, I would like to thank my family. First, my father who taught me to work hard and to always strive to complete tasks with no compromise in effort. Second my sisters on whose stellar example I constantly use to evaluate my own goals. And finally, my late mother who nurtured my interest in science from the very beginning.

TABLE OF CONTENTS

List of Tables vii

List of Figures viii

1 Introduction 1
1.1 Motivation 1
1.2 Literature Review 3
1.2.1 Upper Ocean Response to a TC, Modeling Approach 3
1.2.1.1 Stationary TC 3
1.2.1.2 Moving TC 6
1.2.2 Upper Ocean Response to a TC, In-Situ Approach 9
1.2.3 Upper Ocean Response to a TC, Remote Sensing Approach 14
1.2.4 Upper Ocean Heat Budget Response 19
1.2.4.1 Ocean Heat Content (OHC) 19
1.2.4.2 Hurricane Heat Potential (HHP) 20
1.2.5 Upper Ocean Salinity Response to Precipitation Processes 22
1.2.6 Upper Ocean Response and General Circulation Features 24
1.2.7 The Importance of 2-Way (Atmosphere-Ocean) Coupled Numerical Modeling 26
1.2.8 The Importance of 3-Way (Atmosphere-Ocean-Wave) Coupled Numerical Modeling 33
1.2.9 Previous 1-Way Coupled Model Configurations 35
1.2.9.1 Simple Three-Dimensional Ocean Models (Price 1981, Price et al. 1994) 33
1.2.9.2 PROFS Driven by Re-Analyzed GFS Winds (Oey et al. 2007) 36
1.2.10 Previous 2-Way (Atmosphere-Ocean) Coupled Model Configurations 37
1.2.10.1 BVW Boundary Layer Model to NCOM (Morey et al. 2006) 37
1.2.10.2 GFDL to POM (Bender and Ginis 2000, Shen and Ginis 2003) 38
1.2.10.3 WRF to 1-Dimensional OML (Davis et al. 2008) 41
2 Experiments of Hurricane Isabel (2003) Utilizing WRF Coupled to a 1-Dimensional Ocean Mixed Layer Model 43
2.1 Introduction 43
2.2 Data and Model Configuration 45
2.3 Results and Discussion 47
2.3.1 Track 47
2.3.2 Intensity 49
2.3.3 Sea Surface Condition 50
2.4 Conclusion 51
3 Experiments of an Idealized Tropical Cyclone Utilizing the COAWST Model 53
3.1 Introduction 53

3.2 Coupled Model Design 55
3.3 Idealized Case Configuration 57
3.3.1 Domain Configuration 57
3.3.2 Idealized TC Configuration 57
3.3.3 Atmospheric Model (WRF) 59
3.3.4 Oceanic Model (ROMS) 60
3.3.5 Wave Model (SWAN) 61
3.4 Methodology 62
3.5 Results 64
3.5.1 Track 64
3.5.2 Intensity 65
3.5.3 Ocean Response 66
3.6 Conclusion 68
4 Experiments of Hurricane Ivan (2004) Utilizing the COAWST Model 69
4.1 Introduction 69
4.2 Methodology 71
4.3 Domain and Model Configuration 72
4.3.1 Domain Configuration 72
4.3.2 WRF Configuration (Atmosphere Model) 73
4.3.3 ROMS Configuration (Ocean Model) 74
4.3.4 SWAN Configuration (Wave Model) 76
4.4 Results 77
4.4.1 Track 77
4.4.2 Intensity 77
4.4.3 Ocean Response 79
4.4.4 Conclusion 82
5 Conclusion 83
5.1 Motivation and Literature Review 83
5.2 Experiments of Hurricane Isabel (2003) 87
5.3 Experiments of an Idealized TC Utilizing the COAWST Model 88
5.4 Experiments of Hurricane Ivan (2004) Utilizing the COAWST Model 89
5.5 Considerations for Future Research 91

References 134

LIST OF TABLES

Table 2.1. Track and intensity forecast errors in NHC forecast for Hurricane Isabel, averaged over duration of event. 87

Table 4.1. Track and intensity forecast errors in NHC forecast for Hurricane Ivan, averaged over duration of event. 87

LIST OF FIGURES

FIG. 1.1. Schematic of wind stress vector rotation with TC translation. 88

FIG. 2.1. Spatial domain and NHC best track for Hurricane Isabel (2003). 89

FIG. 2.2. Hurricane Isabel (2003) track comparison between Static SST case (red), Dynamic SST case (green), and WRF OML case (cyan), and NHC best track verification (black). 90

FIG. 2.3. Hurricane Isabel (2003) Sea Surface Temperature (SST) condition comparison at forecast hour 60, valid 12 UTC 17 September 2003. Static case (upper left), Dynamic case (upper right), WRF OML case (lower left), and difference between Dynamic and WRF OML cases where cool colors denote lower SST in Dynamic case (lower-right). 91

FIG. 2.4. Track distance error and average error of simulations against Hurricane Isabel (2003) NHC best track verification from initialization (hour 0, valid 00 UTC 15 September 2003) through landfall (hour 90, valid 18 UTC 18 September 2003). Static case error distance (red), Dynamic case error (green), WRF OML case (cyan), difference between TC positions of Dynamic and WRF OML (black) which are not compared to NHC best track verification. 92

FIG. 2.5. Track comparison at landfall (F090, valid 18 UTC 18 September 2003) between Static SST case (red), Dynamic SST case (green), and NHC best track verification (black). 93

FIG. 2.6. Intensity comparison for Hurricane Isabel (2003) forecast run from initialization (F000, valid 00 UTC 15 September 2003) through termination (F108, valid 12 UTC 19 September 2003). Comparison between Static SST case (red), Dynamic SST case (green), WRF OML SST case (cyan), and NHC best track verification (black). 94

FIG. 2.7. Simulated radar reflectivity derived from model output for Static SST case (upper left), Dynamic SST case (upper right), WRF OML SST case (lower left). Verification radar reflectivity taken at landfall from radar station at KMHX in Morehead City, NC (lower right). Taken at F090, valid 18 UTC 18 September 2003. 95

FIG. 2.8. Sea Surface Temperature change (ΔSST) comparison from model initialization (F000, valid 00 UTC 15 September 2003) through termination (F108, valid 12 UTC 19 September 2003). Static SST case (upper left), Dynamic SST case (upper right), WRF OML SST case (lower left), and difference between Dynamic SST and WRF OML SST cases where cool colors denote lower SST in Dynamic SST case (lower-right). ____ 96

FIG. 3.1. Diagram demonstrating workflow of Model Coupling Toolkit (MCT). ____ 97

FIG. 3.2. Diagram of 3-way coupled model as currently able to be implemented in the COAWST model. ____ 98

FIG. 3.3. Idealized ocean domain configuration. ____ 99

FIG. 3.4. Experimental Case A configuration. ____ 100

FIG. 3.5. Experimental Case B configuration. ____ 100

FIG. 3.6. Experimental Case C configuration. ____ 100

FIG. 3.7. Complete 3-way coupling (not currently available). ____ 100

FIG. 3.8. Comparison of idealized TC track for three experiments: Case A (red), Case B (green), and Case C (blue). ____ 101

FIG. 3.9. SST condition as received by the atmospheric model at F046 for three experiments: Case A (left), Case B (middle), and Case C (right). ____ 102

FIG. 3.10. Comparison of idealized simulations at F068 for three cases: Case A (top row), Case B (middle row), Case C (lower row). Colored surface pressure in hPa and wind vectors (left column); colored magnitude of 10m winds in ms^{-1} and wind vectors (middle column); colored sea surface condition, TC track as red line, and current vectors (right column). ____ 103

FIG. 3.11. Comparison of idealized simulations at F068 for three cases: Case B-A (top row), Case C-A (middle row), Case C-B (lower row). Colored surface pressure difference in hPa (left column); colored magnitude difference of 10m winds in ms^{-1} (middle column); colored sea surface temperature difference (right column). TC track as red and black lines for each respective case in all panels. 104

FIG. 3.12. Simulated radar reflectivity for idealized TC at F068, three experiments: Case A (left), Case B (middle), Case C (right). 105

FIG. 3.13. Comparison of intensity for idealized TCs, three experiments: Case A (red), Case B (green), Case C (blue). 106

FIG. 3.14. SST condition as demonstrated by ocean model at F068 with individual tracks as red lines, three experiments: Case A (left), Case B (middle), Case C (right). 107

FIG. 3.15. Significant wave height as demonstrated by wave model at F055 with individual tracks as red line, one experiment with wave data: Case C (right). 108

FIG. 4.1. Spatial domain configuration and sensitivity of track to initialization times every 12 hours between 00 UTC 10 September 2004 and 12 UTC 13 September 2004: 00 UTC 10 September 2004 (red, solid line marked with x's), 12 UTC 10 September 2004 (green, solid line marked with x's), 00 UTC 11 September 2004 (cyan, solid line marked with x's), 12 UTC 11 September 2004 (black, solid line marked with x's), 00 UTC 12 September 2004 (red, dotted line marked with *'s), 12 UTC 12 September 2004 (green, dotted line marked with *'s), 00 UTC 13 September 2004 (cyan, dotted line marked with *'s), 12 UTC 13 September 2004 (black, dotted line marked with *'s), and NHC best track verification (blue, solid line marked with *'s). 109

FIG. 4.2. Comparison of forecast track, 5 experiments: Static Case (red), Dynamic Case (green), ROMS Case (cyan), WRF-ROMS Case (blue), WRF-ROMS-SWAN (magenta). NHC best track verification (black). 110

FIG. 4.3. Comparison of forecast track, zoomed into area of landfall, 5 experiments: Static Case (red), Dynamic Case (green), ROMS Case (cyan), WRF-ROMS Case (blue), WRF-ROMS-SWAN (magenta). NHC best track verification (black). 111

FIG. 4.4. Track differences through landfall at F090 and respective averages. Five comparisons to verification: Static Case (red), Dynamic Case (green), ROMS Case (cyan), WRF-ROMS Case (blue), WRF-ROMS-SWAN Case (magenta). Static Case and WRF-ROMS-SWAN Case difference (black). 112

FIG. 4.5. Simulated TC intensity from initialization (12 UTC 12 September 2004) through termination (00 UTC 17 September 2004), 5 experiments: Static Case (red), Dynamic Case (green), ROMS Case (cyan), WRF-ROMS Case (blue), WRF-ROMS-SWAN (magenta). NHC best track verification (black). 113

FIG. 4.6. Model simulated radar reflectivity at landfall, 5 experiments: Static Case (upper left), Dynamic Case (upper middle), ROMS Case (upper right), WRF-ROMS Case (lower left), WRF-ROMS-SWAN (lower middle). Verification radar reflectivity taken at landfall from radar station at KMOB in Mobile, AL (lower right). Taken at F090, valid 06 UTC 16 September 2004. 114

FIG. 4.7. SST difference from initialization (12 UTC 12 September 2004) through termination (00 UTC 17 September 2004) for WRF-ROMS Case. 115

FIG. 4.8. SST difference from initialization (12 UTC 12 September 2004) through termination (00 UTC 17 September 2004) for WRF-ROMS-SWAN Case. 116

FIG. 4.9. SST Analysis of the Gulf of Mexico demonstrating two distinct cooling features after the passage of Hurricane Ivan, 17 September 2004 (From Walker et al., 2005). 117

FIG. 4.10. Buoy locations in Gulf of Mexico used for SST analysis in Fig. 4.11 and significant wave height analysis in Fig. 4.17. 118

FIG. 4.11. SST analysis at buoy locations in Fig 4.10 from initialization (12 UTC 12 September 2004) through termination (00 UTC 17 September 2004). Four line colors: Observation (blue), HYCOM model SST (black), WRF-ROMS Case (green), WRF-ROMS-SWAN Case (red). Six panels: Buoy 42001 (upper left), Buoy 42023 (upper right), Buoy 42007 (middle left), Buoy 42039 (middle right), Buoy 42040 (lower left), Buoy sanf1 (lower right). 119

FIG. 4.12. Location of two grid points used for analysis in Figs. 4.13-4.16. 120

FIG. 4.13. Analysis at point U1 in Fig. 4.12 from initialization (12 UTC 12 September 2004) through termination (00 UTC 17 September 2004), 6 panels from top to bottom: wind stress in Nm^{-2}, heat flux in Wm^{-2}, temperature from surface through 100m depth in °C, U velocity from surface through 100m depth in ms^{-1}, V velocity from surface through 100m depth in ms^{-1}, W velocity from surface through 100m depth in ms^{-1}. 121

FIG. 4.14. Analysis of heat budget at point U1 from initialization (12 UTC 12 September 2004) through termination (00 UTC 17 September 2004), panels from top to bottom: horizontal advection term in °C day^{-1} (left), vertical advection term in °C day^{-1} (right), total advection term in °C day^{-1} (left), vertical diffusion term in °C day^{-1} (right), total local rate of change term in °C day^{-1} (left), temperature in °C (right), comparison of contributions of advection and diffusion to local change in temperature integrated through 100m. 122

FIG. 4.15. Analysis at point U2 in Fig. 4.12 from initialization (12 UTC 12 September 2004) through termination (00 UTC 17 September 2004), 6 panels from top to bottom: wind stress in Nm^{-2}, heat flux in Wm^{-2}, temperature from surface through 100m depth in °C, U velocity from surface through 100m depth in ms^{-1}, V velocity from surface through 100m depth in ms^{-1}, W velocity from surface through 100m depth in ms^{-1}. 123

FIG. 4.16. Analysis of heat budget at point U2 from initialization (12 UTC 12 September 2004) through termination (00 UTC 17 September 2004), panels from top to bottom: horizontal advection term in °C day^{-1} (left), vertical advection term in °C day^{-1} (right), total advection term in °C day^{-1} (left), vertical diffusion term in °C day^{-1} (right), total local rate of change term in °C day^{-1} (left), temperature in °C (right), comparison of contributions of advection and diffusion to local change in temperature integrated through 100m. 124

FIG. 4.17. Comparison of observed (blue) and modeled (red) significant wave heights at 4 buoy locations noted in Fig. 4.10: 42001 (upper left), 42007 (upper right), 42039 (lower left), 42040 (lower right). Taken from model initialization (12 UTC 12 September 2004) through termination (00 UTC 17 September 2004), with exceptions to when observations were not available due to extreme waves (as noted in Teague et al., 2007). 125

1. Introduction

1.1 Motivation

The 2005 Atlantic hurricane season was the costliest on record for the United States, with at least 2,280 deaths and damages over $128 billion (Vaccaro, 2006). This tumultuous season highlighted the need for a better understanding of the factors that contribute to hurricane intensity and necessitated the development of more advanced hurricane prediction models to improve intensity forecasts. With a dramatic increase in the amount of people living near the coastline in the past few decades, this trend in increasing damage from tropical systems is only expected to continue (Goldenberg et al., 2001; Oey et al., 2007; Vaccaro, 2006).

As a result of this tumultuous season, the deficiencies in model solutions of these storms have come under increased scrutiny. The lack of skill, particularly in the realm of hurricane intensity forecasting, has been attributed in part to the deficiencies of current model simulations (Chen et al., 2007; Davis et al., 2008). Specific problems have been found with insufficient grid resolution, inadequate surface and boundary layer formulations, and the lack of coupling to a dynamic ocean model (Bao et al., 2000; Bender and Ginis, 2000; Chen et al., 2007; Davis et al., 2008; Morey et al., 2006).

In recent years, a number of studies have been completed that attempt to model the dynamic relationship between atmosphere, ocean, and wave environments which allow interactions of the model solutions (Bao et al., 2000, 2003; Bender and Ginis, 2000; Bender et al., 2007; Chen et al., 2007; Davis et al., 2008; Doyle, 2002; Emanuel et al., 2004; Morey et al., 2006). Most of the coupled atmospheric model simulations that have been run have shown significant improvement in the atmospheric solution over similar simulations based off of a static ocean and wave environment (Bender and Ginis, 2000; Chen et al., 2007; Davis et al., 2008; Morey et al., 2006). Given the recent scrutiny hurricane simulations have come under and in the wake of the unprecedented 2005 hurricane season, more advanced models need to be run operationally. This next generation of numerical simulations should include atmospheric coupling of ocean temperature and wave data to provide feedback for the passing Tropical Cyclone (TC) ((Bender and Ginis, 2000; Chen et al., 2007).

The model to be employed in this thesis research is the COAWST, or Coupled Ocean Atmosphere Wave Sediment Transport, model. COAWST combines the Weather Research and Forecasting (WRF) atmospheric model, the Regional Ocean Model System (ROMS) ocean model, and the Simulating Waves Nearshore (SWAN) wave model. While other experiments have employed 3-way coupling (Chen et al., 2007), utilizing a WRF-ROMS-SWAN configuration is unique in its approach and unprecedented in its execution.

This thesis will examine the differences between utilizing coupled and uncoupled models for tropical cyclone forecasts and hindcasts. The focus of this thesis will be the examining the result of coupling the atmosphere, ocean, and wave models to each other. Examining the sediment transport modeling component of this model will be left to future research.

1.2 Literature Review

1.2.1 Upper Ocean Response to a TC, Modeling Approach

1.2.1.1 Stationary TC

Price (1981) was very detailed in presenting the dynamics of upper ocean circulation, and provided a review of components contributing to upwelling and downwelling features in the deep ocean. An empirical examination of historical observations involving hurricanes passing over a buoy or otherwise data-rich section of the ocean suggests an obvious result – intense, slow moving hurricanes cause the greatest variation in Sea Surface Temperatures (SSTs).

The greatest change in SSTs (ΔSST) occurs on the right side of hurricanes. This relationship was mentioned and studied initially in Price (1981) and was investigated in detail through real cases and through use of an ocean model described further in section 1.2.9.1. In several cited cases, the difference between the ΔSST on the right and left side varied by as much as a factor of four. Originally discussed in Ooyama (1969) and later detailed extensively by Emanuel (1986), numerous numerical simulations of TCs demonstrate that the essential importance of latent and, to a lesser extent, sensible heat flux is from the sea surface. These papers, among others, demonstrate the importance that SST has on the intensity and track of TCs. This cross-track ΔSST change is an important mechanism as both the TC intensity, and to a lesser extent TC track, are dependent on the location of the warm water beneath the storm.

To look into this phenomenon in greater detail, the simple ocean model used in Price (1981), which is detailed in section 1.2.9.1, was initialized with in-situ observations of the ocean prior to the passage of Hurricane Eloise. The initial environment that was constructed was based on several buoy and ship reports in the path of Eloise in the two weeks preceding the event. To simplify things further, the hurricane's winds were taken to be symmetric, and the hurricane translation velocity (forward speed) was not taken into account. Price (1981) therefore could challenge a pre-existing notion that the higher ΔSST values on the right hand side of the hurricane were due to the higher winds on that side of the storm. Stronger winds relative to a fixed position exist in the forward-right quadrant of the TC due to the additive effects of wind direction and hurricane translation velocity.

Important conclusions from the Price (1981) paper include that the reason the ΔSST values are higher on the right side have to do with the wind stress turning with time clockwise on the right side of the storm, thereby creating positive feedback to the inertial currents in the Northern Hemisphere (as demonstrated in Figure 1.1). This feature is dependent on the translation speed of the TC. Price (1981) found that upwelling significantly enhances entrainment under slowly moving (< $4 ms^{-1}$) hurricanes. Upwelling in slow moving storms also reduces the rightward bias of SST response.

Price (1981) considered the contributions to ΔSST by comparing the values of heat flux due to interaction with the atmosphere and heat flux due to upwelling of cool water into the mixed layer from below the thermocline. The model demonstrated a 20 °C m heat flux between the air and sea. The net heat entrainment value within the ocean dwarfed this result at 130 °C m. Therefore, heat entrainment into the mixed layer from upwelling accounted for approximately 85% of the heat exchange in the idealized model from Price (1981).

Additional experiments were undertaken to understand the effect the depth of the mixed layer and the effect of the temperature gradient in the thermocline would have on the SST during and after the passage of a TC. Price (1981) took his model and applied it to a few geographic areas of interest. First 16 °N 20 °W, near the eastern boundary current where there is a sharp thermocline, shallow (30 m) mixed layer, and strong temperature gradient. The ΔSST response here was estimated to be approximately -2.9 °C. Another numerical experiment was performed, with a temperature profile similar to 16 °N 55 °W, where the western boundary current has a deep thermocline and mixed layer, with a low temperature gradient. Here, the ΔSST was estimated to be much smaller, about -0.3 °C.

Price (1981) concludes by stating that the important characteristics of the numerical simulations on the atmospheric solution is based on the strength, translation velocity (speed) and overall size of the TCs. In the ocean, the important characteristics are based on initial mixed layer depth and the temperature gradient. Somewhat surprisingly, experiments into the Price (1981) model determined that the maximum mixed layer current is insensitive to just about everything except hurricane strength winds and is about 1.1 ± 0.2 ms^{-1} over the range in which SST response greatly varies. Another equally surprising conclusion from Price (1981) is that the ΔSST response is insensitive to hurricane size and the local inertial period. As a result of this, larger hurricanes may lower the SST over a larger area, but it was found that the magnitude of the ΔSST is minimally different.

1.2.1.2 Moving TC

Price et al. (1994) continued upon the findings in the Price (1981) paper by executing the model (detailed in section 1.2.9.1) for a hurricane translating over an ocean domain. These simulations examined the forcing and stress caused by a hurricane translating above the upper layers of the ocean. It specifically examines the "forced stage" response during storm passage.

The forced stage is defined as the local (depth and time dependent) ocean response to the strong wind stress of the hurricane Price et al. (1994),. Included in this response are mixed layer currents, substantial cooling of the mixed layer and SSTs, as well as a barotropic response which includes a geostrophic current and an associated trough in Sea Surface Height (SSH). Conversely, the relaxation stage is a nonlocal (three-dimensional and time dependent) baroclinic response to the curl of the wind stress induced by the hurricane. For the purposes of the Price et al. (1994) paper and this thesis, only the initial forced stage response will be examined.

The forced stage response was studied in Price et al. (1994) by examining three hurricane events – Norbert, Josephine, and Gloria. These hurricanes were introduced into a three-dimensional ocean model described further in section 1.2.6.1. Air temperature at the surface of the TC was generally 1-3 °C cooler than the temperature of the sea surface (Riehl 1954 and Emanuel 1986). Price et al. (1994) defined air and dew point temperatures at the surface throughout the domain to be 3 °C and 4 °C less than the initial SST, respectively. This resulted in a 600 W m^{-2} surface heat flux into the atmosphere.

Verification and initialization data were collected by NOAA P3 aircraft deploying 15 AXBTs (Airborne eXpendable BathyThermographs) roughly 40-km apart in a star-like pattern across the area of the three hurricanes. These AXBTs were able to collect temperature data, surface wave information, and current velocity to an error of 0.2 m s^{-1} RMS. The initial upper-ocean currents in the data analysis were treated as random noise under the assumption that hurricane induced currents would be much larger. For model initialization, the initial currents were set to zero.

As to be expected from Price (1981) there was a significant change in mean ocean layer transport in the horizontal structure during TC passage. Again demonstrated here was a rightward bias in transport values, 120 m^2 s^{-1} versus 25 m^2 s^{-1} to the left. This bias in transport vector magnitude was confirmed in the AXBT data as well. As shown in Price (1981) the turning of wind stress vectors in time remain mostly aligned with the clockwise turning of the inertial currents in the northern hemisphere, which contributed to the additive effect. The opposite is true of the left side of the track, the turning of wind stress vectors and the inertial currents were in opposite phase. The net result was that the magnitude of transport vectors were greatly reduced on the left side of the track.

Comparison of the Price (1994) model to the observations from the AXBT data suggests a high skill in simulation of mixed layer currents. There was however significant deviation in regions where the observed current speed was <0.7 m s^{-1} and suggests either imprecise instrumentation on behalf of the AXBTs (based on the RMS error of 0.2 m s^{-1}) or a model failure in those regions.

Upwelling, which significantly enhances entrainment under slowly moving (< $4ms^{-1}$) hurricanes (Price 1981), was considered to be the most important mechanism of density change in the hurricane response. The model data were estimated in these cases by the displacement of 14 ˚C isotherm. Minimal upwelling and pressure coupling was found in the forward section of hurricanes. As a result, the currents in the forward half were trapped within the mixed layer and the transition layers. Vertical current and temperature profiles were given both from the AXCP data and from the model run, these diagrams showed reasonable skill by the model in both temperature change and current velocity with depth.

The Price et al. (1994) paper demonstrated that near-inertial currents in most cases dominated the upper ocean response, a finding that was supported by Price (1981). Also of importance, the vertical mixing is very intense during the forced stage and could penetrate below the mixed layer. Despite this intense vertical mixing, it was also found that the surface mixed layer depth varies only slightly. Although vertical mixing acts to deepen the surface mixed layer, upwelling from below the thermocline pushes the mixed layer closer to the surface.

The extent of the relaxation stage after hurricane passage will briefly reference Brink (1989). Data and conclusions from this study suggest that with time, the thermocline-depth currents will become gradually more intricate during the relaxation phase. This was demonstrated with moored buoy data. The study also found that direction change grew to more than half a cycle a week after the hurricane passage. As mentioned above, this thesis will primarily examine the forced stage response, the relaxation stage is not relevant to this study.

1.2.2 Upper Ocean Response to a TC, In-Situ Approach

Initial observations into the right-side bias phenomenon were described by Church et al. (1989), which documented the effects of the passage of Hurricane Gay above the Pacific. Data from several CTD (Conductivity-salinity, Temperature, and Depth) sensors and Doppler current meters were available throughout the storm. Church et al. (1989) found again that ΔSST and enhanced current velocity occurs much more profoundly on the right side of the track of a moving hurricane. Although this phenomenon is well documented in several models and a few observations, it was not observed in direct current observations until Sanford et al. (1987) and Church et al. (1989).

Data in the Church et al. (1989) paper were collected during a 1985 cruise of the R/V Thomas G. Thompson while making a cross-Pacific CTD and acoustic Doppler current meter section along 24.25 °N. The Doppler imaging was able to provide excellent horizontal (across-track) and vertical resolution of the currents in the hurricane's wake. This dataset also confirmed the strong right-side bias of SST change during this storm. Combining ship position with Doppler data, an absolute current velocity was computed at 30 minute intervals. Noting that the inertial current below 100 m was mostly geostrophic, Church et al. (1989) used the 100 m currents as a reference and subtracted the 20 m currents. When this was displayed, the right-side bias of current strength and its effect on mixed layer and near-surface currents became apparent.

Due to the storm, the ship did not collect data over Hurricane Gay's track until 1.5 days after its passage, and took another 3 days to gather data. As a result, the data presented were not driven synoptically. To bring these data into quasi-synoptic agreement, the current vectors had been back-rotated about one inertial period. This resulted in a much more simplified field of current vectors than the initially analyzed one.

The data from Church et al. (1989) confirm that there was a strong right-sided bias along the track of Hurricane Gay, both in terms of intensity of current and SST. They provided observations within the wake of a hurricane to confirm the cross-track bias demonstrated in the model results from Price (1981). The largest currents, roughly 1.0 m s^{-1} were located 80 km to the right of the track, concurrent with the location of a SST minimum. On the left side of the track, the currents are much weaker and lacked organization. There is no clear current response on either side below 100 m. As a result, the wind-driven currents appear to have only affected the surface mixed layer and transition layer. It is important to consider that this study is not ideally suited to study ΔSST, as there was no data collected before the storm.

Thermocline-depth, pressure-forced currents consistent with the relaxation stage (Price et al. 1994) were not observed during the immediate 4.5-day period following the storms passage. It is assumed that this relaxation stage occurred several days or weeks after the R/V Thomas G. Thompson retrieved this post-storm data.

Ocean response from Hurricane Ivan utilizing in-situ measurements of currents was studied in Mitchell et al. (2005) and Teague et al. (2007) as part of the Slope to Shelf Energetics and Exchange Dynamics (SEED) project. The Naval Research Laboratory has undergone research into the area of examining the slope of the Gulf of Mexico shelf and currents associated with this shelf-break in 2004 with the SEED project. Fourteen Acoustic Doppler Current Profilers (ADCPs) were deployed to measure currents in the Gulf of Mexico through this project. Six of these ADCPs were deployed along the outer continental shelf and slope waters off of the Gulf Coast with moorings at depths of 60 m and 90 m. These six moored instrument packages on the shelf consisted of 300 kHz ADCPs and wave/tide gauges. The ADCPs rested about 0.5 m above the ocean bottom and measured current profiles in 2 m vertical bins with 1 cm s^{-1} accuracy. The remaining eight were deployed along the continental shelf at depths of 500 m and 1000 m, which were too deep to be included in this study of upper-ocean response. All of these instruments were spaced by about 15 km.

After Hurricane Ivan passed over the instrument array, Mitchell et al. (2005) and Teague et al. (2007) examined the ocean response along the continental shelf to Ivan by examining three of the four stages of ocean response. The first stage was represented as the time when the front half of the storm generated downwelling favorable wind conditions. Stage two occurred when the radius of maximum winds (the eyewall for Hurricane Ivan was about 40 km in radius) crossed the outer shelf. Stage three occurred when the rear half of the storm behind the eyewall crossed the outer shelf. Stage four was the relaxation stage as described in Price et al. (1994).

Stage one response (when the front half of the storm generated downwelling favorable wind conditions) was characterized by onshore advection in the upper water column and offshore advection of the lower water column across all six moorings. Given Ivan's average translation speed of 6.3 m s^{-1} in the Gulf of Mexico, stage one was estimated to be about fifteen hours. Some data of the wind stress component showed a linear decrease along with an increase in bottom temperature, suggesting pre-storm downwelling. Fifteen hours prior to eyewall arrival, temperatures increased at a greater rate suggesting enhanced downwelling. The fifteen hours of enhanced downwelling resulted in bottom temperatures rising about 3 °C at all six stations.

The response to stage two (when the radius of maximum winds, or eyewall, crossed the outer shelf) included a rapidly deepening surface Ekman layer that extended nearly to the bottom. Ekman layer thickness depends on friction velocity, which in turns depends on the magnitude of stress applied at each boundary. The wind stress increased monotonically until the eyewall passed over the outer shelf and then decreased. As a result, surface velocities increased and the Ekman layer thickened as the eyewall approached. As the surface wind stress dwarfed the bottom stress by an order of magnitude (10 Pa to 1 Pa), the Ekman layer took only four hours to deepen through to the bottom. Bottom velocities turned offshore at which point bottom temperatures increased about 4 °C due to downwelling. This study concluded that horizontal advection and downwelling resulted in this rapid temperature increase.

The dominant response during stage 3 (when the rear half of the storm outside the eyewall crossed the outer shelf) was characterized near-bottom onshore flows with near-bottom temperature decreases. The rapid rotation of the surface wind stress vector to the left of the eye was a result of the translation of the storm, and eventually slowed surface currents greatly. As stage 3 progressed, the wind stress decreased and the surface Ekman layer thinned, but the bottom currents continued unaffected and rotated clockwise – which resulted in a strong onshore flow that decreased temperatures 11 °C in only six hours. In areas where the eye did not directly pass, the surface Ekman layer remained thicker and the currents became aligned along-shelf.

Stage four, the relaxation response after Ivan's passage as detailed in Price (1994), was not discussed in Mitchell et al. (2005). Stage four response is examined in Teague et al. (2007). This study describes the most distinctive feature of the relaxation stage as the three-dimensional wake of near-inertial internal waves.

The Mitchell et al. (2005) and Teague et al. (2007) studies were significant because the ADCP experiment observed currents in the wake of Hurricane Ivan with unprecedented detail. Four distinct stages were observed during the hurricane's passage, each in response to the wind field. Different responses across the width of the eye were noted during stages two and three as they were increasingly complex as a result of the different rotation of the wind stress vector. Geographic factors, particularly the boot of Louisiana, were noted for accelerating currents over the shelf and enhanced transports to the left of the eye.

1.2.3 Upper Ocean Response to a TC, Remote Sensing Approach

Cornillion et al. (1987) used satellite-derived infrared (IR) images of the western North Atlantic to demonstrate cooling of SST by passing hurricanes as a result of upwelling, specifically during Hurricane Gloria. Hurricane Gloria (1985) formed very late in the hurricane season off of the Cape Verde islands. It moved westward along with the trade winds to the Leeward Islands, and then turned northwest toward the Sargasso Sea. Gloria's minimum central pressure fell to 919 hPa on 25 September, making it one of the most intense Atlantic hurricanes on record. Gloria continued northward and crossed the U.S. coastline along Long Island on 27 September, causing considerable damage to New England despite having been weakened significantly by the cooler waters of the North Atlantic.

The greatest cooling (up to 5 °C) was observed to have occurred north of the Gulf Stream in a region where the seasonal thermocline is shallowest and most compressed. Less intense cooling (3 °C) was observed in the Sargasso Sea where the thermocline is deeper and more diffused. The least cooling occurred near coastal waters (depths of around 20 m or less), which were mostly isothermal before the passage of Gloria. Right-side asymmetry from the passage of Gloria is well observed in this study. The asymmetry was noted as having a factor of four, as Price (1981) also found with in-situ observations of Hurricane Eloise.

The NOAA-Advanced Very High Resolution Radiometer (AVHRR) measured SST using IR satellite images of the western North Atlantic. This study notes the accuracy of this type of measurement to be within 0.2-0.5°C of the actual SST. The satellite data were extrapolated to give 4 km resolution, had been corrected for atmospheric attenuation, and was scan-angle corrected. A pre-hurricane image was compiled during nighttime to remove contamination by diurnal heating, which is very strong in this region. These scans were taken from 19-23 September. A post-hurricane image was collected immediately following the event, on 27 and 28 September. As a result, the post-hurricane data were compiled less than two days after the event, eliminating effects from the relaxation stage (Price et al. 1994) and distortion by horizontal advection. Taking the difference between these two images resulted in a fairly accurate representation of the magnitude of ΔSST.

This study provides an excellent example of regional or along-track variation of ΔSST, consistent with several model studies of the mechanisms of cooling. Previous model studies, Price (1981) and Price (1994), suggest that the upwelling-enhanced entrainment by wind stress is the dominant mechanism of SST cooling. As a result, the strongest cooling will be in regions denoted with a shallow thermocline. Despite the near-linear decrease in hurricane intensity with increase in latitude (due to cooler waters), the strongest ΔSST magnitudes occur in the northern part of the storm track.

Examination of the Hurricane Gloria case in this study attributes one contribution as the shoreward-progression of the track, where the coldest water is found near the sea surface (shallower thermocline). However, there was a limit to this, as when the depths approached less than 20 m along the coastline, the thermal layering was non-existent in late September and ΔSST was minimal. Cornillion et al. (1987) demonstrated that Hurricane Gloria provided a good test case for several known phenomena regarding

ΔSST with hurricane path. Gloria's effect on the sea surface was characterized by a strong right side bias, and advection of cooling by strong Gulf Stream currents. This study also confirmed the lack of change to the sea surface by hurricanes passing over weak, shallow, or non-existent thermoclines. Hurricane Gloria's initial east-west and then north-south oriented track allowed for asymmetries to be demonstrated along both dimensions.

Utilizing satellite composite imagery, Walker et al. (2005) was able to examine the effects of upwelling on SST, SSH and chlorophyll-*a* enhancement in the wake of Hurricane Ivan. After Hurricane Ivan passed overhead in the Gulf of Mexico in September 2004, clear skies allowed for satellite remote sensing of surface conditions. These conditions were sufficient to provide a unique understanding of the upper-ocean response to a passing hurricane utilizing satellite remote sensing data.

SST was examined using NOAA GOES-12 nighttime composite images. SSH was examined using altimeter data from Jason-1, TOPEX/POSEIDON, and Geosat Follow-on using techniques described in Leben et al. (2002). Chlorophyll-*a* concentrations were calculated using SeaWiFS data along with the NASA OC2 algorithm.

Hurricane Ivan was a classic hurricane that began forming over the tropical Atlantic Ocean on 2 September 2004. After entering the Gulf of Mexico, it rapidly strengthened to a category four hurricane, with winds in excess of 62 m s^{-1}. Ivan translated a north-northwestward course across the Gulf of Mexico towards New Orleans at a speed of 5.4 m s^{-1}. It slightly changed course on 15 September and made landfall as a strong category three storm near Gulf Shores, AL.

Walker et al. (2005) makes mention that despite this importance of SSTs on forecasting hurricane intensity fluctuations, most current hurricane models do not incorporate dynamic SSTs. The lack of this crucial data from model runs is considered to be one of the biggest contributing factors to less accurate hurricane intensity forecasts, including the forecast for Hurricane Ivan. Two rapid 3 m s^{-1} decreases in Ivan's wind intensity were noted during its trek across the Gulf of Mexico. Walker et al. (2005) directly correlates these sudden drops in intensity to the near-instantaneous cooling of the SST to 20-26 °C (from 28-30 °C before storm passage) over a wide swath of ocean surface, 38,000 km^2, by Ivan.

Average storm-related SST changes were computed to be around -4 °C. SSH changes were also reflective of this. SST/SSH change maxima were found to be 40-90km east (right) of Ivan's track, consistent with a right-side bias. Regions of extreme cooling (ΔSST greater than -5 °C) were found further westward of the track than expected. This feature was attributed to a strong pre-storm current (about 60 cm s^{-1}) located on the outer margin of one of the warm core ring features in the Gulf of Mexico. The data presented in this study revealed cooling around 1-6 °C in most areas after hurricane passage, with maximum cooling in regions of cyclonic circulation along Ivan's track.

Walker et al. (2005) demonstrated that cyclonic circulation features in the Gulf of Mexico have been found in regions of vigorous sub-surface upwelling and upward doming of cool water where the top of the thermocline is typically 50-60 m below the surface. Walker et al. (2005) utilized a number of calculations and formulas can be employed to find the displacement of the thermocline due to upwelling caused by Ivan. Using values consistent with conditions in the Gulf of Mexico with the passage of hurricane Ivan, there would be upward isotherm displacement of 32.7 m for every 10 cm decrease in SSH. Utilizing the satellite observed SSH change of -15 to -20 cm yields an isotherm displacement of 50-65 m. This is consistent with calculations of surface wind stress affecting the mixed layer (Walker et al, 2005).

Time-sequenced SeaWiFS imagery reveals large-scale enhancement of Chl-*a* concentrations within two upwelling regions. Peak concentrations lagged Ivan's passage by three and four days in the northern and southern features, respectively. The aforementioned 50-65 m upward isotherm displacement would have injected higher concentrations of nitrate into the surface waters, as previous study has shown that nitraclines within the Gulf of Mexico are typically found at the 50-70 m depth. Two features of hurricane-induced Chl-*a* enhancement are upward entrainment of phytoplankton to the surface and new production. Study into this hurricane event revealed that both sources were likely present. A three-way fully coupled model would be able to provide the oceanic dynamics necessary to study phytoplankton blooms in the wake of TCs. This implementation of the model system was not experimented with in the scope of this thesis.

Walker et al. (2005) showed that SST, SSH, and Chl-*a* observations all confirm enhanced upwelling along and east (to the right) of Ivan's track, as expected from previous studies. This study also confirms the importance of accurate SST/SSH forecasts for passing hurricanes by examining the SST/SSH fluctuations with Ivan's intensity fluctuations. This study also shows that hurricane-forced eddy pumping of nutrients into surface waters is an important biogeochemical process to be considered in future modeling studies.

1.2.4 Upper Ocean Heat Budget Response

1.2.4.1 Ocean Heat Content (OHC)

Hurricane intensification/decay has been directly correlated to the 26 °C isotherm. This has been mentioned in numerous studies (e.g. Leipper and Volgenau 1972, Emanuel 2005) as being the critical value. It has been demonstrated that TCs in environments of SSTs less than 26 °C usually experience decay while TCs in environments of SSTs greater than 26 °C experience intensification. Areas in the ocean with deeper mixed layers (greater than 150 m) are of particular importance to forecasting hurricane intensity fluctuations due to the greater amount of heat energy present. Hurricane winds result in surface mixing, with particularly strong mixing to the right of the hurricane's track.

Leipper and Volgenau (1972) introduced OHC as a quantity that would determine regions conducive to storm intensification based on temperature and depth of the 26 °C isotherm. The OHC formula is:

$$OHC = \rho_0 C_p \int_{Z_{26}}^{\eta} (T-26)\,dz, \ \mathrm{T} \geq 26\ {}^{\circ}\mathrm{C}$$

where Z_{26} (greater than 0 m) is the depth of the 26 °C isotherm, η is the SSH, ρ_0 is the density of the sea water, and C_p is the specific heat of the sea water. Based on this, regions of OHC greater than 60-90 kJ cm^{-2} have been found to be conducive to storm intensification. This value is truly dependent on the dynamics of the upper-ocean. Upwelling and vertical mixing can raise the depth 26°C isotherm (Z_{26}) and reduce the value of the temperature at the surface (T), thereby reducing the value of OHC.

Equally important, and leading to the intensification of TCs, downwelling is prevalent in modeling studies including Oey et al (2007) (the configuration is discussed in section 1.2.11.1). Downwelling due to convergent flows onto coastlines of southern Cuba and the northeastern Yucatan are demonstrated utilizing model data for Hurricane Wilma in October 2005. Downwelling, pushing the 26 °C isotherm to deeper depths, is able to increase the OHC in some regions by 50 kJ cm^{-2} or more over less than three days. This OHC increase can have drastic effects on the intensity of the TC.

1.2.4.2 Hurricane Heat Potential (HHP)

Morey et al. (2006) created a dynamic modeling system to pass information between the atmospheric and ocean environments during a passing TC in order to look at the contribution of different fluxes to the heat budget. A major hurdle in accurate SST and TC modeling and forecasting is the lack of a highly accurate wind field compared to observations during TCs. Techniques presented in Morey et al. (2006) provide interpolation of satellite scatterometer data with numerical weather prediction (NWP) data. Interpolating these fields has been found to result in highly accurate wind fields, properly gridded in space and time for input into numerical ocean models (Morey et al. 2006). These interpolated fields seem to produce a more accurate simulation of the ocean during TC forcing events rather than using NWP winds alone. The coupled flux model configuration in Morey et al. (2006) is discussed further in section 1.2.10.1.

Morey et al. (2006) examine the effect of Hurricane Dennis (2005) as it moved through the Gulf of Mexico. Results from this study confirm that there is a large amount of heat loss from the ocean to the atmosphere during a passing TC. In order to closely look at the heat budget of the ocean, four model experiments were run with heat and momentum surface flux active or inactive: one with no flux, one with heat flux, one with momentum flux, and one with both heat and momentum flux. Hurricane Heat Potential (HHP) from Leipper and Volgenau (1972) was used to examine the differences between the four cases. The study was able to show the dominance of the momentum flux over the heat flux in cooling the water column of deep ocean areas, in agreement with Shen and Ginis (2003). Hurricane Heat Potential can not be calculated in the coastal areas, where the entire water column temperature is greater than 26° C. As a result, his model was not able to look into the amount of HHP lost to the atmosphere in coastal regions. SST comparisons demonstrated rapid cooling along the coastline as the negative heat flux from the surface quickly mixed through the shallow water. The strongest cooling was still offshore, where mechanical mixing demonstrated the greatest effect to ΔSST (Shen and Ginis 2003).

Taking a closer look at the heat budget in the four experiments, Morey et al. (2005) is able to demonstrate the effect of various contributions of different processes.

The combined net surface heat flux (which was found in the heat and momentum flux experiment) and radiation terms show a -30 to -50 MJ m^{-2} contribution to the HHP budget. Considering a solar radiation contribution of 70 to 100 MJ m^{-2} in heat gained by the ocean, the amount of heat lost to the atmosphere is between -100 and -150 MJ m^{-2}. Modeled HHP values near the storm track range from 300 to 1000 MJ m^{-2}. Therefore, the amount of heat utilized by the atmosphere in a passing TC may be estimated to be within a range of 10-50%. This is much greater than the original estimates of 2-8% presented in Cione and Uhlhorn (2003).

1.2.5 Upper Ocean Salinity Response to Precipitation Processes

Price et al. (1979) was an initial observational study into the role of precipitation processes on the upper-layers of the ocean. Fresh water falling over the ocean surface creates a negative salinity anomaly within the first few meters of the ocean surface. This fresh stable layer plays an important role in mesoscale air-sea interaction processes. The fresh layer examined in Price et al. (1979) was a very thin layer that was the result of a brief (<2 hr) rain event that accumulated approximately 6 cm of rain. This fresh layer immediately deepened by entrainment and merged with an existing mixed layer approximately 25 m thick within 20 hr. The Price et al. (1979) observational study was a relatively simple example of wind-driven mixed layer deepening.

Bao et al. (2003) demonstrated the response of the upper-ocean to fallen precipitation utilizing the Princeton Ocean Model (POM). In order to accurately represent these thin layers, the POM is configured in Bao et al. (2003) with fine vertical grid spacing in the top layers, as low as 1 m. This vertical grid spacing is necessary as the ocean's response to the surface atmospheric forcing by precipitation occurs within in the upper few meters of the ocean. Depending on the atmospheric event (TC, squall line, etc) this ocean response may occur over only a few hours.

Bao et al. (2003) utilized an initially homogenous (in the horizontal and vertical) ocean environment. Rainfall was introduced into the model at an intensity of 15 mm hour^{-1} within a circle of 100 km and lasted for five hours. Running the POM in this configuration resulted in a maximum salinity anomaly of -0.3 to -0.35 psu (practical salinity units) within the top 2-3 m in five hours, and with a small (-0.05 psu) anomaly contour reaching below 10m depth. The stable layer gradually mixed over the course of few hours decreasing the magnitude of the anomaly but spreading it to a depth of 11-13 m. This modeled data correlates well with observations taken during a similar storm that took place during the Tropical Ocean Global Atmospheres/Coupled Ocean Atmosphere Response Experiment (TOGA/COARE) in the western Pacific warm pool, at 156 °E 2 °S.

Another experiment is carried out in Bao et al. (2003) that introduced a downward heat flux of 200 W m^{-2} by shortwave radiation to the surface after the rainfall is stopped. The results of this are compared to the same heat flux being applied to the surface, except with no precipitation-induced stable layer. An increased SST anomaly of 0.13 °C is noted in the case with the precipitation-induced stable layer. This anomaly is nearly three times larger than the case with no precipitation-induced stable layer, 0.035 °C. Likewise, the warming of the upper-layers of the ocean lasted longer in the case where there was a precipitation-induced stable layer. As a result, the rainfall-induced fresh layer responds to warming much more rapidly than the rest of the ocean.

The Bao et al. (2003) study concludes that the upper-ocean responds to surface forcing from the atmosphere much more rapidly when precipitation has formed a stable layer at the surface. However, it is also quick to note that a two-way coupled model including ocean-to-atmospheric feedback would be necessary to further study the problem. The current implementation of the coupled model does not allow for examination into this problem and will not be tested in this thesis. It remains an interesting problem that will utilize a fully coupled ocean-atmosphere-wave model for future study.

1.2.6 Upper Ocean Response and General Circulation Features

Oey et al. (2006) investigated the results of loop current warming on TCs, specifically Hurricane Wilma. Hurricane Wilma, during its duration from 16 October through 26 October 2005 became the strongest Hurricane on record in the Atlantic basin. The storm originated southwest of Jamaica over a region of high OHC. It strengthened rapidly to a Category 5 storm, weakened briefly and made landfall on the island of Cozumel and part of the Yucatan Peninsula. After making landfall it weakened again, but was pushed back to sea and strengthened again as it passed over the warm loop current as it headed towards Florida.

Wilma's unusually large size, combined with strong intensity and slow translation caused a decrease in SST at National Data Buoy Center (NDBC) buoys well before the storm arrived (Oey et al. 2006). Price (1981) and Shay et al. (2000) suggest that SST decreases are common and to be expected prior to the arrival of a TC, but on the scale of a few hours and within 100-200 km of the storm's center. In the case of Wilma, the SST at buoy 42056 decreased gradually (by approximately 0.5 °C per day) from 18-19 October 2005 while the storm center was still 400-600km from the site.

Data provided by buoy 42003 presents a more complicated problem due to its proximity to the Loop Current. Observed SST showed a 0.4°C decrease in SST, then an increase in SST of the same magnitude, followed by a sharp drop in SST of 0.8°C after Wilma passed to the south of the site. Oey et al. (2006) attributed the brief oscillation in SST before Wilma passed through to momentary shifting in the loop current due to the massive transport of warm water into the Gulf of Mexico by Wilma. The path of Wilma was unique in that it followed along the Yucatan Channel, thus pushing water northward. This massive volume transport is demonstrated in both model and satellite data.

Oey et al. (2007) continued this examination of Wilma and the loop current in the Gulf of Mexico by using a numerical model of the ocean, which is described in detail in section 1.2.9.2. Oey et al. (2007) utilized the numerical model and removed the loop current from the general circulation of the Gulf of Mexico. The model demonstrated that Hurricane Wilma would have traversed over a larger area of high OHC before making landfall in Florida. When the loop current was included in the solution, the massive volume flux of warm water as Wilma pushed through the Yucatan channel was channeled by the loop current away from the storm. As a result, the loop current in the Gulf of

Mexico and the general circulation, have huge impacts on the track and intensity of storms (Oey et al. 2007)

1.2.7 The Importance of 2-Way (Atmosphere-Ocean) Coupled Numerical Modeling

Bender and Ginis (2000) examined four realistic cases: Hurricanes Opal (1995) and Gilbert (1988) in the Gulf of Mexico, and Hurricanes Felix (1995) and Fran (1996) in the western Atlantic. Several experiments were run comparing uncoupled and coupled model cases, refer to section 1.2.10.2 for a detailed explanation of the model configuration.

In Bender and Ginis (2000), the uncoupled model forecast used for comparison is the Geophysical Fluid Dynamics Laboratory (GFDL) model, which was operational at the time of publication. According to Bender and Ginis (2000), beginning in 1995 the GFDL hurricane prediction system became the operational hurricane model for the National Weather Service, run on all TCs in the east Pacific and Atlantic basins during the hurricane season. The coupled model used for comparison is the same operational GFDL model coupled to the POM (Bender and Ginis 2000).

The GFDL forecasting system had performed very well in providing accurate track forecasts (Kurihara et al. 1998). Intensity forecasts were less accurate as the performance of the model has shown little skill and had a tendency to overintensify weak storms and underintensity strong TCs (Bender and Ginis 2000).

Hurricane Gilbert (1998) made landfall on the eastern edge of the Yucatan peninsula, and quickly re-entered the Gulf of Mexico over the northern edge. After reentering the Gulf, Gilbert experienced a slight 4 hPa deepening to 946 hPa as it translated westward before making landfall in Mexico 48 hours later. The uncoupled GFDL, had incorrectly deepened the storm 26 hPa to 934 hPa over that same period, an over-intensification of 22 hPa. Utilizing the coupled model, the forecast was much closer to the observed with the storm deepening about 10 hPa to 940 hPa, over-intensifying it merely 6 hPa.

In Bender and Ginis (2000), simulations of Hurricane Opal (1995) suffered from time incongruity to verification, the modeled storm moving too quickly and making landfall too soon. Comparing forecast intensity to a time-shifted verification also demonstrates that the model's 1/6° resolution was not able to deepen Opal as intensely as the verification provided. Ocean coupling had the most important effect on Opal during the initial part of the forecast, when Opal drifted to the north at a slow rate of speed. During this period, as Opal moved slowly though the Gulf of Mexico the SST decreased rapidly underneath the storm. As a result, the coupled solution most closely represented the intensity of the storm, as the uncoupled storm intensified much quicker than realized (Bender and Ginis 2000).

Simulations of Hurricane Felix (1995) in Bender and Ginis (2000) demonstrated better timing than Opal across all experiments. The coupled model resolved cross-path SST changes well, with a strong rightward-bias apparent but weakening as the storm's translation speed slowed in the Sargasso Sea. After a 72 hour forecast, the minimum sea level pressures were 963 hPa (verification), 960 hPa (coupled) and 945 hPa (uncoupled). This SST cooling due to the storm's slow translation speed through the Sargasso Sea led to a decrease in intensity in verification and the coupled solution. Clearly, the uncoupled solution had over intensified the storm (Bender and Ginis 2000).

Hurricane Fran (1996) was unique in the Bender and Ginis (2000) study because the TC followed in the wake of another major hurricane, Hurricane Edouard. As a result of the cold wake from Hurricane Edouard, Fran only deepened to 963hPa. The coarse grid spacing of the National Center for Environmental Prediction (NCEP) SST analysis, utilized in the operational model, was unable to resolve the cold wake generated by Edouard. As a result, the operational GFDL forecast incorrectly deepened Fran to 941 hPa in 72 hours, an over-intensification of 22 hPa. Another uncoupled simulation was executed, this time correctly resolving the cooler SSTs from Edouard, and the model intensified Fran to 951 hPa, an over-intensification of 12 hPa. A similar result was achieved by running the coupled model utilizing the sparse NCEP SST data. The closest result was when the coupled model was run with Edouard's wake resolved, which resulted in Fran having a 957 hPa minimum pressure after 72 hours.

Shen and Ginis (2003) examined multiple idealized comparisons of TCs translating above deep and coastal ocean areas. Multiple experiments had already been done over the deep ocean, which demonstrated that the primary SST cooling is due to mixing. The Shen and Ginis (2003) study looked into TC interaction above coastal waters. What they found was that the mixing in shallow water was less prevalent because there was no deep cold water to mix. As a result of this, surface heat fluxes have a much larger contribution to ocean cooling in near-coastal shallow ocean regions.

Utilizing the Shen and Ginis (2003) implementation of a coupled modeling system over deep water (see section 1.2.9.1 for the detailed configuration), appreciable differences in both SST change and resulting hurricane intensity are noted. The surface heat loss in the deep water (500 m depth) experiment is dominated, as expected from Price (1981), by entrainment of the lower layer water and by turbulent mixing. Some additional cooling is noticed when the surface heat fluxes are turned on, but the magnitude of this is small compared to mixing.

The SST anomalies (SSTA) between the coupled and uncoupled cases (within a 100 km radius of the eye) were used to judge the effectiveness of surface fluxes to overall cooling. A reduction by SSTA of 0.14° C (-0.53°C with surface fluxes on to -0.39° C with surface fluxes off) was noted by turning on surface fluxes in the deep-water case to account for about 20% of the total SSTA. The storm intensity reduction between the coupled and uncoupled cases was used to compare the effect of SSTA on the TC. For the deep-water case, the storm intensity reduction was 0.7 hPa (6.4 hPa with surface fluxes on to 5.7 hPa with surface fluxes off) or 11% of the total storm intensity reduction.

Shen and Ginis (2003) state that the surface heat fluxes result in SST cooling in two ways. First, by evaporation-induced cooling which is a direct heat sink into the atmosphere. Second, by vertical mixing caused by changing convective instability in the mixed-layer. To test this, they implemented their solution with the idealized TC over shallow water and compared to the deep-water case. Surface heat fluxes in shallow water (35 m depth) were more important as the mixing accounted for less heat loss. Turning off the surface fluxes resulted in a SSTA 0.17° C greater than with the surface fluxes included (-0.34° C with surface fluxes on against -0.17° C with surface fluxes off) or 50% of the total SSTA. This difference in SST anomaly averaged under the eye resulted in the TC being stronger with the warmer water by 1 hPa (3.8 hPa against 2.8 hPa) or 26% of the total reduction in intensity.

A cooling bias on the right-side of the track was prevalent in the shallow water case of Shen and Ginis (2003). This is typically attributed to the stronger mixing due to faster currents on the right side of the storm in the open ocean (Price 1981). However, due to the lack of a significant source of cool water below the mixed layer in the shallow water, this source of biased SST cooling is ruled out. Shen and Ginis (2003) attribute the right-sided cooling in the shallow water experiments to a 2-stage feedback mechanism. First, the winds in the front (leading-edge) right quadrant of a storm are the strongest as a result of the cyclonic circulation of hurricane winds and the translation direction. As a result of this, the surface fluxes are stronger, resulting in enhanced sensible and latent heat flux and cooler SSTs. Second, the cyclonic circulation causes dryer parcels from the cold wake of the storm to advect around and enhance the evaporation on the right side. This further accelerates the cooling of the sea surface.

Any SST difference beneath the eye can have drastic effects on the heat and moisture fluxes from the surface, which play important roles in TC evolution (Bender and Ginis, 2000). The location and amount of upwelling is of great importance in the prediction of the intensity and location of landfalling hurricanes. Unfortunately the patterns of SST change under the eye are not very well documented because this is also a region where instrumentation is rare and accurate satellite observations are scarce.

Oey et al. (2007) reiterated the importance of a time-varying upper ocean in the prediction of hurricanes, also demonstrated in Bender and Ginis (2000). One possible solution to implementing upper-ocean data is to use along-track altimeter data, which provides near-instantaneous and high resolution (5 km) Sea Surface Height Analysis (SSHA) during a hurricane. SSHA data are not limited by cloud coverage and have also been used operationally in other oceanographic applications where rapid observation is necessary, such as with Tsunami detection as demonstrated in Geist et al. (2006). Unfortunately, TC track and satellite orbit rarely overlap so SSHA does not provide a realistic solution. Oey et al. (2006) utilize the available SSHA data, among other data sources, to provide verification for model data during spatial and temporal alignment with the model grid.

According to Oey et al. (2007), SSHA data were extremely important in the prediction of Hurricane Wilma (2005). Immediately after passing over a warm eddy with a high OHC, the storm rapidly intensified into the strongest Atlantic hurricane on record (minimum surface pressure of 882 hPa and maximum sustained wind speeds of around 78 m s^{-1}). Contoured plots of the resultant change in sea surface height from satellite altimetry confirms that Wilma dramatically decreased SST's. Right-side SST cooling bias was evidenced, but Wilma had a slow translation speed. As a result of the slow translation speed, Wilma had less pronounced right-side bias, demonstrated in Price et al. (1994) and Church et al. (1989). After running the numerical simulation (the configuration is detailed in section 1.2.9.2) and comparing the data, there was some accuracy in predicting the SST drop in the Oey et al. (2007) study.

Experimentation into improving hurricane intensity forecasts in Davis et al. (2008) centered around three areas for forecast error reduction. First, improved surface-entropy-flux formulation, with a constant drag coefficient for winds greater than 30 m s^{-1} (Donelan et al. 2004). Second, finer resolution of the inner core, where the authors reduced the inner grid spacing from 4 km to 1.33 km (Chen et al. 2007). Third, which will be explored in depth, incorporation of the storm-induced ocean mixing and cooling of SST.

Davis et al. (2008) modeled (the model configuration is explained in detail in section 1.2.10.3) Hurricane Katrina (2005), which devastated the Gulf Coast. Intensity forecasts of Katrina were overestimated as they called for the hurricane to reach peak intensity just prior to landfall (Davis et al. 2008). Unreasonably high SSTs of 31° C from the Reynolds SST analysis may have contributed to this overintensification (Davis et al. 2008). While these high SSTs may have occurred, it is highly unlikely they existed underneath the eyewall (Davis et al. 2008, Scharroo et al. 2005). The major source of error in overestimating intensity in the Katrina forecast is attributed to this high SST input and the lack of ocean cooling feedback to the atmosphere (Davis et al. 2008).

Including an Ocean Mixed Layer (OML) model solution in with the atmospheric model revealed a strong right-side bias as Katrina moved through the Gulf of Mexico. Modeled SST changes reached a maximum of 3.5 °C on the right side but were observed to vary from 2-4.5 °C. This deficiency is attributed to not including the spatial variance of thermodynamic structure of the upper ocean in the OML model. Intensity at landfall was given as: 920 hPa (verification), 906 hPa (uncoupled) and 920 (OML). Strength at landfall was given as 57 m s^{-1} (verification), 64 m s^{-1} (uncoupled), 56 m s^{-1} (OML). The lower SST caused by ocean cooling reduced the strength of the storm 8 m s^{-1} prior to landfall and greatly improved accuracy when compared to an identical setup without contributions from the OML model. The addition of feedback from the OML model to WRF provided a more realistic solution for the strength of the storm at landfall, and was closer to verification.

1.2.8 The Importance of 3-Way (Atmosphere-Ocean-Wave) Coupled Numerical Modeling

Chen et al (2007) described the importance of three-way numerical modeling in helping to remove the lack of skill in hurricane intensity forecasting. This paper suggested the framework for a three-way coupled model and the parameter exchanges between the individual models. The authors suggested utilizing MM5 or WRF for the atmospheric model. A three-dimensional primitive equation, hydrostatic model, such as the one employed in Price et al. (1994) or the HYCOM model could be used to resolve the ocean. A third generation surface wave model, such as Wavewatch III, could be used to provide wave conditions.

Several parameters would be exchanged between the three models in this setup. The atmospheric model would pass surface heat and moisture fluxes to the ocean model. The ocean model would pass SSTs to the atmospheric model. The wave model would pass wave-induced shear to the ocean model. The ocean model would pass current velocity information to the wave model. The atmospheric model would pass surface wind to the wave model. Lastly, the wave model would pass wave-induced stress to the atmospheric model.

As stated in section 1.2.7, an ocean-atmosphere coupled model may improve hurricane intensity prediction as current atmospheric models feature an unrealistic constant SST condition that may overintensify storms. Including an atmospheric-oceanic coupling will reduce this effect as the SST decreases due to surface stress applied by the atmosphere.

Three-way, ocean-atmosphere-wave coupling seeks to better reduce the underestimation of surface winds (strength) as another problem in hurricane forecasting. This underestimation occurs even if the minimum sea level pressure (intensity) is correctly forecast. Chen et al. (2007) states that beyond a wind speed of 33 ms^{-1}, the surface does not become any rougher aerodynamically. Therefore, surface stress parameterizations in atmospheric models are pushed to their limits in hurricane conditions. Current models treat surface roughness as a scalar quantity (Bao et al. 2000, Doyle 2002), which is not realistic for the variable swirling winds in a TC. According to Chen et al. (2007), directionally coupling the wind and waves will provide a better solution than computing a scalar roughness from the total stress of the TC. Including wave coupling to the atmospheric model will reduce the underestimation of strength while inclusion of ocean coupling to the atmospheric model will reduce overestimation of intensity.

1.2.9 Previous 1-way Coupled Configurations

1.2.9.1 Simple Three-Dimensional Ocean Models (Price 1981, Price et al. 1994)

Price (1981) constructed a simple ocean model around the following physical approximations: Coriolis is held constant, pressure is hydrostatic, Boussinesq's approximation is made throughout, and diffusive processes (not including entrainment) are excluded. Density is computed from a linear equation of state. The sea surface is treated as a rigid lid. The subthermocline ocean is taken as infinitely deep and unable to sustain a pressure gradient. Temperature and salinity are assumed to have linear depth dependence and vertical density gradients are held constant.

Price et al. (1994) used the Price (1981) model that had to be modified when the varying speed and direction of the hurricane paths (Norbert, Josephine, and Gloria) resulted in systematic phase errors. Experimentation revealed that this would result whenever there was either 30° or greater shift in direction or a change in residence time greater than 2 hours. This problem was dealt with by initializing the hurricane well outside of the domain, then moving it along the correct track and speed until it reaches the central point of the domain. The model was then stopped and computations were integrated and saved to determine the resulting effect. The mixed layer depth in Price (1981) was significantly deeper than observed. For this model, the issue was resolved by adopting a hybrid mixed layer formulation that allows for possible mixing below the mixed layer.

1.2.9.2 PROFS Driven by Re-Analyzed GFS Winds (Oey et al. 2007)

Oey et al. (2007) utilized an ocean model driven by atmospheric winds to demonstrate the ocean effect of Hurricane Wilma in October 2005. The model used was the Princeton Regional Ocean Forecast System (PROFS), based off of the original Princeton Ocean Model (POM). The initialization wind field was pulled from the Global Forecast System (GFS) winds rerun using analyzed winds from the Hurricane Research Division of the NHC.

Wind stress was calculated from a wind-speed limited drag coefficient (C_d):

$$
\begin{aligned}
C_d \times 10^3 &= 1.2, \ |u_a| \leq 11\,\mathrm{ms}^{-1} \\
&= 0.49 + 0.065|u_a|, \ 11 < |u_a| \leq 19\,\mathrm{ms}^{-1} \\
&= 1.364 + 0.0234|u_a| - 0.00023158|u_a|^2, \\
&\quad 19 < |u_a| \leq 100\,\mathrm{ms}^{-1}
\end{aligned}
$$

where $|u_a|$ represents the magnitude of wind speed. This formulation would stay constant for low winds, increase linearly for moderate winds, reach a broad maximum for hurricane winds, and decrease for extreme winds. Donelan et al (2004) suggest the leveling of C_d at high winds is due to flow separation from steep waves. Moon et al (2004) find that C_d decreases for younger waves that predominate in hurricane-forced wind fields. Bye and Jenkins (2006) put the cause of the broad C_d maximum to the effect of sea spray flattening the sea surface by transferring energy to lower wavelengths.

Surface heat and evaporative fluxes for the Oey et al. (2007) model were set to zero due to the internal dynamics of the model. This was justified by referencing the assertion in Price (1981) that surface heat flux out of the ocean surface accounts for a small amount of the overall cooling, which is dominated by internal mixing.

1.2.10 Previous Two-way coupled Atmosphere-Ocean Configurations

1.2.10.1 BVW Boundary Layer Model to NCOM (Morey et al. 2006)

The numerical simulations in Morey et al. (2006) were conducted using the Bourassa-Vincent-Wood (BVW) atmospheric boundary layer model and the Navy Coastal Ocean Model (NCOM) of the Gulf of Mexico. The NCOM has been successfully used in the past to compute large and small domains. It is a primitive equation three-dimensional ocean model with the hydrostatic and Boussinesq approximations and employs a hybrid sigma/z-level vertical coordinate. This model was configured for use in the Gulf of Mexico with a 1/20° horizontal resolution and 60 vertical layers. The vertical layers were 20 evenly spaced sigma (terrain-following) layers for the upper 100m and 40 z-level (geopotential-following) grid levels from 100m to the bottom of the ocean with stretched grid spacing. This resulted in about 5m spacing for the upper 100m, with closer spacing near shallow coastal regions. The model domain encompassed the entire Gulf of Mexico and northwestern Caribbean Sea. The model domain has an open boundary to the east with radiation and upwind advection used for outgoing waves and atmospheric flow. Freshwater forcing was implemented into the domain from 30 rivers discharging into the Gulf by finding the net river discharge (evaporation minus precipitation).

The atmospheric flux model was based on the Bourassa-Vincent-Wood (BVW) boundary layer model (Bourassa et al. 1999) and was coupled to the NCOM. This BVW flux model takes its input from momentum, heat, and moisture roughness length parameterizations and then calculates the air-sea fluxes of momentum, latent heat, and sensible heat dependent on the air-SST and humidity differences. Also considered in the flux model were the sea state and influence provided from small capillary waves. The model domain was simplified by assuming local wind-wave equilibrium, a prescribed surface air humidity of 98% and a 2m specific humidity of 20 gkg^{-1}. This is in line with calculations from the NOAA National Data Buoy Center (NDBC) station 42039 demonstrating that the specific humidity during Hurricane Dennis was roughly between 18.0-20.5 gkg^{-1}. Downward momentum fluxes and upward latent and sensible heat fluxes were then calculated using three formulas, eliminating the need for estimating transfer coefficients for calculating the fluxes.

1.2.10.2 GFDL to POM (Bender and Ginis 2000, Shen and Ginis 2003)

Both Bender and Ginis (2000) and Shen and Ginis (2003) utilized the NOAA Geophysical Fluid Dynamics Laboratory (GFDL) hurricane model described in Kurihara et al. (1998) coupled with the Princeton Ocean Model (POM) developed by Blumberg and Mellor (1987). The latest version of POM may be referenced by Mellor (1998).

In Bender and Ginis (2000), the GFDL hurricane model described in Kurihara (1998) was used to model Hurricanes Opal (1995) and Gilbert (1988) in the Gulf of Mexico, and Hurricanes Felix (1995) and Fran (1996). In Shen and Ginis (2003), a vortex similar to Hurricane Fran (1996) is used. The model is a primitive equation model formulated using latitude, longitude, and sigma (σ) coordinates (18 levels in the vertical). A triply nested movable mesh (of 1°, 1/3°, 1/6° grid spacing, respectively) was used with the GFDL to represent TC features on a finer scale. The parent domain was set based on the TC's initial and 72 hour locations, the two child domain meshes follow the storm center.

The GFDL model was run using a cumulus parameterization scheme described in Kurihara (1973) with some changes from Kurihara and Bender 1980, appendix C. Surface flux calculation was done by using a Monin-Obukhov scheme. A level-two turbulence closure scheme from Mellor and Yamada (1974) was applied with a background diffusion coefficient added. Additional information regarding the GFDL hurricane model may be referenced in the Bender and Ginis (2000) publication.

The POM was chosen due to highly accurate representation of upper ocean mixed layer physics, a requirement for accurately reproducing the horizontal and vertical mixing processes under a TC. It is a three-dimensional, primitive equation model with thermohaline dynamics. The vertical levels are based on a terrain-following sigma (σ) coordinate. The second-order turbulence closure scheme described in Mellor and Yamada (1982) is employed to provide mixing parameters so that surface mixed layer dynamics are well represented. One of two ocean domains were specified based on the case they were studying (in the Gulf of Mexico or the western Atlantic). A 1/6° grid spacing was used for both ocean domains. 21 and 23 vertical layers were specified for the Gulf of Mexico and western Atlantic domains, respectively. Two land-ocean lateral boundaries were closed using a no-slip condition in the velocity field. The two open lateral boundaries utilized transport and thermal observations available at the time. Additional information regarding the POM may be referenced in the Bender and Ginis (2000) publication.

In Bender and Ginis (2000), the initial atmospheric fields for the GFDL hurricane model were derived using a scheme from Kurihara et al. (1995) and Kurihara et al. (1998). The NCEP T126 global analysis and storm messages from the National Hurricane Center (NHC) were merged to provide the best wind field generation. Producing axisymmetric and symmetric components of the TC within the environmental fields from the global analysis is a technique known as producing a "bogus vortex" (Singh et al. 2005). Lateral boundaries for the hurricane model were established using the NCEP global model.

In Shen and Ginis (2003), idealized oceanic and atmospheric conditions were used to integrate a solution over 60 hours. A "normal size" initial vortex was placed in an idealized atmospheric environment of uniform horizontal and vertical conditions. A -5ms^{-1} (easterly) wind was applied in the model where the TC was required to translate over the domain, some experiments were also carried out using a stationary storm. For the deep-water case, ocean depth was set to 500m, which was well below the layer that is typically perturbed by tropical cyclones, 150 m or less. The shallow water case was configured to a depth of 35m with a mixed layer depth of 25m.

1.2.10.3 WRF to 1-Dimensional OML (Davis et al. 2008)

The model in Davis et al. (2008) utilized the WRF model coupled to an OML model from Pollard et al. (1973). The atmospheric model was initialized on three domains. The fixed outer domain was composed of 12 km grid spacing and utilized the Kain-Fritsch cumulus parameterization scheme. A movable inner nest consisted of a 4 km grid spacing. A smaller movable nest with 1.33 km grid spacing was used in order to resolve the rapid deepening of Katrina on 28 Aug. Nest repositioning was based on the location of the 500 hPa minimum geopotential height and was called every 15 minutes in the simulation. Neither of the child nests used a cumulus parameterization scheme. All of the domains used the WSM-3 microphysics package and YSU planetary boundary layer scheme. Initialization for Davis et al. (2008) on 27 Aug was based on the GFDL model, with data positioned on a 1/6° grid. This model was chosen because of its sophisticated bogusing scheme described in Bender, 2005.

Simulations used a simple one-dimensional ocean mixed layer (OML) model applied to columns of ocean at individual grid points. This model, following Pollard et al. (1973), parameterizes ocean feedback in the presence of a TC in an attempt to capture the first-order negative feedback experienced in ocean-atmospheric coupling. As a result, this model does not feature pressure gradients or horizontal advection, but does include Coriolis. The inclusion of Coriolis is vital to demonstrating the rotation of inertial currents and the right-side bias of SST cooling. The model applies a stress to the top of the mixed layer, which deepens and cools as a result of entrainment from the water below. The mixed layer depth and lapse rate are specified in the model for the entire domain, a significant source of error as this varies spatially. The initial mixed layer current is set to zero, under the assumption that the TC will induce currents of much larger magnitudes. The OML model is called every model timestep across every grid point and the SST is then fed back into the atmospheric model. The initial ocean mixed layer depth was set to 30 m and the lapse rate was chosen to be 0.14 K m^{-1}.

2. Experiments of Hurricane Isabel (2003) Utilizing WRF Coupled to a 1-Dimensional Ocean Mixed Layer Model

2.1 Introduction

The reasoning behind an air-sea-wave coupled numerical model was explored in great depth in the first Chapter of this thesis. The most robust product that offers Sea Surface Temperature (SST) feedback from the ocean to the atmosphere that is openly available is the Weather Research and Forecasting (WRF) model. The ocean-atmospheric feedback mechanism is a simple 1-dimensional ocean mixed layer (OML) model based on Pollard et al. (1973). This basic atmospheric-ocean model that features SST coupling has been explored in depth in Davis et al. (2008) for Hurricane Katrina, examined in section 1.2.7 of this thesis.

The purpose of this thesis is to examine the effects of OML model coupling on Hurricane Isabel, which devastated North Carolina's Outer Banks in September of 2003. According to the NHC Tropical Cyclone Report (Beven and Cobb, 2004), Hurricane Isabel was a category 2 storm on the Saffir-Simpson scale when it made landfall, but the size of the storm was quite massive. Isabel has been directly attributed to the deaths of 16 people in the United States, mainly due to the torrential rainfall it produced in the state of Virginia, where 10 people perished. Total insured damage caused by the storm is estimated at $1.685Bil, with total damage estimates to be nearly twice that at $3.37Bil.

As demonstrated in Table 2.1 from Beven and Cobb (2004), the National Hurricane Center (NHC) track forecasts of Hurricane Isabel were very accurate, with forecasts statistics favoring 51-64% smaller error than forecasted storms during the 10 year period (1993-2002). This study does not seek to necessarily improve the track forecast for Hurricane Isabel, as Marks and Shay (1998) state that track prediction is primarily dependent on large-scale processes. As a result, track forecasting has improved considerably in the last several years. Little, if any improvement, in the track will be found in this case over the official NHC forecast by utilizing a coupled air-ocean model passing SST information (Davis et al., 2008).

Strength forecasts during the same period reached less favorable results (Bender and Ginis, 2000; Shen and Ginis, 2003). This is attributed to both an underestimation of how quickly Isabel would strengthen over the eastern Atlantic and an overestimation of how intense Isabel would remain as it reached the cooler waters of the western Atlantic (Beven and Cobb, 2004). Isabel's strength forecast compared to the previous 10-year average showed less skill across the board, with losses of 8 to 23% in accuracy

Chen et al. (2007) suggests that the current lack of skill in hurricane intensity forecasting is due to: deficiencies in current models, insufficient grid resolution, inadequate surface and boundary-layer formulations, and the lack of coupling to a dynamic ocean. The problem of insufficient grid resolution will improve over time with faster computational resources being developed and implemented. Inadequate surface and boundary-layer formulations is a problem that is being dealt with in other studies, including frequent updates to numerical models such as the WRF model. The issue of coupling to a dynamic ocean was addressed in the latest version of WRF and is what will be examined in this thesis. Three experiments will be used to demonstrate differences among the model solutions.

2.2 Data and Model Configuration

The WRF model version 3.0.1 from August 2008 was used in simulating Hurricane Isabel as it approached and made landfall off of the Outer Banks of North Carolina. The WRF Preprocessing System (WPS) version 3.0.1 from August 2008 was utilized to create the input and boundary conditions for the TC to operate within.

Atmospheric data are input from the Global Forecast System (GFS) 1° analysis. No bogusing scheme was used to initialize the TC, all the fields are derived from the 1° GFS grid. Atmospheric initialization data for the three experiments were identical. The WRF model was run for 4.5 days between 00Z 15 September 2003 and 12Z 19 September 2003. This initialization point was chosen as providing significant lead time (90 hours) before landfall, without having to utilize a large and computationally expensive grid.

The spatial domain was chosen to center over the southeastern U.S. with 3 km grid spacing (Figure 2.1). This level of spacing was used over the entire domain in order to adequately resolve the mesoscale processes that occur within the storm (Done et al 2004) and to negate the need to use a cumulus parameterization scheme. Nesting was not used in order to maintain some congruity to coupled air-sea studies (where nesting capabilities are currently unavailable) that will be discussed in later chapters. 31 vertical levels were used with a 9 second timestep, the top of the model domain was set to 50hPa.

The model spatial and temporal domains were identical in the three experiments. Internal dynamics were updated with regard to the lateral boundary conditions every 6 hours.

Model physics parameters were chosen to best support TC development and promote an accurate simulation. Precipitation processes were held entirely on the grid scale, with the WRF Single-Moment 6-class microphysics scheme (WSM-6) from Hong and Lim (2006). This first-order microphysics scheme was chosen as it is quite robust and includes water vapor, cloud water, cloud ice, rain, snow and graupel. Radiation schemes selected included the Rapid Radiative Transfer Model (RRTM) to represent the longwave radiation, and the Dudhia scheme for shortwave radiative processes, called every 8 minutes. The Monin-Obukhov surface layer physics option was used along with the thermal diffusion land surface physics scheme (selected because it must be used with the OML model). The Mellor-Yamada-Janjic turbulent kinetic energy planetary boundary layer (PBL) model was called every timestep. The model physics between the three experiments were identical except for the inclusion of different sea surface conditions. One of the new features included in WRF v.3 is the addition of a modified bulk drag and enthalpy (C_k, C_d) coefficients designed for tropical storm applications. This was not employed in order to maintain some congruity between this and later case studies using WRF v.2.

SST condition was derived from the 0.5° Real Time Global (RTG) SST and was utilized for the different sensitivity experiments. The control condition (hereafter referred to as Static) utilized the RTG SST condition at initialization that remained the same throughout the simulation. This represents what hurricane forecasts are based on without the inclusion of any ocean feedback. The first experiment (hereafter referred to as Dynamic) used analyzed RTG SST data to provide the sea surface condition for the storm. However, the RTG SST dataset is only available every 24 hours, so 6 hourly interpolations are made to provide additional SST data to the atmospheric mode. This represents the best available solution to including ocean feedback in hindcast simulations. The second experiment (hereafter referred to as WRF OML) utilized the WRF model's built-in ocean model that was available as of version 3. The thermocline depth was set to 50 m with a $\frac{dT}{dz}$ (Γ) of 0.14 °C m^{-1} over the entire domain.

2.3 Results and Discussion

2.3.1 Track

Figure 2.2 demonstrates how the model tracked the storm through the domain at 12-hourly intervals. The resultant model output demonstrates the assertion of Marks and Shay (1998) that track prediction is dependent primarily on large-scale processes. Little deviation was found between the three cases and most demonstrated high forecast skill 90 hours from landfall, consistent with the NHC forecast for this event.

Some slight deviation in track can be found after forecast hour 60 (F060, 12Z 17 September) and before landfall (F090). The Static and WRF OML case tracks closely follow each other, while the dynamic deviates slightly to the southwest. The three experiments then converge again at landfall. Given that the only difference between the three runs over this time period is the SST condition, an examination of the change in SST yields possible explanation for this difference. Figure 2.3 demonstrates the SST condition at F060 along with the tracks from initialization through F060 for the respective cases. The bottom right panel demonstrates the difference in SST between the Dynamic and WRF OML case along with their respective tracks after they diverge. As shown in the bottom right panel, the Dynamic SST on the far right side of the track (away from the track) cooled much more than the far right side when compared to the WRF OML. As convection inside of a hurricane would tend to be stronger with a warmer sea surface, the lowest sea level pressure (SLP) followed the stronger convection and deviated slightly to the southwest in the Dynamic case. This excessive right-sided cooling in the Dynamic case could be a result of erroneous SST data or possibly due to the 6-hourly interpolation method cooling water asymmetrically before the storm actually passed over the sea surface.

This track deviation was very minor, as shown in Figure 2.4 which shows the difference (in km) of the tracks between the different cases, which can be used as a proxy for modeled track skill. The three experimental cases ranged between an average track deviation of 46-57 km from initialization until landfall (F090) with the WRF OML case performing the worst. From model initialization until immediately before landfall (F072), the WRF OML case performed quite well and was the most consistent. An examination of 6-hourly track data immediately prior to and after landfall (Figure 2.5) shows that the WRF OML hurricane accelerated towards the coast faster than verification and the other two cases. This resulted in a temporal error in the forecast and a poorer forecast for the WRF OML case from F072 through landfall, although the resulting difference was quite small.

Forecast verification data from NHC (Table 2.1) from 72-hours and 96-hours over the course of the hurricane show errors of 148 km and 193 km. Forecast verification data compared to the average error of these model runs at F072 and F096 of 58 km and 93 km, respectively. All three model runs showed exceptional skill in predicting the point of landfall, with an improvement over the average NHC forecasted track error for this hurricane at F072 and F096 of 61% and 52%, respectively. Spatially, the three cases intersected the coastline at almost the exact point, less than 80km from the actual point of landfall at F090.

As mentioned in section 2.1, little, if any improvement in track prediction would be expected in the two experimental cases. All of the model runs did a very good job of giving a track hindcast. The control run and experimental runs yielded very nearly the same track, validating the hypothesis in section 2.1.

2.3.2 Intensity

As shown in Figure 2.6, improved skill is demonstrated in utilizing any type of ocean feedback compared to the Static case in most forecast periods. The initial deepening of the hurricane was quite rapid due to the incorporation of the 3-km grid spacing. Figure 2.7 demonstrates how well the grid spacing did to resolve the mesoscale features in and around the eyewall. As discussed in section 2.3.1, the hurricane in the WRF OML case made landfall a couple of hours before the others, as shown in this figure. While this had an effect on the accuracy of the track prediction, this is not resolved in the intensity comparison (Figure 2.6) as the NHC best track and intensity product is available on 6-hourly intervals.

The static case over intensified the storm due to the fact that the SSTs in and around the hurricane were treated as constant and were therefore too warm. As shown in the upper left panel of Figure 2.8, the initial SST (shown in the upper left panel of Figure 2.3) did not vary during the simulation. As a result, the TC in the other cases experienced cooler SSTs, which directly affected the contributions of heat and moisture fluxes – the driving mechanisms of the hurricane. As these resulted in a much better forecast, the magnitude of the ocean cooling should be considered realistic.

Demonstrated in Figure 2.6, at F072, the intensity error given by the Static, Dynamic and WRF OML cases were -13 hPa (overintensification), +4 hPa (underintensification), and +3 hPa, respectively. At F084, just prior to landfall, the intensity errors were -12 hPa, +1 hPa, +1 hPa, respectively. As mentioned in Section 2.1, the intensity prediction forecasts by NHC for this hurricane were quite poor when compared to the previous 10-year average. Given the very small difference of forecast surface pressure compared to verification, the strength forecast would be greatly improved with the introduction of SST feedback.

2.3.3 Sea Surface Condition

As mentioned in section 2.3.2 and shown in Figure 2.8, the sea surface condition in the static case did not vary as designed. As discussed in section 2.3.1, a mere 2.5 days into the simulation the difference in ΔSSTs between the Dynamic case and the WRF OML case resulted in minor track deviations between those two cases.

The right-side cooling bias discussed in Price (1981) and Price et al. (1994) is clearly evident among the Dynamic and WRF OML cases in Figure 2.8. In the Dynamic case, warming is noted along the coastline at the end of the simulation. This could be due to the transport of water from the Sargasso Sea by the TC, which is not included in the 1-Dimensional WRF OML model. As the TC moves across the continental shelf, the large volume transport of water by the TC could result in downwelling along the coast. Unfortunately, this hypothesis cannot be tested without the use of a fully coupled atmosphere-ocean-wave model resolving 3-dimensional ocean currents and wave energy.

2.4 Conclusion

This study sought to quantify the differences in model forecasts of Hurricane Isabel, starting at 90 hours before landfall. Hurricane Isabel devastated the Outer Banks of North Carolina in September 2003. The NHC track forecasting for the event was excellent, an average of 50-65% better than NHC track forecasts for the previous 10 years (Beven and Cobb, 2004). The NHC strength forecasting for the same storm was poor, with errors 8 to 23% greater error than NHC strength forecasts in the previous 10 years (Beven and Cobb, 2004).

Based on the recommendations from other studies, utilizing a coupled model to include the effects of mixing on the SST should yield a better intensity forecast, although track forecasts are mostly subject to large-scale forces. Three different model configurations (a control and two varying SST cases) were run to examine the effects of SSTs on the hurricane. The 1-Dimensional OML model showed no increased skill in track between the three modeled solutions, although the overall skill in predicting the TC track was excellent. The use of a 1-Dimensional OML model based on Pollard et al. (1973) demonstrated high skill in reducing error of the intensity from a +13 hPa (overintensification) error to a -1 hPa (underintensification) error. A right-side asymmetry in SSTs were noted in both cases which included a varying ocean temperature. Additional studies utilizing 3-Dimensional ocean and wave models could provide the benefits of examining specific ocean feedback features and a more robust atmosphere-ocean-wave coupled system.

3. Experiments of an Idealized Tropical Cyclone Utilizing the COAWST Model

3.1 Introduction

The need for advanced coupled numerical modeling of the atmosphere-ocean-wave system was a topic broadly explored in the first chapter of this thesis. Track forecasting has greatly improved over the last several years due to advances in model design and computational resources. As demonstrated in section 2.1, the track forecasts for Hurricane Isabel, a hurricane that devastated the Outer Banks of North Carolina in 2003, showed substantial improvement over the average forecasted track error during the prior 10-years. While the skill in predicting TC track has improved greatly, the skill in predicting TC intensity has remained the same for the last several decades. Chen et al. (2007) attributes this lack of skill to, among other deficiencies, the lack of full coupling to a dynamic ocean.

A small degree of ocean-atmosphere coupling exists with currently available numerical models, such as the Advanced Hurricane WRF explored in section 1.2.7 and the latest version (v. 3.1) of the WRF model explored in Chapter 2. However, neither of these atmospheric models resolve the ocean as a 3-dimensional system, and deficiencies in simulations result. Furthermore, no three-way coupled model is currently operational that combines the feedback mechanisms between the atmosphere, ocean, and wave systems – the need for which is presented in Section 1.2.8 of this thesis.

Two operational models exist that feature ocean-atmosphere coupling. The first, the GFDL model (operational with coupling since 2001) features coupling of the GFDL atmospheric model to the POM. There is no reference that mentions inclusion of wave coupling to this atmosphere-ocean coupled model (Bender et al., 2007). The second, the HWRF model (operational since 2007) currently features coupling of the WRF atmospheric model to the POM ocean model. There are plans to incorporate coupling to the WaveWatch III wave model (Environmental Modeling Center, 2009).

The Coupled Ocean Atmosphere Wave Sediment Transport (COAWST) model seeks to improve hurricane forecasting in that regard. The COAWST model represents the latest in air-sea interaction and numerical model coupling. The COAWST model was designed from three state-of-the-art numerical models representing the atmosphere, ocean and wave environments. Using the Model Coupling Toolkit (MCT), the COAWST model is able to couple the following models together:

Weather Research and Forecasting (WRF) model – Atmosphere

Regional Ocean Modeling System (ROMS) – Ocean

Simulating Waves Nearshore (SWAN) – Wave

Implementing this three-way coupling strategy will demonstrate the proper feedback mechanisms that occur when a significant meteorological event, such as a hurricane, interacts with the ocean. Coupling to the Community Sediment Transport Model (CSTM) is available but outside of the scope of this thesis.

This chapter seeks to provide a proof of concept for the COAWST model as a TC makes landfall in an idealized situation. The interaction and feedback mechanisms between the atmosphere, ocean and wave environments to be shown in this study will demonstrate the necessity and feasibility in using this three-way coupled model for realistic TC simulations within the atmosphere, ocean and wave models. The effects and interactions of the TC making landfall over an idealized coast will be examined in all three systems.

3.2 Coupled Model Design

Coupling the three models is accomplished through use of the Model Coupling Toolkit (MCT). MCT is a fully parallelized system that uses Message Passing Interface (MPI) to exchange model state variables. The coupled system operates as demonstrated in Figure 3.1. First, the master program initializes MPI and distributes each model component onto different sets of processors. Each individual model enrolls into MCT and configures its own domain, dynamics and physics parameters as defined by their respective documentation. Data exchange occurs by MCT at initialization between the models, after which the models integrate by their specified timesteps to a defined synchronization point. At that instance data is exchanged between the models. Model integration then continues until the next synchronization point where data is exchanged again. This process continues through the end of the models' integrations. At the end of the models' iteration, the master program finalizes the MCT and MPI and terminates the program.

In order to fully realize a three-way (atmosphere-ocean-wave) coupled system, data must be exchanged between the three models with reasonable frequency. The first feedback mechanism, which was explored to some extent as SST cooling in Chapter 2 of this thesis, is between the atmosphere (WRF) and ocean (ROMS) models. As explored in depth in the first chapter of this thesis, a TC translating above an open ocean will usually result in decreased SST due to mixing and heat loss to the atmosphere. This relationship has a large effect on the lowering the intensity of the TC, which in turn induces less mixing in the ocean than in a 1-way model configuration.

While the SST is passed from ROMS to WRF, several variables are passed from WRF to ROMS. The 10 m wind vectors ($\overline{U}_{10}$) , air temperature (T_{air}), atmospheric pressure (P_{air}), humidity, downward long wave radiation, and net shortwave (SW) radiation are passed from WRF to ROMS for use in a set of bulk flux formulas. The wave (SWAN) model exchanges variables of wavelength (L-wave), significant wave height (H-wave), and wave period (P-wave) to ROMS. From there, stress (τ), heat flux (hf), and pressure are passed as output from the bulk formulas to the ROMS model (Fairall et al., 2003, Taylor and Yelland, 2001).

SWAN passes surface wave parameters (direction, significant height, average length, relative peak period), wave breaking and dissipation parameters, and bottom wave parameters (period, orbital velocity) to ROMS. Currents (u, v) are passed from ROMS to SWAN. WRF sends the 10 m wind to SWAN but no heat flux information (for example, as a result of wave breaking, sea foam) is currently passed back from SWAN to WRF. This will be pursued in future research. The bulk flux parameterizations used in the COAWST model are based on: Fairall et al. (1996), Fairall et al. (1996), Liu et al. (1979), Fairall et al. (2003), Taylor and Yelland (2001), and Oost et al. (2002). These parameterizations have been extensively validated and used for the low to moderate wind conditions. Their utility in the high wind scenarios is subject to further investigation (section 3.4.3).

It is important to recognize that the COAWST modeling system is a new modeling tool that is under rapid development. We first applied COAWST to an idealized case in order to demonstrate what is expected to occur, based on the literature review, and provide a proof of concept before moving on to more complicated studies of realistic cases.

3.3 Idealized Case Configuration

3.3.1 Domain Configuration

The COAWST modeling system is configured for a closed ocean basin with 12 km grid spacing. The domain has 200 and 150 points in the X, and Y directions, respectively. For the sake of simplicity in the idealized case, this same grid is shared by all three models to eliminate the need for any grid interpolation. The model was run for 120 hours (5 days) from 1 September 00Z to 6 September 00Z. September was chosen to represent the shortwave radiation flux near the height of the hurricane season.

3.3.2 Idealized TC Configuration

The domain was initialized using a modified version of the WRF Standard Initialization (WRFSI) product. Modifications were made to allow initialization of the idealized TC above a specified land-water domain. Terrain height across the entire domain was taken to be a constant 0 m with defined land and sea points to demonstrate reasonable heat and moisture fluxes over the land. In order to have the TC make landfall roughly perpendicular to the coastline, the idealized input files were further modified to have the Coriolis force (f) held constant (f-plane) at $f \approx 4.9880 \times 10^{-5}$ s^{-1} (f at 20°N). This eliminated a cause of possible northward shift in the TC track (β-drift) as on an f-plane, $\frac{\partial f}{\partial y} = 0$.

An algorithm designed by Kevin Hill with the Department of Marine, Earth and Atmospheric Sciences at North Carolina State University was used to generate the initial and boundary conditions for the TC (Hill, 2006). This algorithm initialized an axissymetric vortex within the mean environmental temperature and SSTs found within the region 8.5°N to 15° N and 60° to 40° W during the month of September 2005, near the peak of the Atlantic hurricane season. The average SST was defined to be 29° C. The vortex structure was designed with reference to Kwok and Chan (2005) with a slightly different initial strength and size. Hill's algorithm first defines the wind speeds, and then calculates temperatures by thermal wind balance. Pressure perturbations are then calculated from the hypsometric equation, and gradient balance is used to set the geopotential heights. In order to get the TC to translate westward to make landfall perpendicular to the coast, Hill implemented a modification to his original code that instituted a North-South pressure gradient, which established a uniform 5 m s^{-1} easterly flow across the domain from an initial point, located at grid points X=150, Y=75.

The maximum wind of the vortex was set to 20 m s^{-1}, established at a radius of 50 km from the center. The minimum sea level pressure was approximately 1000 hPa. Hill used the Chan and Williams' (1987) horizontal wind profile to set the horizontal wind field, V_T (r) according to the formula:

$$V_T(r) = V_{\max}\left(\frac{r}{r_{\max}}\right)\exp\left\{\frac{1}{b}\left[1-\left(\frac{r}{r_{\max}}\right)^b\right]\right\}$$

where r is defined as the radius, r_{max} is defined as the radius of maximum wind (V_{max}). B is a constant that is related to the size of the vortex, set to b = 0.33 for all of the experiments. Vertical structure is established by multiplying the horizontal wind field, V_t (r), by a function $w(p)$ that decreases with pressure above an established point:

$$w(p) = \left[\frac{3(p/p_m)}{2+(p/p_m)^3}\right]$$

where p_m is the vertical level of maximum tangential wind (set to 850 hPa in all experiments).

3.3.3 Atmospheric Model (WRF)

The WRF model v.2.2 (released December 2006) is configured on the spatial domain described in section 3.3.1 with 31 vertical levels, and no nesting was used. The timestep was defined as 75 seconds. Internal dynamics were updated with regard to the lateral boundary conditions every 24 hours. The Lin et al. (1983) microphysics scheme was used to represent precipitation processes on the grid scale. The Kain-Fritsch cumulus parameterization (CP) scheme was also used to account for precipitation on the sub-grid scale. Longwave and shortwave radiation physics were computed using the Rapid Radiative Transfer Model (RRTM) and the Dudhia scheme respectively, called every 10 minutes. The Monin-Obukhov (the version implemented in the Eta model) surface layer physics option was used along with the thermal diffusion land surface physics scheme. The Mellor-Yamada-Janjic turbulent kinetic energy planetary boundary layer (PBL) model was called every timestep.

3.3.4 Oceanic Model (ROMS)

ROMS (updated through February 2008) is a state-of-the-art, free-surface, hydrostatic, and primitive-equation model which is currently used for several applications including simulations of estuarine, coastal and basin-scale ocean applications (Marchesiello et al. 2003; He and Wilkin, 2006, He et al., 2008). The model computes using vertically stretched terrain-following (σ) coordinates. ROMS includes includes high-order advection and time-stepping schemes, weighted temporal averaging of the barotropic mode to reduce aliasing into the slow baroclinic motions, and conservative parabolic splines for vertical discretization. A redefinition of the barotropic pressure-gradient term is also applied to reduce the pressure-gradient truncation error, which has previously limited the accuracy of terrain-following coordinate models. ROMS utilized installed physics that allows total implementation of advective processes, Coriolis, and viscosity in 3-dimensions. The Mellor-Yamada level-2.5 turbulence closure scheme was used (Mellor and Yamada, 1982).

ROMS is configured on the spatial domain described in section 3.3.1 with 21 vertical levels, and no nesting was used. The oceanic domain configuration is shown in Figure 3.3. The number of interior ρ points was set as 198 along the X-axis, 148 along the Y-axis and a 25 second timestep was used. A closed ocean basin was designed in the grid in order to ensure that any oceanic heat lost or gained would be as a result of atmospheric interaction and not advection into or out of the domain. Closing the ocean basin also removed the need for boundary conditions to be generated. As shown in Figure 3.3, the grid was defined along the X-axis as land from 1-50 (the location of landfall), water from 51-196, and land from 197-200. Along the Y-axis, the grid points were laid out as land from 1-15, water from 16-146, and land from 147-150.

To replicate a typical continental shelf with the minimum depth set to 10 m, the ocean bottom bathymetry is defined as a set of linear functions of offshore distance X. The bathymetry of the first section, representing the continental shelf, was defined with a downward slope of 10 m every 12 km for every grid point from the shoreline (X=50) through X=69. The bathymetry of the second section, representing the shelf break, has a defined downward slope of 40 m for every 12 km from grid points X=70 through X=89. The bathymetry of the final section, representing the deep ocean, is set to a constant 1000 m depth from grid points X=90 through X=197. The TC is placed three-quarters to the west of the domain (X=150), and halfway to the north (Y=75).

3.3.5 Wave Model (SWAN)

The SWAN model is integrated on the same grid as the ROMS model. The wave model is introduced to provide mixing to the ocean model. As discussed earlier, no feedback mechanism exists from the SWAN model to WRF model. The wave model is configured on a Cartesian grid. A circular grid in directional space was utilized with 36 directional bins. The model represented waves with a spectral frequency resolution between 1 s and 25 s, divided into 24 1 s bins. Waves are computed in 5-dimensions: west-east, south-north, time, frequency, and direction of propagation. The depth-induced breaking constant, the wave height to water depth ratio for breaking waves, was set to 0.73. Wind-wave growth was generated using the Komen formulation (Komen et al. 1984). A backward-in-space, backward-in-time advection scheme was used for iteration.

3.4 Methodology

Three experiments are undertaken to understand the role of ocean coupling and demonstrate proof of concept in using the COAWST model. The experiments are designed from case to case to introduce additional exchange of model state variables to allow interactions of physical processes in the models. Each case will be examined to determine whether the apparent feedback mechanisms are realistic, based on previous literature.

The first experiment, Case A, represents 1-way coupling as oceanographers currently use to force the ocean. As demonstrated in Figure 3.4, several variables are passed from WRF to ROMS via a set of bulk parameterizations. 10 m wind vectors ($\overline{U}_{10}$), air temperature (T_{air}), atmospheric pressure (P_{air}), humidity, and net shortwave (SW) and downward long wave radiation are passed from WRF to the bulk formulas (Fairall et al., 2003). Surface Stress (τ), net surface heat flux (hf), and surface pressure are computed and then passed as the forcing to the ROMS model. There is no SST feedback from the ocean to the atmosphere.

The second experiment, Case B, represents 2-way coupling similar to what was examined in Chapter 2 of this thesis. As demonstrated in Figure 3.5, SST is now passed from ROMS back to WRF, allowing the ocean model to provide feedback to the atmospheric model. While Chapter 2 examined this effect using a simple 1-Dimensional Ocean Mixed Layer model, this chapter will seek to examine ocean feedback from a 3-Dimensional model.

The third experiment, Case C, represents the more complete coupling that can be currently implemented using the COAWST model. As demonstrated in Figure 3.6, the wave (SWAN) model inputs variables wavelength (L-wave), significant wave height (H-wave), and wave period (P-wave) into the set of bulk formulas. The ocean model (ROMS) provides current vectors to the wave (SWAN) model. SWAN passes surface wave parameters (direction, significant height, average length, relative peak period), wave breaking and dissipation parameters, and bottom wave parameters (period, orbital velocity) to ROMS. The 10 m wind is given from the atmospheric (WRF) model to the wave (SWAN) model. This configuration is not a complete 3-way coupled model as described in Chen et al. (2007) and demonstrated in Figure 3.7. The current version of the COAWST model lacks the surface roughness (wave induced stress) and heat flux exchange feedback mechanism that SWAN would provide to WRF. Despite this missing feature, wave feedback to the ocean will be explored.

3.5 Results

3.5.1 Track

As demonstrated in Figure 3.8, the idealized TC translated across the domain almost perfectly to the west. Despite running the simulation with a total westward wind and on a f-plane, some northward drift was apparent just before landfall, particularly in the coupled cases. It is important to note that the drift accelerated as the TC moved closer to shore. It is also important to note that the drift was strongest in the fully-coupled case, and weakest in the uncoupled case.

This northward drift may be attributable to two causes related to the cyclonic motion of the storm. The first, evidenced by the slight northward drift in the uncoupled case is that the cyclonic nature of the TC causes the northward drift. As the TC nears shore, the cyclonic winds pull drier air from the land into the southern part of the TC. This causes the convection in the northern half of the TC to be slightly stronger than the southern part, causing the TC to drift northward slightly.

The second cause is due to the left hand bias of cooling in the TC. As demonstrated in Figure 3.9, the SST used in the atmospheric model remains at a constant 29° C in Case A across the entire domain. The red spot in the figure demonstrates the TC location in the domain at hour 46 (F046) of the model run. This position was chosen as it represents the location where the TC begins to make a slight northward shift. The SST cooling coupled to the atmospheric model shows significant cooling behind the storm and a profound right side bias is shown. As the cooler air is wrapped around the TC, the convection in the southern half is less intense. As a result, the TC shifts slightly to the north, putting it more into the cold wake.

These two effects cause the slight northward shift in the TC before it makes landfall. As shown in Figure 3.8, after landfall all of the simulated TCs move south rapidly due to interaction with the western boundary. The TC in Case A interacts with the western boundary faster and is pushed to the south sooner. Due to the lack of ocean feedback, the TC in Case A becomes much larger than the TCs in the two coupled cases. This is demonstrated in Figure 3.12, the simulated reflectivity of the three cases during landfall. Interaction with the western boundary forces the idealized TCs in all three experiments to the south, however because the TC in Case A is much larger, it reaches the western boundary earliest, forcing it further south than the other two cases.

3.5.2 Intensity

As predicted, the intensity of the TCs across the three cases varies greatly by the coupling of the atmosphere, ocean, and wave models. Introducing additional feedback in the coupling results in a generally weaker storm. As shown in Figure 3.9, the SST as "seen" by the atmospheric model remains a constant 29° C through development. As a result, this storm is allowed to grow without any restriction on the intensity (Figure 3.10 and Figure 3.13), strength (Figure 3.10), or size (Figure 3.12) and only weakens after landfall at F070, reaching a minimum shortly before landfall of 924 hPa. As a result, this unchecked and drastic increase in TC intensity, strength, and size demonstrates the effect of coupling on an atmospheric numerical model solution.

The introduction of atmosphere-ocean coupling in Case B greatly reduces the intensity (Figure 3.10, Figure 3.11 and Figure 3.13), strength (Figure 3.10 and Figure 3.11), and size (Figure 3.12) of the developing TC as it is subject to the surface ocean cooling feedback mechanism (Figure 3.10). This feedback has a drastic effect on the intensity as the storm does not deepen as quickly, and it reaches a minimum intensity of 960 hPa shortly before landfall, resulting in a difference of 36 hPa compared to the uncoupled Case A.

The same mechanism applies in the atmosphere-ocean-wave coupling in Case C. The additive mixing provided by the wave model further decreases the SST in and around the TC environment (Figure 3.10 and Figure 3.11) when compared to Case B. As a result, the TC in the 3-way coupled simulation is smaller (Figure 3.10) and less intense (Figure 3.10, Figure 3.11 and Figure 3.13) than both Cases A and B, reaching a minimum SLP of 967 hPa shortly before landfall. Resulting in a difference of 43 hPa and 7 hPa when compared to Case A and Case B, respectively.

3.5.3 Ocean Response

The upper ocean temperature response given by the ocean model differs among the three model cases, as expected. Figure 3.14 demonstrates that the SST differs as the TC makes landfall, despite nearly identical tracks. SST cooling demonstrates a profound bias to the right side of the track in all three cases, although the magnitude of cooling varies among the experiments. SST cooling resolved by the ocean model is most intense in Case A, because the intensity of the storm is much greater. As explained in section

3.5.2, the atmospheric model does not resolve the cooler SSTs and maintains a constant 29° C SST condition (Figure 3.9), resulting in a more intense storm. The SST condition is cooler (Figure 3.10 and Figure 3.11) in Case C than in Case B, this is due to the wave feedback tied with the ocean solution which enhances mixing. The additional surface cooling in Case C results in a weaker and less intense TC (Figure 3.10, Figure 3.11 and Figure 3.13). Despite the weaker surface wind, the wave influence continues to mix cooler water to the surface efficiently.

Significant wave height data from Case C before the TC generated waves impact the shore (Figure 3.15) demonstrates that the highest wave heights are found in the front-right quadrant of the TC. The additive effect of cyclonic wind velocities and storm translation velocities result in the highest wind speeds being located in this area. As a result of the strong surface winds, strong surface stress is sent to the ocean model, which results in the strong surface current velocities sent to the wave model (Figure 3.6). A fully coupled ocean model (Figure 3.7) would include sea surface roughness being passed to the atmospheric model which would increase the surface area of the ocean. Heat and moisture fluxes, the driving forces of the TC, would increase as the surface area becomes larger. Increased sea surface roughness would also act to weaken surface winds as a result of greater surface friction. Therefore, future study of a complete 3-way coupled model is necessary in order to examine which process has the greater effect and whether or full 3-way coupling that would act to intensify or weaken the TC.

3.6 Conclusion

As demonstrated, introducing 2-way and 3-way coupling to the TC simulation provides a reasonable and realistic feedback mechanism to the atmosphere. Slight fluctuations exist in track due to the right side maximum of SST cooling across all coupled cases. The passing TC cools the sea surface below in the ocean model. Where the atmospheric model receives the cooling feedback, there is a large decrease in TC intensity. Ocean response of SST cooling is proportional to the strength of the TC, with a stronger TC inducing more mixing and subsequent cooling. Additional mixing and SST cooling was noted when the wave model was activated, resulting in diminished TC intensity. The wave simulation demonstrated the largest significant wave heights in the TC quadrant of greatest wind speed. Additional coupling with passing the sea surface roughness from the wave model to the atmospheric model may help increase storm intensity by introducing greater heat and moisture fluxes to the surface. At the same time, increased surface friction may result in diminished strength of the TC.

4. Experiments of Hurricane Ivan (2004) Utilizing the COAWST Model

4.1 Introduction

The need for a coupled numerical modeling system has been explored extensively in the previous three chapters. The first chapter examined the problem, proposed solutions, and some earlier models through literature review. The second chapter examined experiments into ocean coupling using the newest version of the Weather Research and Forecasting (WRF) system coupled with a built-in 1-Dimensional Ocean Mixed Layer (OML) model. The third chapter introduced the formulation of the Coastal Ocean Atmosphere Wave Sediment Transport (COAWST) model. This model features 3-way coupling feedback mechanisms between the atmosphere, ocean, and wave environments. The third chapter used an idealized case to act as a proof-of-concept before moving onto a realistic case, the focus of this chapter. The realistic case chosen to demonstrate model skill is Hurricane Ivan in September 2004.

According to the NHC Tropical Cyclone Report (Stewart, 2005), Hurricane Ivan was a classical hurricane that reached Category 5 strength on the Saffir-Simpson Hurricane Scale three times while devastating the southeastern Caribbean Sea. Hurricane Ivan was unique in that it intensified rapidly at a relatively low latitude (9.7° N) and it experienced many rapid intensification and decay cycles over the course of its lifetime. Upper-level shear and entrainment of dry air was attributed to these cycles (Stewart, 2005). As Ivan approached the Gulf Coast of the US, it devastated the oil and natural gas industry causing the disruption of the flow of these commodities, along with their refinement (Stewart, 2005). Ivan made its first landfall in the US at 0650 UTC on 16 September, just west of Gulf Shores, Alabama. The direct effects of the hurricane resulted in 25 US deaths, 14 in Florida alone. The total loss in the US was estimated at $14.2 billion, with total insured damage of $7.11 billion. Ivan weakened over the southeast US and entered the Atlantic Ocean off of Maryland, it re-intensified to a tropical storm and made its second landfall near Holly Beach, LA at 0200 UTC on 24 September as a weak tropical depression. As a point of clarification, this study will focus on its first, and much more intense, landfall.

Table 4.1 from Stewart (2005) demonstrates that NHC track forecasting for Ivan was generally well done; with 9-45% better track forecasting over 12 to 120 hours than in the previous 10 year period (1994-2003). The hurricane watch and warning issued by NHC 51 and 42 hours, respectively, prior to landfall were both directly in Ivan's track. Table 4.1 also demonstrates that NHC intensity forecasting for Ivan was considerably less accurate; with skill 8 to 71% worse over the 12 to 120 hour forecast periods than in the previous 10 year period (1994-2003). There is a noteworthy exception, as intensity forecasts were improved 20% and 21% over the F48 and F72 periods, respectively. The lack of skill in intensity forecasting is attributed to Ivan's frequent, and unpredicted, fluctuations of intensity (Stewart, 2005).

Hurricane Ivan presented a unique case for model coupling due to the drastic effects it had on the Gulf Coast and the intensification and decay cycles over the course of its lifetime. This study will use five different configurations of the WRF, ROMS, and

COAWST models to make comparisons of increasing complexity in air-sea-wave interaction and feedback.

4.2 Methodology

First, the simplest configuration available is to use the WRF model uncoupled to a static sea surface (Static case). This represents a complete lack of feedback to the atmospheric model, as there is no SST cooling signature present during and after Tropical Cyclone (TC) passage. As a result, this configuration could be used as a forecast model.

Next, a little more complexity to the system is introduced by using dynamic SST observations throughout the model domain over the course of the run (Dynamic case). This represents the best possible SST solution for running a hindcast for a storm with only the WRF, but the 4.5 day ocean surface observations would not be available for a forecast product.

A ROMS hindcast is introduced next to WRF to demonstrate a dynamic ocean providing feedback to the atmosphere (ROMS case). ROMS, driven by the Global Forecast System (GFS) and H-Wind solution of the wind stress provided by the atmosphere to the ocean surface, is run through the simulation period uncoupled to any atmospheric model. This represents how oceanographers currently utilize atmospheric data to get a hindcast solution for the ocean model. Then this hindcast ocean solution provides sea surface information for WRF. While running an ocean model in forecast mode and using SST information from it is possible, this particular ROMS configuration is hindcast. As a result, this would not be available for use in forecast mode.

The COAWST model is then used in a 2-way, ocean-atmosphere, coupled configuration. This configuration demonstrates the effect of 2-way coupling with the COAWST model for a realistic case. This could be used to provide a true forecast solution as initial oceanic and atmospheric conditions are used in conjunction with modeled lateral boundary conditions to run the model.

A 3-way coupled simulation, as described in section 3.2, utilizes ocean-atmosphere-wave coupling to create a dynamic system. This configuration will demonstrate the effect of 3-way coupling with the COAWST model for a realistic case. This could be used to provide a true forecast solution as the model is initialized from model output providing conditions of the ocean-atmosphere-wave system.

4.3 Data and Model Configuration

4.3.1 Domain Configuration

The WRF model domain shown in Figure 4.1 was chosen to incorporate the entire ROMS and SWAN model domains (which are co-located), outlined in blue. Additional grid points were added to the south and east in order to provide Ivan sufficient model space in order to develop and strengthen after initialization. The WRF model utilizes a coarser (8 km) grid than the ROMS and SWAN grids (5 km). Grid points had to be interpolated before model initialization for proper data exchange in the MCT.

After establishing the spatial domain, the temporal domain was chosen by running 8 WRF-only simulations from 00Z 10 September through 12Z 13 September utilizing their respective initial input and boundary conditions and a static SST. All of the iterations were terminated at 00Z 17 September. The best configuration of initialization conditions were based on three conditions. First, the model would need sufficient time to execute in order to demonstrate forecast skill during the forecast simulations. Second, the model would need to demonstrate a reasonable track forecast, including time at landfall. This was done so that any improvements through coupling would be based on the best available initialization and boundary condition data. Third, the model would need to demonstrate a reasonable intensity forecast with rapid initial deepening. Similar to the forecast track condition, the purpose was to give the best possible initialization and boundary conditions for the experiments to iterate. By choosing the temporal domain in this fashion, its reasonable to presume that the domain that yields the best uncoupled simulation would also yield the best coupled simulation. The simulation that performed best was initialized at 12Z 12 September and terminated 00Z 17 September (4.5 days). This simulation had a slight westward track error, but demonstrated excellent timing for landfall and comparatively rapid deepening in intensity.

4.3.2 WRF Configuration (Atmosphere Model)

The WRF model is initialized on 12Z 12 September 2004 and integrated through 00Z 17 September 2004 using the sea surface temperature conditions described in section 4.2 for each respective case. The atmospheric initial and boundary conditions for the entire domain are based on GFS model output, with boundary condition updates every 6 hours. The grid dimensions are 500 (east-west) by 450 (north-south) with 31 vertical levels and 8 km grid spacing. The model timestep is defined as 24 seconds. No nesting was used as it can not currently be implemented in the COAWST coupled modeling system.

Grid scale precipitation was computed using the WRF Single-Moment 6-class microphysics scheme (WSM-6) from Hong and Lim (2006). This first-order microphysics scheme features water vapor, cloud water, cloud ice, rain, snow and graupel. Given the 8 km grid spacing, the Kain-Fritsch CP scheme was used to parameterize precipitation processes on a sub-grid scale. Longwave and shortwave radiation physics were computed using the Rapid Radiative Transfer Model (RRTM) and the Dudhia scheme respectively, called every 8 minutes. The Monin-Obukhov (the version implemented in the Eta model) surface layer physics option was used along with the Noah land surface model. The Mellor-Yamada-Janjic turbulent kinetic energy planetary boundary layer (PBL) model was called every timestep.

4.3.3 ROMS Configuration (Ocean Model)

For realistic hurricane hindcast simulations, our ROMS domain encompasses both the south Atlantic Bight and the Gulf of Mexico (hereinafter, SABGOM ROMS), with a horizontal grid spacing of 5 km. There are 36 terrain-following vertical levels with higher resolution near the surface and bottom in order to better resolve ocean boundary layers. A 25 second baroclinic timestep was used. Open boundaries were used along the eastern and southern portions of the domain, closed boundaries were used along the northern and western portions of the domain.

To specify the open boundary conditions for the SABGOM ROMS, we nested it inside the global ocean simulation provided by HYCOM/NCODA [Hybrid Coordinate Ocean Model /NRL Coupled Ocean Data Assimilation: http://hycom.rsmas.miami.edu/dataserver]. NCODA is a multivariate optimal interpolation technique that assimilates surface observations from satellites, including altimeter and multi-channel sea surface temperature, and also profile data such as expendable bathythermographs (XBTs), conductivity-temperature-depth (CTDs) and ARGO floats (Chassignet et al., 2006). As a part of the Global Ocean Data Assimilation Experiment (GODAE), HYCOM/NCODA provides daily three-dimensional ocean state estimates at 1/12 degree resolution. Because the domain of SABGOM ROMS covers a significant deep ocean portion, where energetic boundary current, meanders and eddies present, HYCOM/NCODA fields are very appealing for our regional-scale coastal circulation simulation in that the timing and extent of such deep-ocean processes can be well represented through HYCOM data assimilation.

A one-way nesting approach was used to downscale HYCOM/NCODA ('parent model') to the regional-scale SABGOM ROMS ('child model'). Specifically, open boundary conditions (OBCs) were applied to ROMS tracers and baroclinic velocity following Marchesiello et al. (2001), whereby Orlanski-type radiation conditions were used in conjunction with relaxation (with timescale of 0.5 days on inflow and 10 days on outflow) to HYCOM/NCODA solutions. The free surface and depth-averaged velocity boundary conditions were specified using the method of Flather (1976) with the external values defined by HYCOM/NCODA. Mellor and Yamada (1982) was used to compute vertical turbulent mixing, as well as the quadratic drag formulation for the bottom friction specification.

For realistic ocean circulation simulation, the surface atmospheric conditions from North America Regional Reanalysis (NARR) provided by NOAA NCEP was utilized. The spatial and temporal resolutions of NARR are 32-km and 3 hourly, respectively. Air-sea fluxes of momentum and buoyancy were computed by applying the standard bulk formulae (Fairall et al. 2003) to NARR marine boundary-layer winds, air temperature, relative humidity, air pressure, along with ROMS generated surface currents. The SABGOM ROMS realistic circulation hindcast is run from November 1, 2003 to January 1, 2008. The resulting hydrodynamics conditions at 12Z, September 12, 2004 were then used as ocean initial conditions for both the WRF-ROMS 2-way coupled and WRF-ROMS-SWAN 3-way coupled simulations for Hurricane Ivan.

4.3.4 SWAN Configuration (Wave Model)

The SWAN model is solved on the same grid as the ROMS model. Boundary conditions are derived from fields provided by the WaveWatch 3 (WW3) model. The wave model is configured on a Cartesian grid. Other SWAN parameters are identical as outlined in section 3.3.5.

4.4 Results

4.4.1 Track

The track forecasting gradually improved with greater complexity in ocean representation of the experiments and demonstrated good skill in predicting the timing and location of landfall. Figure 4.2 demonstrates that there is slight improvement in track prediction as complexity of coupling is introduced. Given the Marks and Shay (1998) assertion that track is largely dependent on large-scale processes, there is minimal difference between any of the runs. Figure 4.3 and Figure 4.4 demonstrates that the 2-way coupled model fared the best as far as landfall location. Overall track error against verification at F090 (at landfall) among the experiments were: 133 km (Static), 126 km (Dynamic), 103 km (ROMS), 45 km (2-way), 62 km (3-way). The track difference between the Static and 3-way experiments was 76 km. The 2-way track average during the simulation against verification was also the best among the experiments.

4.4.2 Intensity

Intensity prediction across the five simulations was quite poor. This is attributable to the coarse 8 km grid spacing employed in these simulations. The Kain-Fritsch CP scheme was employed in all of the model runs. Any kind of parameterization on the convective process would have a drastic effect on the intensity of the simulated storm. This is particularly true of TCs, any CP scheme is pushed to its limits in attempting to parameterize convection, resulting in diminished intensity (Rosenthal 1979). As a result, the convective processes of the TC, and the vital source of latent heat release is diminished. In order to more properly represent this process, explicit convection should be utilized, at a computation expense well beyond the resources of this study. Model nesting is currently not available to the COAWST modeling system, but will be considered in future versions.

The intensity prediction of the two coupled simulations (WRF-ROMS, and WRF-ROMS-SWAN) demonstrate the benefit of utilizing atmosphere-ocean-wave coupling. As demonstrated in Figure 4.5, the modeled TC intensifies during model initialization and “spin-up”. After reaching 18-24 hours during the forecast run, the feedback mechanism between the ocean and atmosphere is apparent. As the TC gains intensity, the ocean model responds by cooling the upper ocean. This results in less surface heat and moisture fluxes, and less energy for the TC to utilize.

This ocean response is apparent in verification as there is a discrete decrease in intensity at F36-F72 in the 2 and 3-way coupling cases, which coincide with the TC translating over cool water eddies in the Gulf of Mexico shown in Figure 4.7 and 4.8. This response is not observed in both WRF-only models (Static and Dynamic cases). In the WRF-only cases, the TC intensifies through F24 and maintains roughly the same intensity until landfall. While the intensity at landfall is closest in these uncoupled cases, its important to recognize that the trend is incorrect. In the WRF-only cases, significant decreases in intensity are completely absent throughout the analysis until landfall, so the TC wrongly maintained the same intensity throughout the model run. The 1-way coupled (ROMS) case showed decreasing intensity, as a result of the cooling of the water surface in the ocean model. While this showed improvement over the uncoupled runs, the diminished intensity was not of comparable magnitude (15 hPa) when compared to observed (26 hPa).

The coupled model runs both showed considerable improvement in predicting the trend of Ivan's intensity. After entering Gulf of Mexico, the storms in the 2-way and 3-way experiments weakened 24 hPa and 28 hPa, respectively. Modeling this weakening correctly, if combined with a good initial condition for Ivan would drastically improve the intensity forecast for this storm, which was quite poor. Unfortunately in this evaluation, the poor intensity initialization for Ivan is apparent, upon entering the Gulf of Mexico, the 2-way and 3-way models resolve Ivan with a minimum pressure of 941 and 946 hPa, respectively. As the observed Ivan was at 914 hPa during this period, a stronger TC entering the cooler waters may yield better results.

4.4.3 Ocean Response

As shown in Figures 4.7 and 4.8, the ocean cooling response is quite strong in two distinct regions. Microwave imagery from Walker et al. (2005), shown in Figure 4.9, confirms the presence of two cold core cyclones in the Gulf of Mexico. NHC's best track data on intensity, shown in Figure 4.5 and discussed in Section 4.4.2, demonstrates that Ivan had two distinct intensity decreases as the TC passed over those cooler areas of the Gulf of Mexico.

Comparison of the modeled ocean data to SSTs obtained at buoy stations distributed in the Gulf of Mexico (Figure 4.10) is shown in Figure 4.11. The 2-way and 3-way experiments resolved SSTs within a degree in most cases. The 3-way coupled case cools the storm much more intensely than the 2-way case, as evidenced in Figure 4.7, Figure 4.8, and buoy 42040 of Figure 4.11. The 2-way case represents SST cooling directly under the storm (buoy 42040) very well, to within 0.5°C.

Utilizing the 2-way case as it represented the SST condition the best, an examination of the reaction of the upper-ocean to the TC is examined in two locations (Figure 4.12). U1 was selected to represent the temperature and heat budget of the deep ocean. U2 was used to demonstrate the effects along the continental shelf.

Figure 4.13 demonstrates the reaction of the mixed layer to Ivan's passage. Surface wind stress (τ) gradually builds up, peaks, and rapidly falls off as Ivan moved over the location. Solar radiation, the dominant term of heat flux going into the ocean, shows a clear diurnal cycle through the model run. Ivan's track through this location on 14 September limited the solar radiation term due to the increased albedo from cloud coverage. The surface stress enhanced mixing through the mixed layer, resulting in a cooler surface temperature and eroded thermocline. The U and V currents demonstrate an inertial oscillation after the TC's passage.

Figure 4.14 breaks the heat budget equation:

$$\frac{\partial T}{\partial t} = -u\frac{\partial T}{\partial x} - v\frac{\partial T}{\partial y} - w\frac{\partial T}{\partial z} + \frac{\partial \frac{k\partial T}{\partial z}}{\partial z}$$

into its individual terms: $-u\frac{\partial T}{\partial x} - v\frac{\partial T}{\partial y}$ (horizontal advection), $-w\frac{\partial T}{\partial z}$ (vertical advection), $-u\frac{\partial T}{\partial x} - v\frac{\partial T}{\partial y} - w\frac{\partial T}{\partial z}$ (total advection), $\frac{\partial \frac{k\partial T}{\partial z}}{\partial z}$ (vertical diffusion), $\frac{\partial T}{\partial t}$ (local rate of change in temperature) measured in °C day^{-1}. These terms are calculated from output of the ocean model. The horizontal advection term has a large magnitude during the event, but oscillates continuously afterwards with an inertial period of about 1 day. Vertical advection also oscillates with a large magnitude, however out of phase with horizontal advection. As a result, the combined advection terms do not account for very much heat transfer during much of the event. As the curl of wind stress vectors correlate with inertial currents, there is a strong upwelling signature. Upwelling from advection combines with negative diffusion on 15 September to erode the thermocline and entrain cool water throughout the column. A time-series of $\int_{mid} F(z)\frac{\partial z}{MLD}$, or the vertically integrated heat transfer, confirms the findings of Price (1981) that entrainment of cooler water accounts for roughly 85% of the total heat transfer in the deep ocean.

Examination of the mixed layer on the continental shelf in Figure 4.15 reveals many similarities to the mixed layer at U1. There is a steady increase in surface stress as the TC approaches, and then a rapid decline. A diurnal cycle is apparent in the overall heat flux. The mixed layer is eroded after Ivan cools the surface water. There is a distinct inertial oscillation signature in the U and V fields after TC passage.

Examination of the heat budget in Figure 4.14 reveals some additional similarities to U1. The horizontal and vertical advection terms largely cancel out, except when the curl of wind stress strongly correlates with the inertial oscillation. As a result of this, there is strong upwelling that erodes the thermocline. In contrast with point U1, the upwelling in the shallow region accounts for much less heat transfer. As a result, diffusion is a comparable term in the heat transfer equation on the continental shelf, in agreement with Shen and Ginis (2003).

Significant wave height data, available in the 3-way case, was used in comparison with buoys located close to Ivan's track (42001, 42007, 42039, 42040). Figure 4.17 demonstrates high correlation of the modeled significant wave height with observations. Buoy 42040, directly in Ivan's track, suffered a mechanical issue and was unable to measure significant wave height after 06Z 15 September.

4.5 Conclusion

Hurricane Ivan served as a test case for the newly developed COAWST model in order to look at a modeled TC in unprecedented detail. The best available initialization and boundary conditions were chosen to experiment with Ivan and compare modeled results to observations. Track changes were minimal, as expected. Intensity predictions compared well in trend analysis. Unfortunately, coarse grid spacing and initialization conditions did not enable the simulated TC to gain sufficient intensity before entering the cool waters of the Gulf of Mexico. Examination into the ocean response demonstrated the erosion of the thermocline and mixed layer. Ivan translating over deep ocean proved that the entrainment term dwarfed the diffusion term in cooling the mixed layer, however the two terms were of similar magnitude near the continental shelf.

5. Conclusion

5.1 Motivation and Literature Review

The research goals of this thesis were to examine the effects of implementing a coupled ocean-atmosphere-wave model. This thesis specifically sought out the effects of coupling on numerical models representing Tropical Cyclones. Section 1.1 provided motivation with significant improvements in numerical environmental models that can be found utilizing at least some representation of feedback (Bao et al. 2000, Bender and Ginis 2000, Bender et al. 2007, Chen et al. 2007, Davis et al. 2008, Morey et al. 2006, Emanuel et al. 2004). Motivation for this study is found in the improvement in individual solutions that will result from utilizing coupling and from the ability to analyze the dynamics present in the atmosphere-ocean-wave fields.

An extensive literature review was first undertaken in section 1.2, in order to provide a basis upon which to draw hypotheses during implementation of the coupled model. First, in sections 1.2.1 through 1.2.6, the upper ocean response to a moving TC was examined. This examination took place in the form of numerical modeling (section 1.2.1), in-situ measurements (section 1.2.2), and remote sensing studies (section 1.2.3). An important result of this early research was the appearance of the right-side SST cooling bias and the role of entrainment and upwelling in cooling SSTs (Price 1981, Price et al. 1994).

In-situ measurements in Church et al. (1989), and Sanford et al. (1987) provided initial observations into the right side SST bias. ADCP measurements during Hurricane Ivan in Mitchell et al. (2005) and Teague et al. (2007) demonstrated that ocean response to a passing TC can represented as four distinct stages having drastic effects over the depth-profile of the ocean.

Remote sensing studies of Cornillion et al. (1987) demonstrated the complexity of the SST cooling as the thermocline depth of the ocean varied along the track of Hurricane Gloria (1985). As a result of this, areas with a shallower thermocline experienced additional SST cooling due to upwelling-enhanced entrainment. Walker et al. (2005) examined the effects of upwelling on SST, SSH and chlorophyll-*a* enhancement in the wake of Hurricane Ivan. Significant cooling was found in the wake of Hurricane Ivan, around 1-6 °C in most areas. Enhancement of Chl-*a* concentrations were found within two upwelling regions. Modeling Chl-*a* concentrations in the wake of a tropical cyclone is possible using a coupled numerical model and provides an interesting problem for future study. Walker et al. (2005) showed that SST, SSH, and Chl-*a* observations all confirm enhanced upwelling along and east (to the right) of Ivan's track.

Upper ocean heat budget response was also examined in section 1.2.4. Ocean heat content (OHC), introduced in Leipper and Volgenau (1972), is frequently utilized as a quantity to determine areas of ocean that would be conducive to TC growth, and is examined in section 1.2.4.1. The effects of downwelling due to convergent flows on increasing OHC is examined in Oey et al. (2007). In section 1.2.4.2, Morey et al. (2006) utilized hurricane heat potential (HHP), also from Leipper and Volgenau (1972), in order to examine the loss of oceanic heat to a TC in their numerical experiments.

The upper ocean response to fresh water input from precipitation in TCs is examined in section 1.2.5 through study of Price et al. (1979) and Bao et al. (2003). Both papers look into the effects of the stable fresh layer after input of precipitation into the ocean. Price et al. (1979) does so using in-situ measurements, and Bao et al. (2003) utilizes a numerical modeling approach. The current implementation of the coupled model does not feature this input of fresh water from the atmosphere into the ocean. It is a problem that coupling an atmospheric numerical model to a 3-dimensional ocean model would be capable of solving, and is left to future research.

The upper ocean response and influence of general circulation features is examined in section 1.2.6. Oey et al. (2006) investigated the interaction of the loop current on TC in a numerical modeling study. By removing the loop current in the model domain, Oey et al. (2006) was able to demonstrate that there was a large volume flux of water with high OHC was transported away from Hurricane Wilma (2005). As a result of this, Oey et al. (2006) demonstrated that the general circulation features have large impacts on storms translating within an ocean domain.

Section 1.2.7 provides a number of papers that examine the 2-way coupling of atmosphere and ocean numerical models. Bender and Ginis (2000) demonstrated marked improvement in the intensity of TCs through examination of four hurricane events. Shen and Ginis (2003) carried out several experiments examining the effects of surface heat fluxes on SST cooling over several regions of varying thermocline depth and bathymetry. The right-side SST cooling bias was prevalent in shallow regions in the Shen and Ginis (2003) numerical solution, despite presence of a well-mixed shallow column of water. Shen and Ginis (2003) attribute this to the circulation of the storm. Oey et al. (2007) suggested the use of along-track satellite altimeter data to reduce sea surface height anomalies to temperature anomalies during TC events. The lack of sufficient satellite data during TC events pointed Oey et al. (2007) to the development of a coupled numerical model as a more efficient solution. Davis et al. (2008) modeled Hurricane Katrina with a simple 1-dimensional ocean mixed layer (OML) model, which provided significant improvement in the intensity resolved by the atmospheric model.

Section 1.2.8 provided motivation for the 3-way coupling of the atmosphere, ocean, and wave models through Chen et al. (2007). This paper suggested the framework for a three-way coupled model and the parameter exchanges between the individual models, which were mostly utilized in the model of study for this thesis. Chen et al. (2007) stated that the constant SST condition used by many atmospheric models leads to the over intensification of TCs. Conversely, Chen et al. (2007) demonstrated that the lack of directional coupling between the wind and waves leads to an underestimation of TC strength in maximum wind speed.

Section 1.2.9 provided the configurations for the previously referenced 1-way coupled numerical studies. The simple 3-dimensional ocean models of Price (1981) and Price et al. (1994) are explained in section 1.2.9.1. The configuration of the PROFS ocean model driven by re-analyzed GFS winds from Oey et al. (2007) is explained in section 1.2.9.2.

Section 1.2.10 provided the configurations for the previously referenced 2-way coupled atmosphere-ocean numerical studies. Section 1.2.10.1 describes the BVW coupling to NCOM utilized in Morey et al. (2006). Section 1.2.10.2 describes the GFDL to POM coupling of Bender and Ginis (2000) and Shen and Ginis (2003). Section

1.2.10.3 describes the utilization of the WRF coupled to a 1-dimensional OML model in Davis et al. (2008).

5.2 Experiments of Hurricane Isabel (2003)

Based on the motivating factors described in the introduction and literature review provided for in the first chapter of this thesis, a simple case using an available model was first considered to examine the effects of ocean feedback on the atmospheric solution of a TC. The model used was the Weather Research and Forecasting (WRF) model coupled to a 1-dimensional ocean mixed layer (OML) model from Pollard et al. (1973). This configuration was previously used for numerical investigations into Hurricane Katrina (2005) in Davis et al. (2008). Hurricane Isabel was chosen as it devastated the Outer Banks of North Carolina.

The NHC track forecast for the storm was good, featuring 51-64% less error in track than TCs of the previous 10-year period. Intensity forecasts for the event were less favorable due to both an underestimation of how quickly Isabel would strengthen over the eastern Atlantic and an overestimation of how intense Isabel would remain as it reached the cooler waters of the western Atlantic (Beven and Cobb, 2004).

Three experiments were used to demonstrate differences in the atmospheric model solution. The first experiment (Static SST) employed an unchanging SST, based on the SST condition at initialization. The second experiment (Dynamic SST) allowed the SST to change based on a 6-hourly interpolation of the analyzed SST. The third experiment (WRF OML SST) utilized the 1-dimensional OML to provide the SST condition.

Based on the assertions of Marks and Shay (1998), a hypothesis was made that the TC track would be largely unaffected by the SST condition. This first hypothesis was verified. Based on the results from Davis et al. (2008), Bender and Ginis (2000), and Shen and Ginis (2003) a hypothesis was made that the intensity would be greatly improved by introducing ocean feedback from a 1-dimensional OML model. This second hypothesis was verified.

The lack of coupling to a fully 3-d ocean model left the testing of hypotheses involving the upper ocean response to the fully coupled simulations in the third and fourth chapters of this thesis. However, the 1-dimensional OML model was able to resolve the right-side SST cooling bias, a similar result was found in Davis et al. (2008). This is attributed to the inclusion of Coriolis which is vital to demonstrating the rotation of inertial currents and the right-side bias of SST cooling (Price, 1981; Price et al., 1994).

5.3 Experiments of an Idealized TC Utilizing the COAWST Model

The configuration of the Coupled Ocean Atmosphere Wave Sediment Transport (COAWST) model is introduced in section 3.1 and discussed in depth in section 3.2. The configuration of the atmosphere, ocean, and wave models for the idealized case is discussed in section 3.3. Three experiments are carried out using the COAWST model in order to provide a proof of concept for the model. The first case features 1-way coupling of the atmospheric model to the ocean model. The second case features 2-way coupling between the atmospheric and ocean models. The third case features the most coupling currently available to the atmosphere, ocean, and wave models.

Based on the assertions of Marks and Shay (1998), a hypothesis is drawn that the track of the idealized TC will be largely unaffected by coupling. This first hypothesis is verified. Based on the results of Davis et al. (2008), Bender and Ginis (2000), and Shen and Ginis (2003), a hypothesis was made that the intensity would be greatly affected by the introduction of 2-way and 3-way coupling. This hypothesis is also verified. Based on the right-side SST cooling bias of TCs translating across an ocean demonstrated in several papers referenced in the first chapter of this thesis, a hypothesis is made that the SST cooling will be much more significant to the right side of the track. This hypothesis is verified. Based on the addition of wind and TC translation direction vectors, a hypothesis is made that the largest significant wave heights would be found in the front-right quadrant of the idealized TC when 3-way coupling is employed. This hypothesis is verified.

Based on the aforementioned verified hypotheses, the COAWST model was successfully tested with an idealized TC as the subject.

5.4 Experiments of Hurricane Ivan (2004) Utilizing the COAWST Model

As the COAWST model was able to demonstrate several features reviewed in the first chapter of this thesis within the scope of an idealized TC, the final step would be to implement its use with a realistic TC. Hurricane Ivan (2004), detailed in section 4.1, was chosen as a unique and very powerful storm that translated through the Gulf of Mexico.

NHC track forecasting for Ivan was generally well done; with 9-45% better track forecasting over 12 to 120 hours than in the previous 10-year period. NHC intensity forecasting for Ivan was considerably less accurate; with skill 8 to 71% worse over the 12 to 120 hour forecast periods than in the previous 10-year period (with exception to improvement of 2 forecast periods within that timeframe).

Five experiments were conducted in order to demonstrate the effects of manipulating the atmosphere, ocean, and wave conditions and are detailed in section 4.2. The first two cases were run with only the atmospheric model. The first, Static case, used a static SST condition based on the SST condition at the time of initialization. The other simulation using only the atmospheric model, Dynamic case, used a dynamic SST condition updated with interpolated SST data every 6-hours. The first case to utilize the ocean model (Regional Ocean Modeling System, ROMS) was the ROMS case. The SST condition from a ROMS hindcast run with re-analyzed surface winds was input into the atmospheric model. The first case to use the COAWST model was the 2-way (ocean-atmosphere) coupled case. The final case, representing complete coupling of the COAWST model was the 2-way (ocean-atmosphere-wave) coupled case. Section 4.3 describes the configuration of the 3 models used for experimentation.

Based on Marks and Shay (1998) and the track result from section 3.5.1 of this thesis, a hypothesis was made that little deviation would occur in track based on additional coupling. This hypothesis was verified. Based on the results of Davis et al. (2008), Bender and Ginis (2000), and Shen and Ginis (2003), a hypothesis was made that the intensity and size of the simulated TC would be greatly affected by the manipulation of the SST condition. Due to the poor initial condition in this realistic case, improvements in all 5-cases will be sought in future research. Despite this, the intensity and size were greatly affected by SST condition and this hypothesis was verified. Based on the additional wave mixing in the 3-way configuration from the 2-way configuration, a hypothesis was made that the SST cooling would be more significant in the 3-way coupling than the 2-way coupling. This hypothesis was verified. A hypothesis was made based on the analytical results of Price (1981) and Price et al. (1994) as well as the in-situ results of Mitchell et al. (2005) and Teague et al. (2007) that the heat budget off of the continental shelf would be dominated by heat loss due to entrainment of cooler water, whereas on the shelf the terms would be largely similar. To verify this, two grid points (one on the continental shelf, the other off) were used and the depth-integrated heat budget was determined. This hypothesis was verified.

In addition, significant wave height data was analyzed and compared to buoy data during the passage of Hurricane Ivan. A high correlation between the two was found, demonstrating the utility of coupling the ocean and atmosphere models to a wave model. Although there was significant error in the initial condition of the TC, the coupled model was able to verify several hypothesis and prove the ability of the COAWST model to simulate realistic TCs.

5.5 Considerations for Future Research

A comparison between the COAWST model and the 1-dimensional WRF OML model in resolving TC events is a problem considered for future research. The WRF model with OML capability is currently available only for WRF version 3.1 and higher. The COAWST model used in the Hurricane Ivan simulations was coupled to WRF version 2.2. A comparison of Hurricane Ivan spread across these two different model versions would be flawed and incongruent. Recent updates to the COAWST model feature coupling to the newest version of WRF at the time of this writing. Future research will look into comparisons between the COAWST and 1-dimensional OML models for Hurricane Ivan to see how well each model resolves the TC and the SST condition.

Updating the COAWST model to include passing Sea Surface Roughness directionally coupling the wind and waves (Chen et al., 2007; Fig. 3.7) is also being researched. Implementing this in the COAWST model would represent the completion of the 3-way coupling mechanisms in Chen et al. (2007). Investigating idealized and realistic TCs with this implementation is considered for future research.

Walker et al. (2005), reviewed in the section 1.2.3 of this thesis, utilized satellite data in order to demonstrate the Chl-*a* distribution in the wake of Hurricane Ivan. This hurricane provided a unique opportunity for the remote sensing of Chl-*a* as the skies were clear for several days after passage of the TC. A 3-dimensional ocean model, featuring a biological model, with 3-way (ocean-atmosphere-wave) coupling would answer some questions the ability to hindcast and forecast Chl-*a* blooms in the wake of TCs. Comparison of the resolved Ivan solution, with a biological ocean model implemented, to this satellite Chl-*a* data would be an interesting test of the COAWST model with biology.

Investigation into the precipitation-induced stable layer at the ocean surface was undertaken in section 1.2.5. Price et al. (1979) demonstrated in-situ observations of a precipitation-induced stable layer. Bao et al. (2003) used a 3-dimensional ocean model in order to examine the effects of precipitation on the ocean surface. Numerical investigations of the precipitation-induced stable layer require a 3-dimensional ocean model (Bao et al., 2003), and would take advantage of the COAWST model.

The cases that served as the basis of this thesis were all based on Tropical Cyclone simulations. These TCs tested the limits of model parameterizations (Chen et al., 2007; Davis et al., 2008; Bender et al., 2007) and were able to provide a good proof of concept for the COAWST model. Implementing the COAWST model for other types of coastal meteorological events such as Nor'easters, blizzards, typical mid-latitude cyclones, etc. provides many alternate avenues for future research.

TABLES

Table 2.1. Track and intensity forecast errors in NHC forecast for Hurricane Isabel, averaged over duration of event.

Forecast Error	**F12**	**F24**	**F36**	**F48**	**F72**	**F96**	**F120**
Track (km)	41	72	96	111	148	193	270
Track, 10-yr Avg (km)	83	150	215	278	417	522	693
Track, Improvement	51%	52%	55%	60%	64%	63%	61%
Strength (ms^{-1})	3.6	5.7	7.2	8.7	11.3	12.9	13.9
Strength 10-yr Avg. (ms^{-1})	3.1	5.1	6.7	7.7	9.8	10.8	11.3
Strength, Improvement	-17%	-10%	-8%	-13%	-16%	-19%	-23%

Table 4.1. Track and intensity forecast errors in NHC forecast for Hurricane Ivan, averaged over duration of event.

Forecast Error	**F12**	**F24**	**F36**	**F48**	**F72**	**F96**	**F120**
Track (km)	44	87	146	200	298	411	535
Track, 10-yr Avg (km)	81	144	207	270	402	459	591
Track, Improvement	45%	40%	29%	26%	26%	10%	9%
Strength (ms^{-1})	4.6	6.2	6.7	6.2	7.7	12.3	18.5
Strength 10-yr Avg. (ms^{-1})	3.1	5.1	6.2	7.7	9.8	10.3	10.8
Strength, Improvement	-50%	-20%	-8%	20%	21%	-20%	-71%

FIGURES

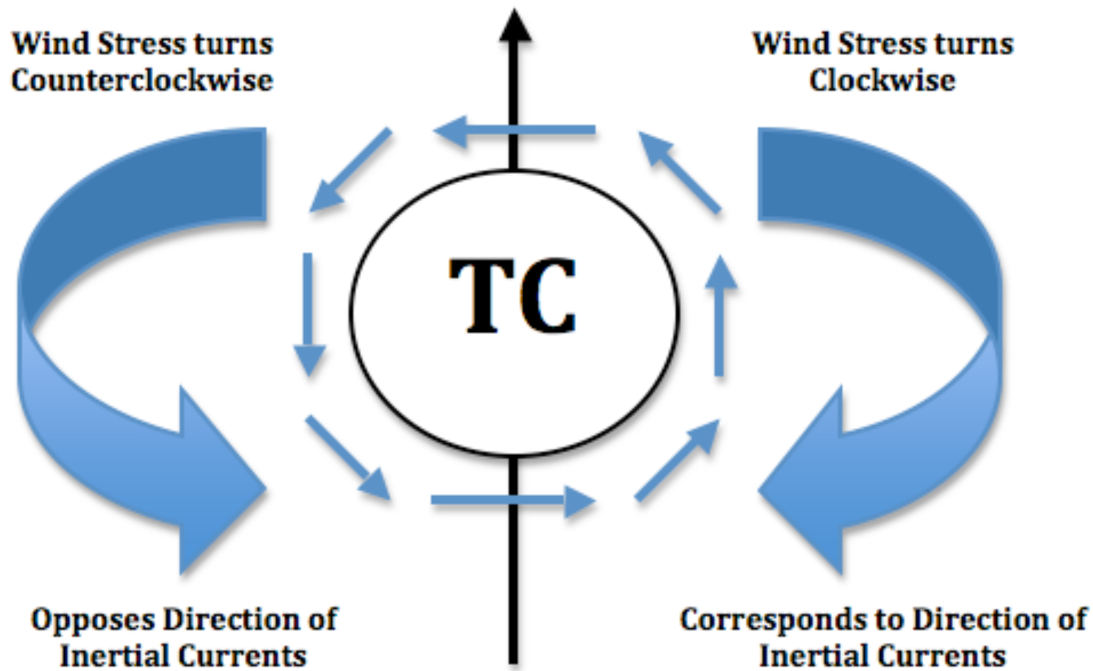

FIG. 1.1. Schematic of wind stress vector rotation with TC translation.

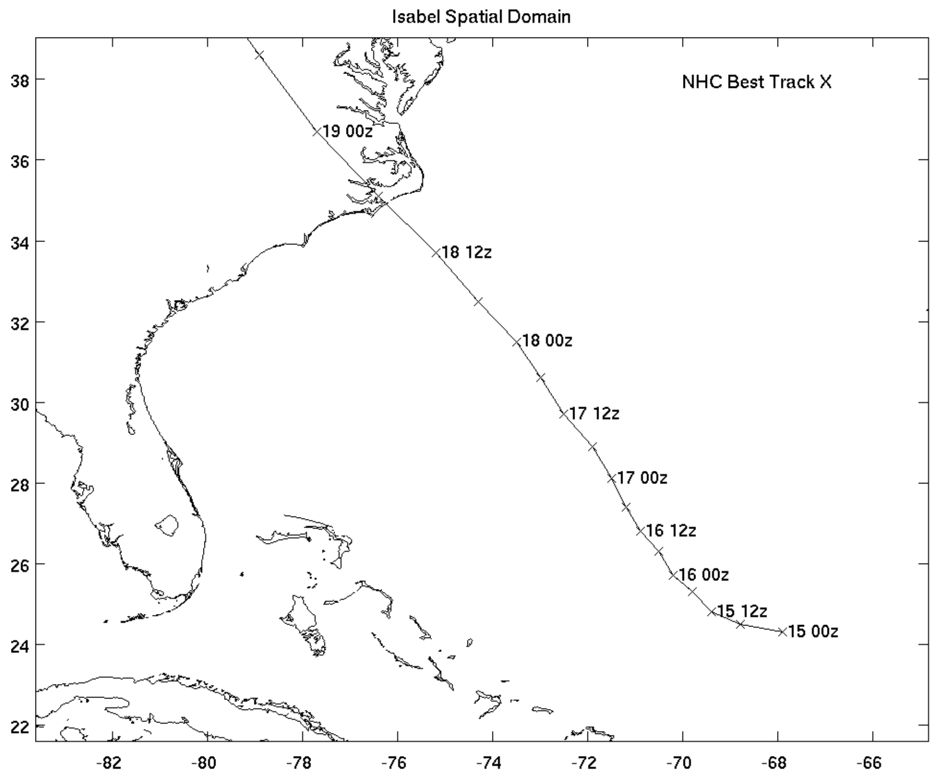

FIG. 2.1. Spatial domain and NHC best track for Hurricane Isabel (2003).

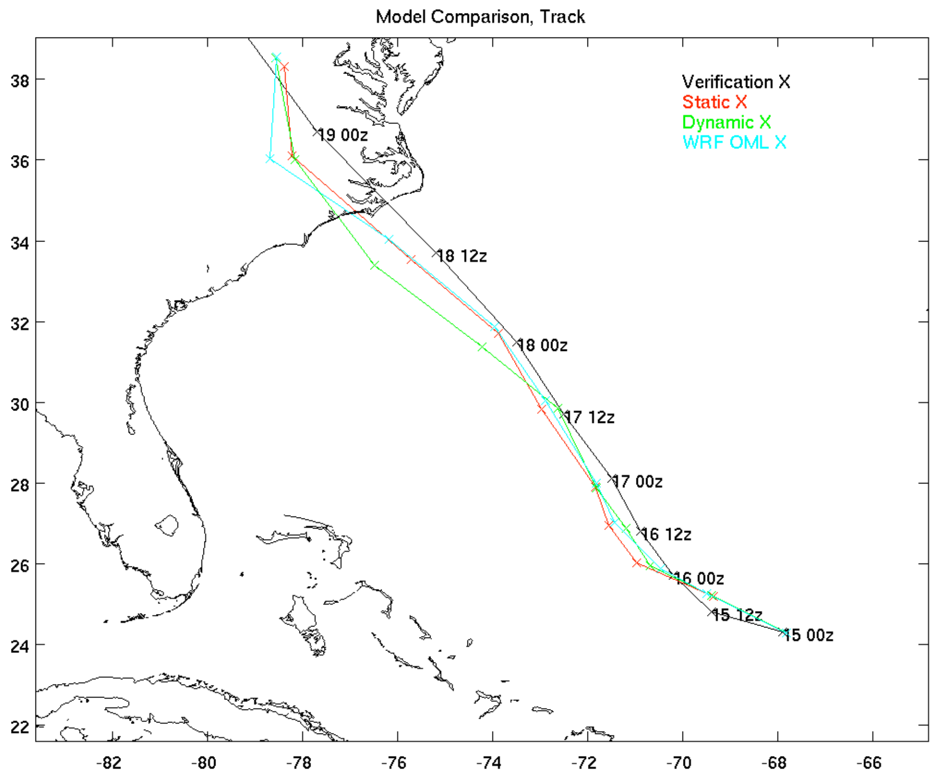

FIG. 2.2. Hurricane Isabel (2003) track comparison between Static SST case (red), Dynamic SST case (green), and WRF OML case (cyan), and NHC best track verification (black).

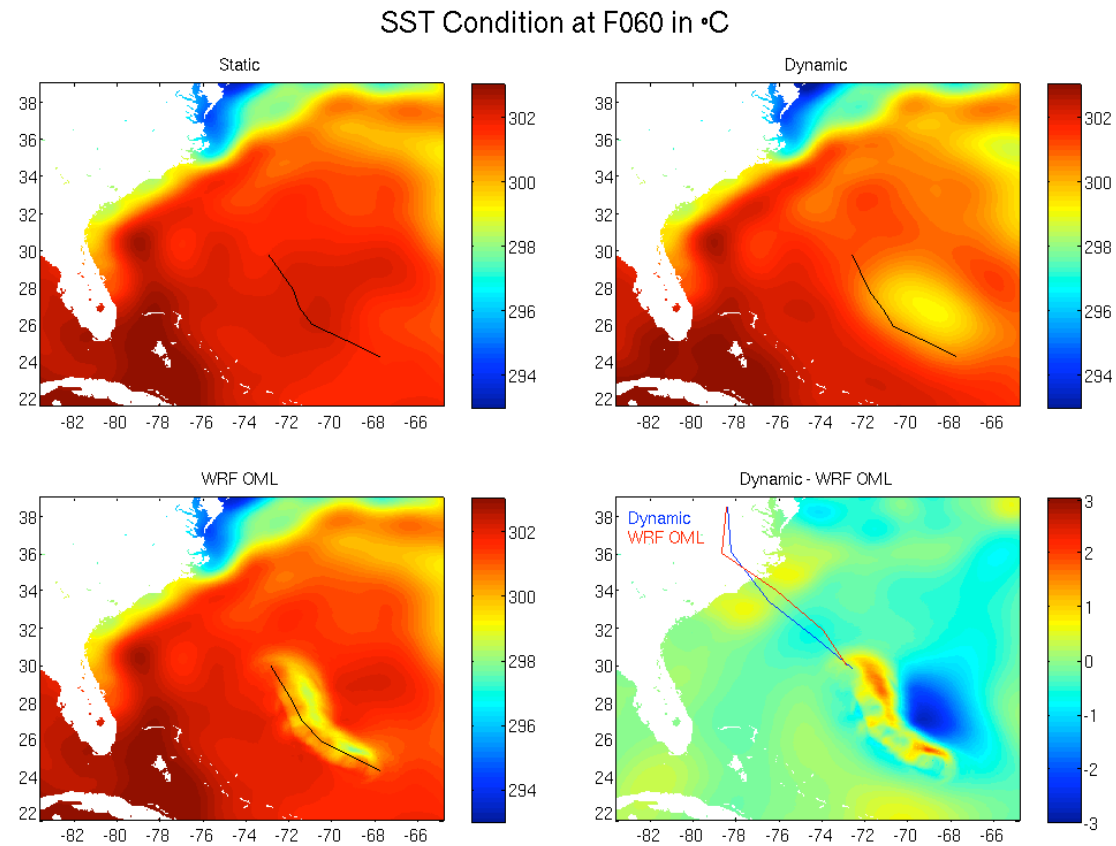

FIG. 2.3. Hurricane Isabel (2003) Sea Surface Temperature (SST) condition comparison at forecast hour 60, valid 12 UTC 17 September 2003. Static case (upper left), Dynamic case (upper right), WRF OML case (lower left), and difference between Dynamic and WRF OML cases where cool colors denote lower SST in Dynamic case (lower-right).

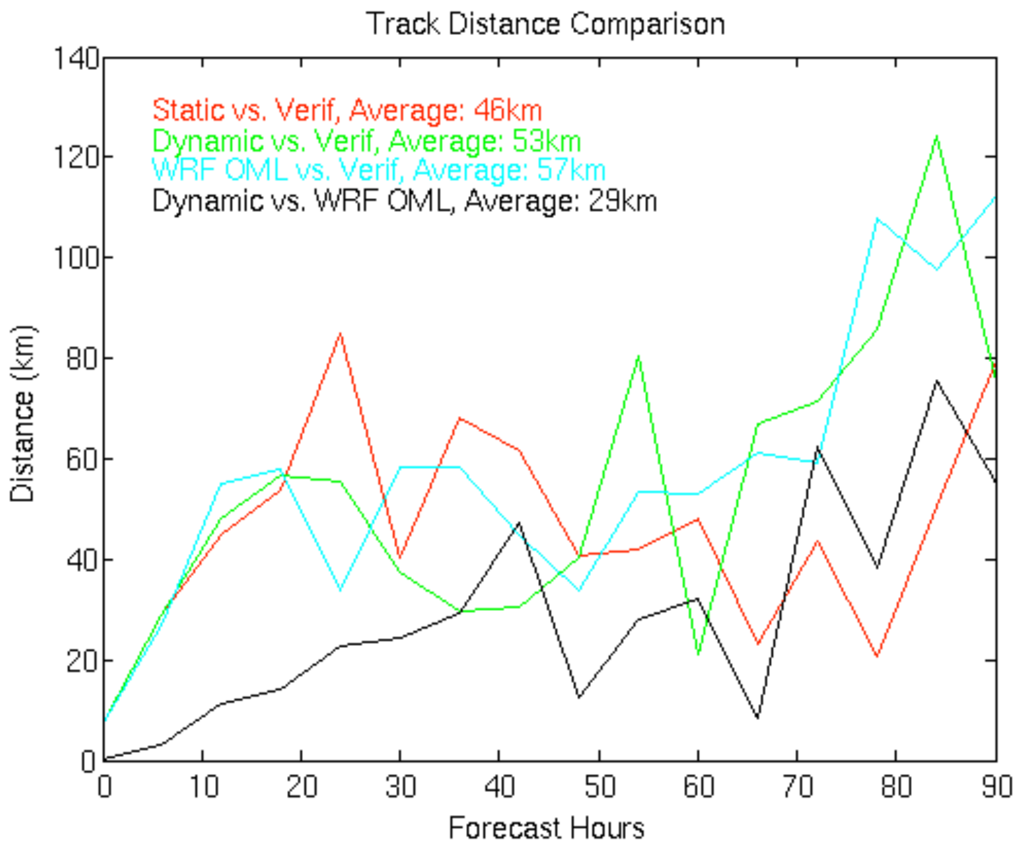

FIG. 2.4. Track distance error and average error of simulations against Hurricane Isabel (2003) NHC best track verification from initialization (hour 0, valid 00 UTC 15 September 2003) through landfall (hour 90, valid 18 UTC 18 September 2003). Static case error distance (red), Dynamic case error (green), WRF OML case (cyan), difference between TC positions of Dynamic and WRF OML (black) which are not compared to NHC best track verification.

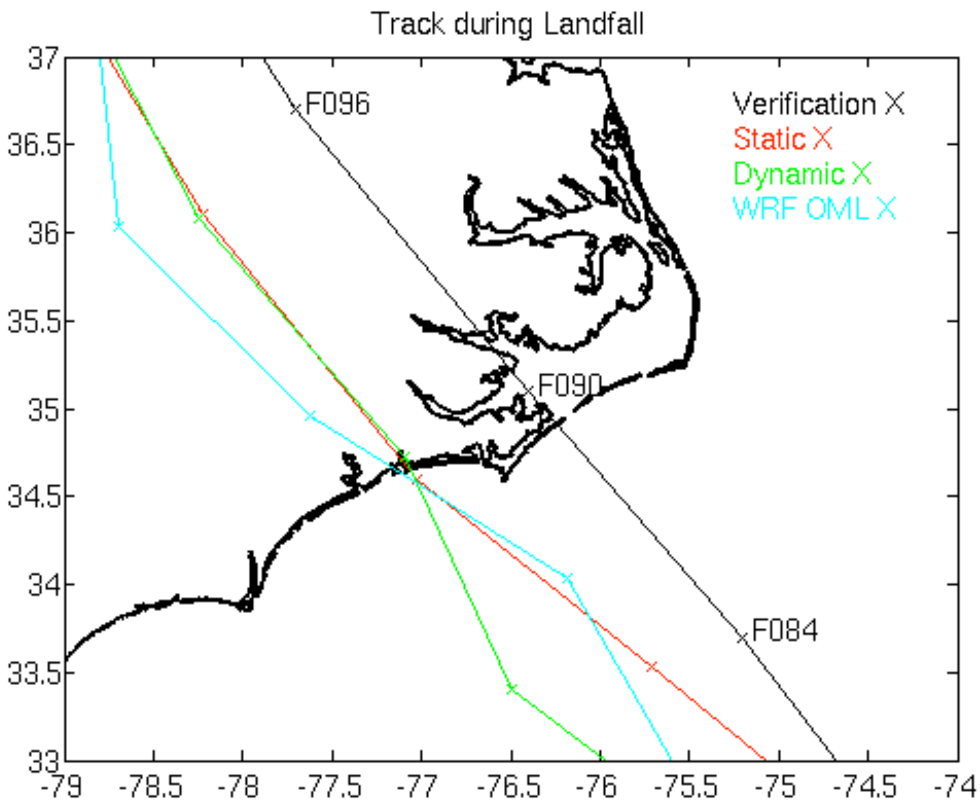

FIG. 2.5. Track comparison at landfall (F090, valid 18 UTC 18 September 2003) between Static SST case (red), Dynamic SST case (green), and NHC best track verification (black).

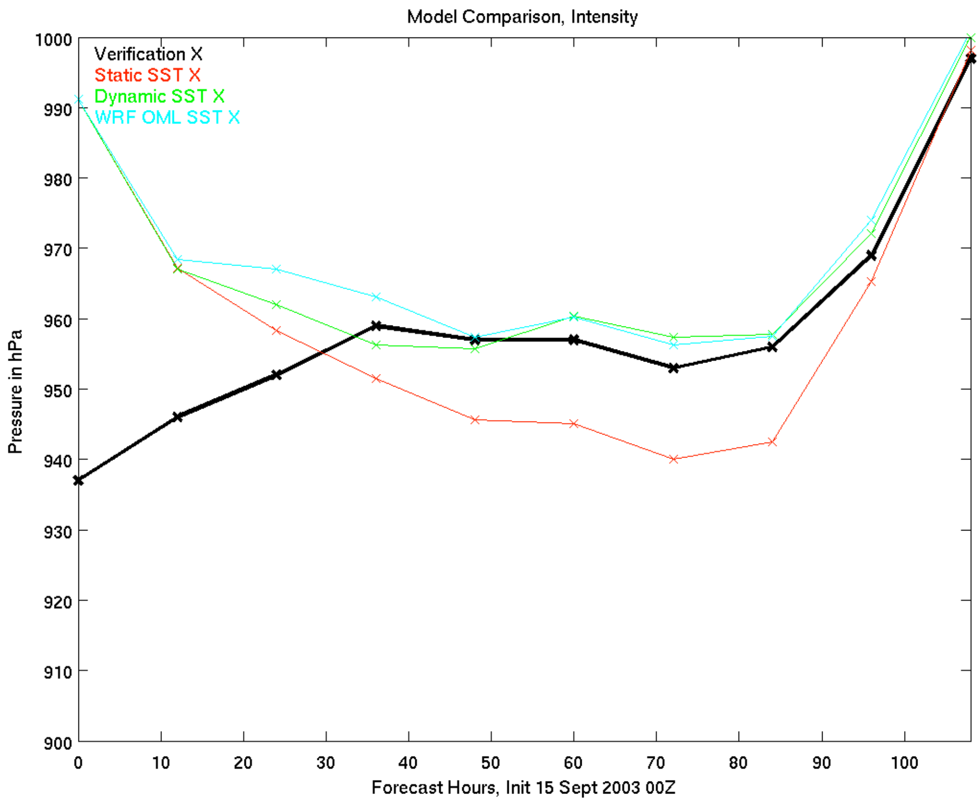

FIG. 2.6. Intensity comparison for Hurricane Isabel (2003) forecast run from initialization (F000, valid 00 UTC 15 September 2003) through termination (F108, valid 12 UTC 19 September 2003). Comparison between Static SST case (red), Dynamic SST case (green), WRF OML SST case (cyan), and NHC best track verification (black).

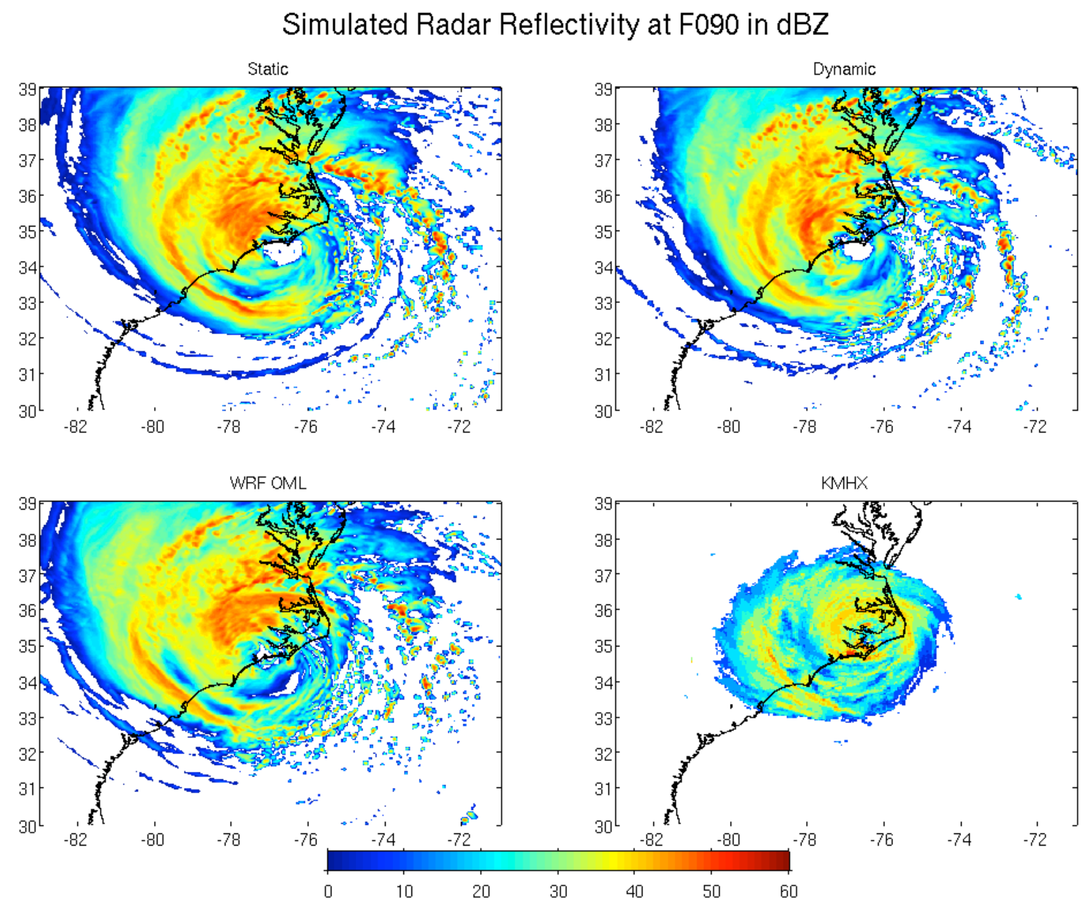

FIG. 2.7. Simulated radar reflectivity derived from model output for Static SST case (upper left), Dynamic SST case (upper right), WRF OML SST case (lower left). Verification radar reflectivity taken at landfall from radar station at KMHX in Morehead City, NC (lower right). Taken at F090, valid 18 UTC 18 September 2003.

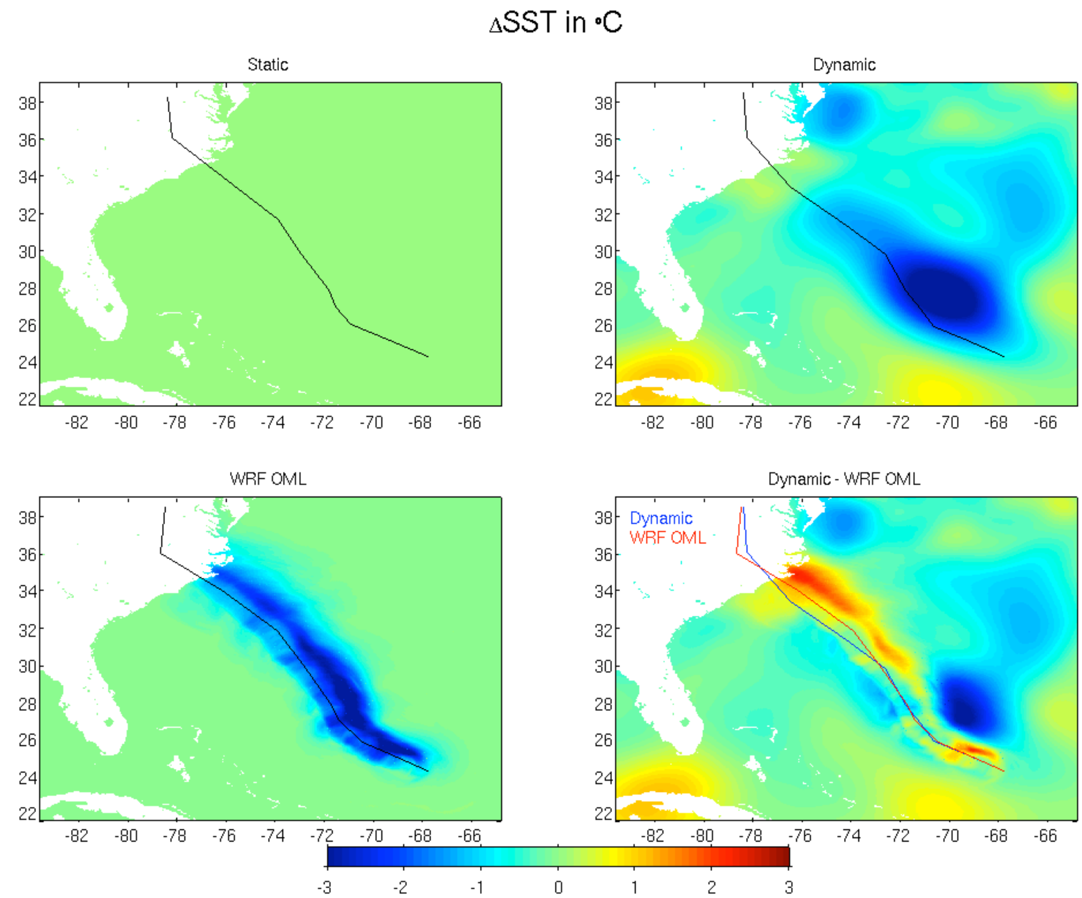

FIG. 2.8. Sea Surface Temperature change (ΔSST) comparison from model initialization (F000, valid 00 UTC 15 September 2003) through termination (F108, valid 12 UTC 19 September 2003). Static SST case (upper left), Dynamic SST case (upper right), WRF OML SST case (lower left), and difference between Dynamic SST and WRF OML SST cases where cool colors denote lower SST in Dynamic SST case (lower-right).

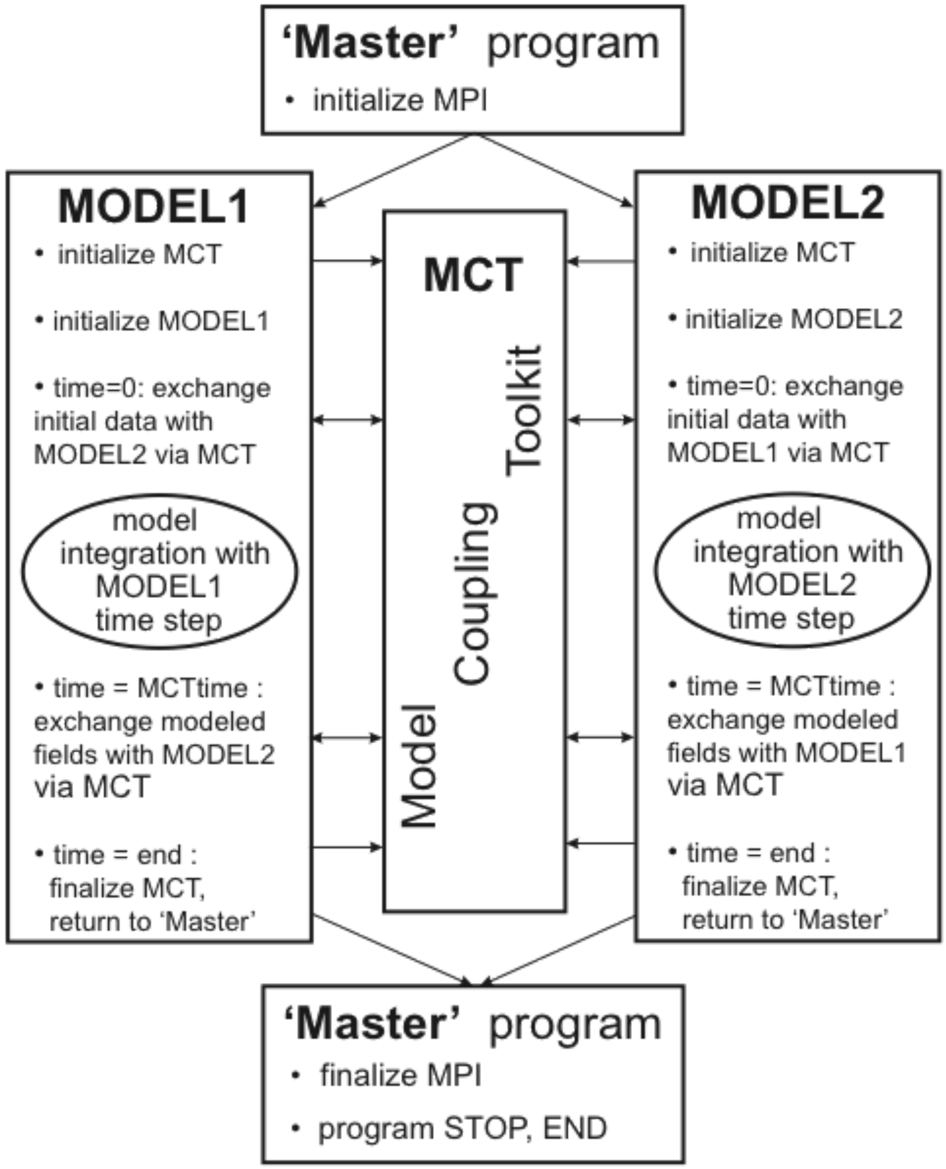

FIG. 3.1. Diagram demonstrating workflow of Model Coupling Toolkit (MCT).

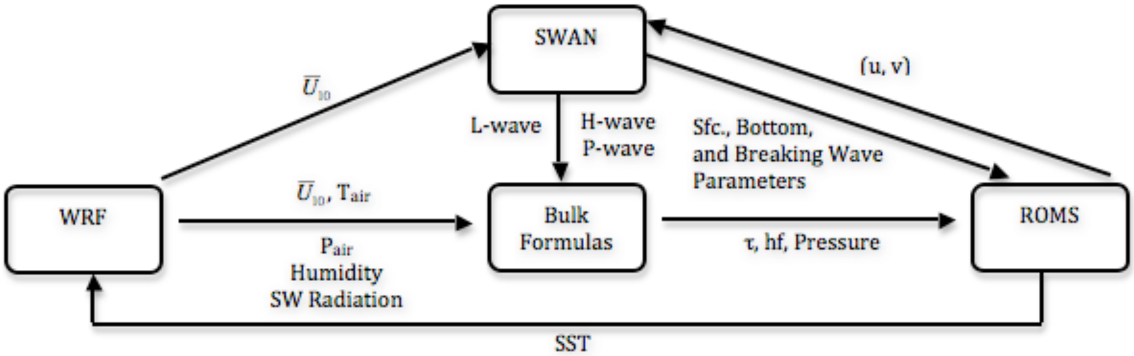

FIG. 3.2. Diagram of 3-way coupled model as currently able to be implemented in the COAWST model.

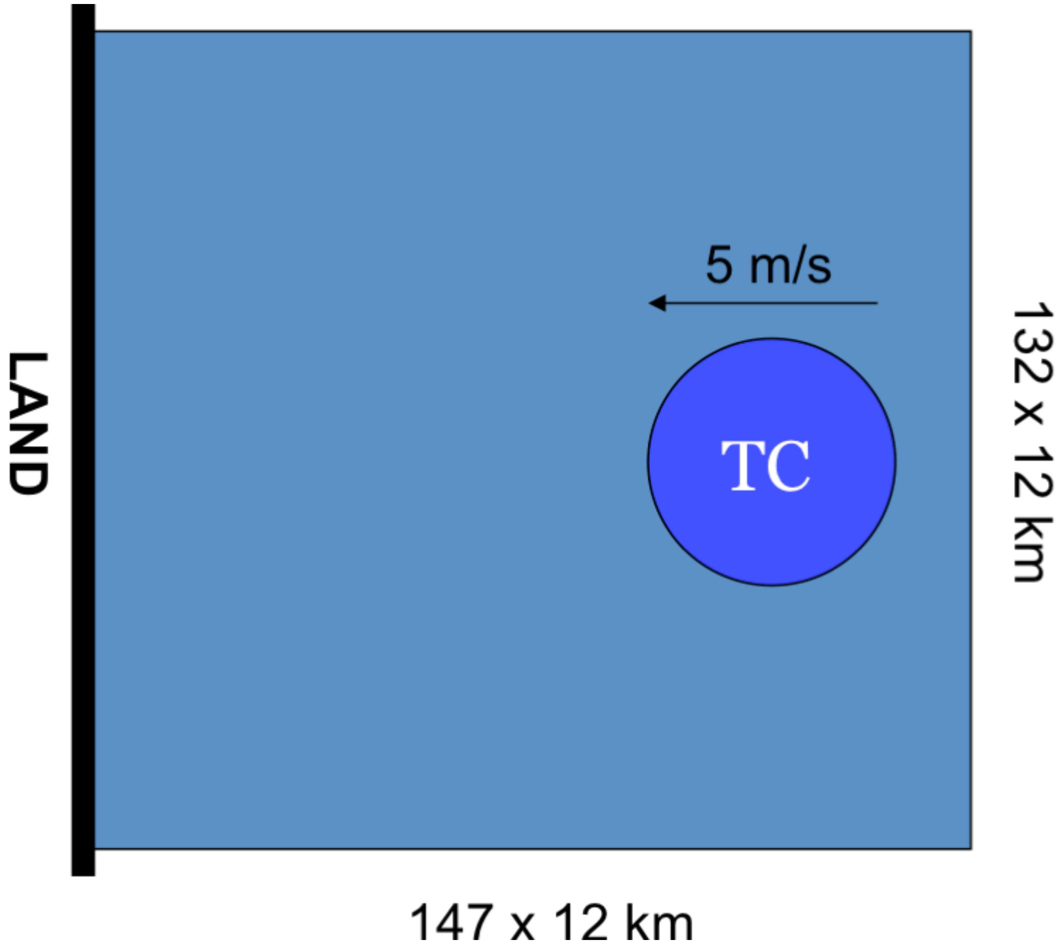

FIG. 3.3. Idealized ocean domain configuration.

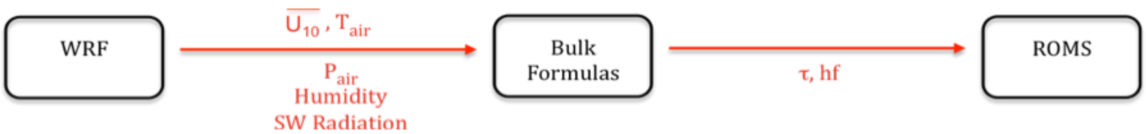

FIG. 3.4. Experimental Case A configuration.

FIG. 3.5. Experimental Case B configuration.

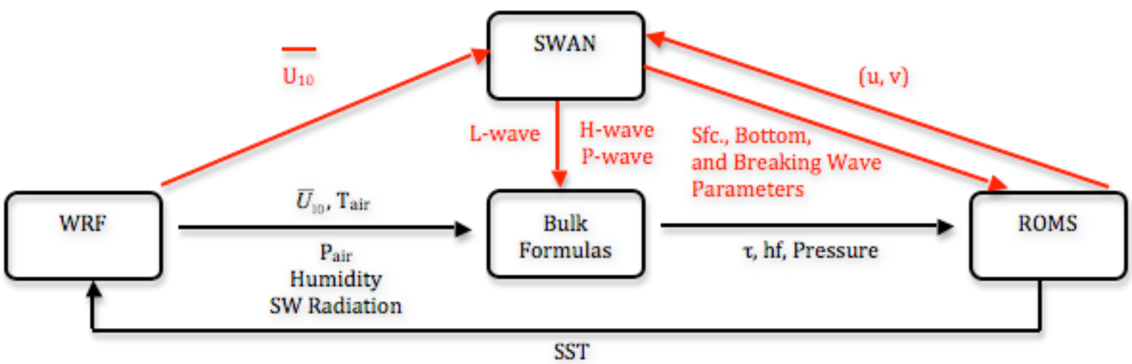

FIG. 3.6. Experimental Case C configuration.

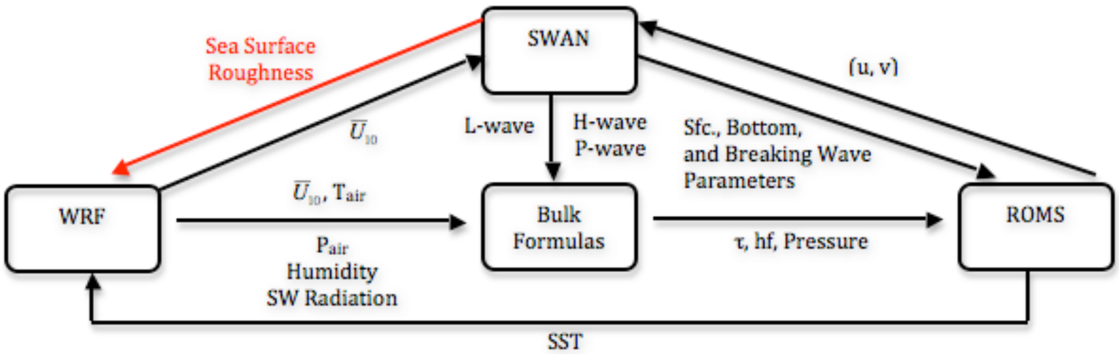

FIG. 3.7. Complete 3-way coupling (not currently available).

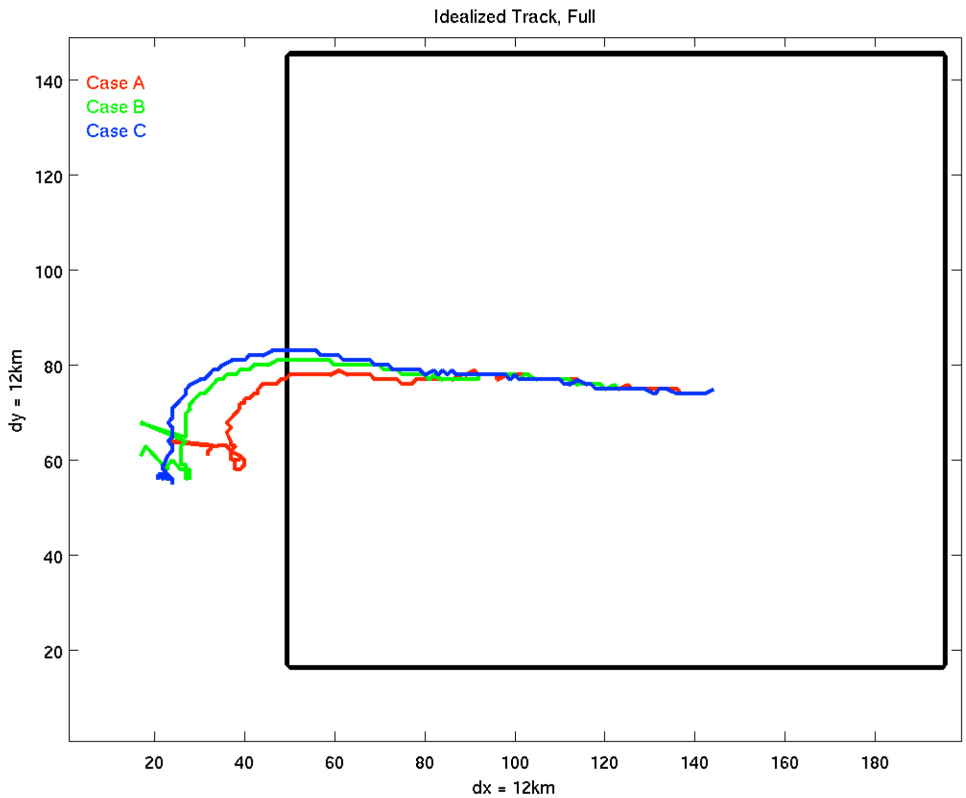

FIG. 3.8. Comparison of idealized TC track for three experiments: Case A (red), Case B (green), and Case C (blue).

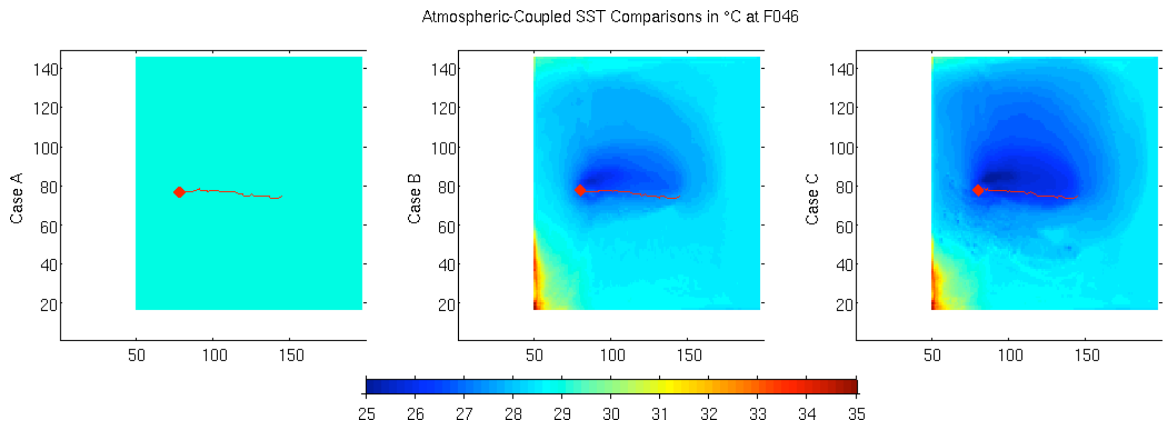

FIG. 3.9. SST condition as received by the atmospheric model at F046 for three experiments: Case A (left), Case B (middle), and Case C (right).

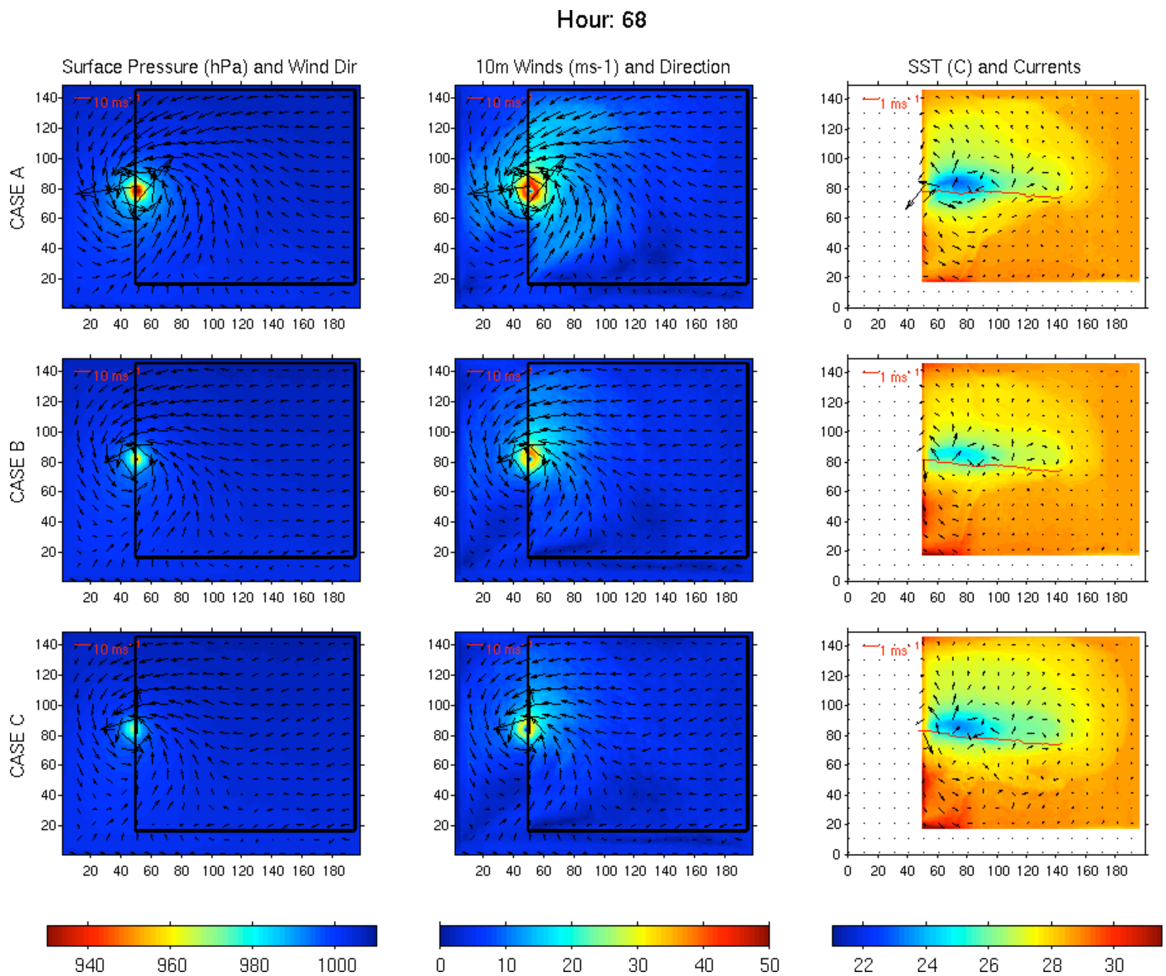

FIG. 3.10. Comparison of idealized simulations at F068 for three cases: Case A (top row), Case B (middle row), Case C (lower row). Colored surface pressure in hPa and wind vectors (left column); colored magnitude of 10m winds in ms^{-1} and wind vectors (middle column); colored sea surface condition, TC track as red line, and current vectors (right column).

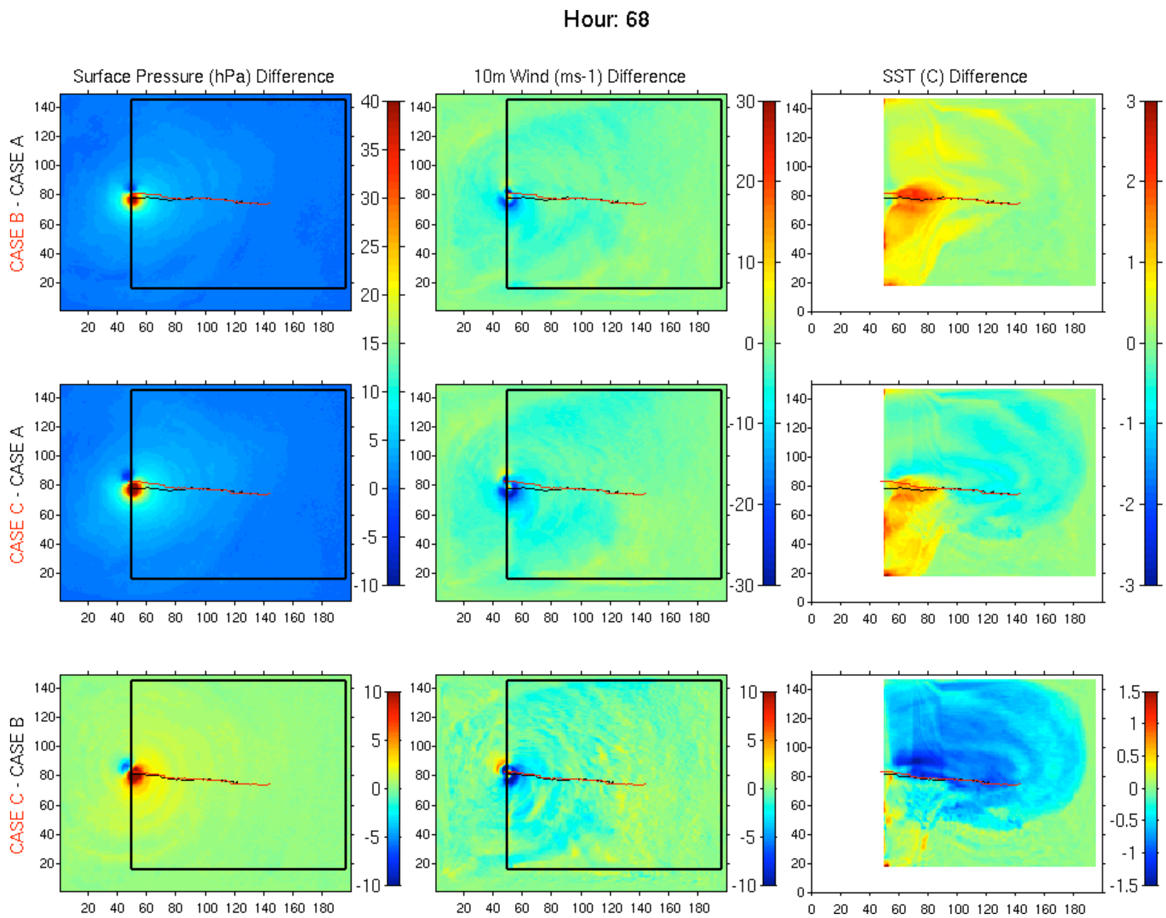

FIG. 3.11. Comparison of idealized simulations at F068 for three cases: Case B-A (top row), Case C-A (middle row), Case C-B (lower row). Colored surface pressure difference in hPa (left column); colored magnitude difference of 10m winds in ms^{-1} (middle column); colored sea surface temperature difference (right column). TC track as red and black lines for each respective case in all panels.

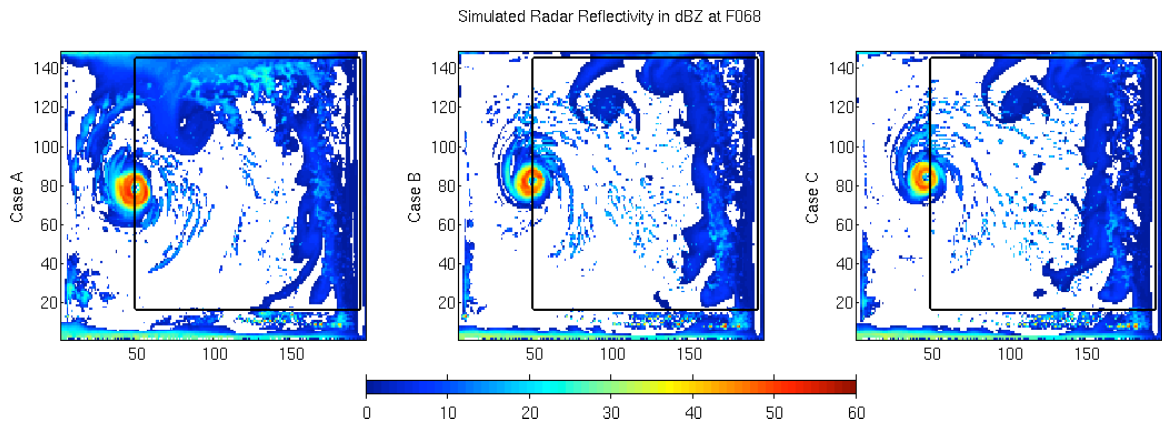

FIG. 3.12. Simulated radar reflectivity for idealized TC at F068, three experiments: Case A (left), Case B (middle), Case C (right).

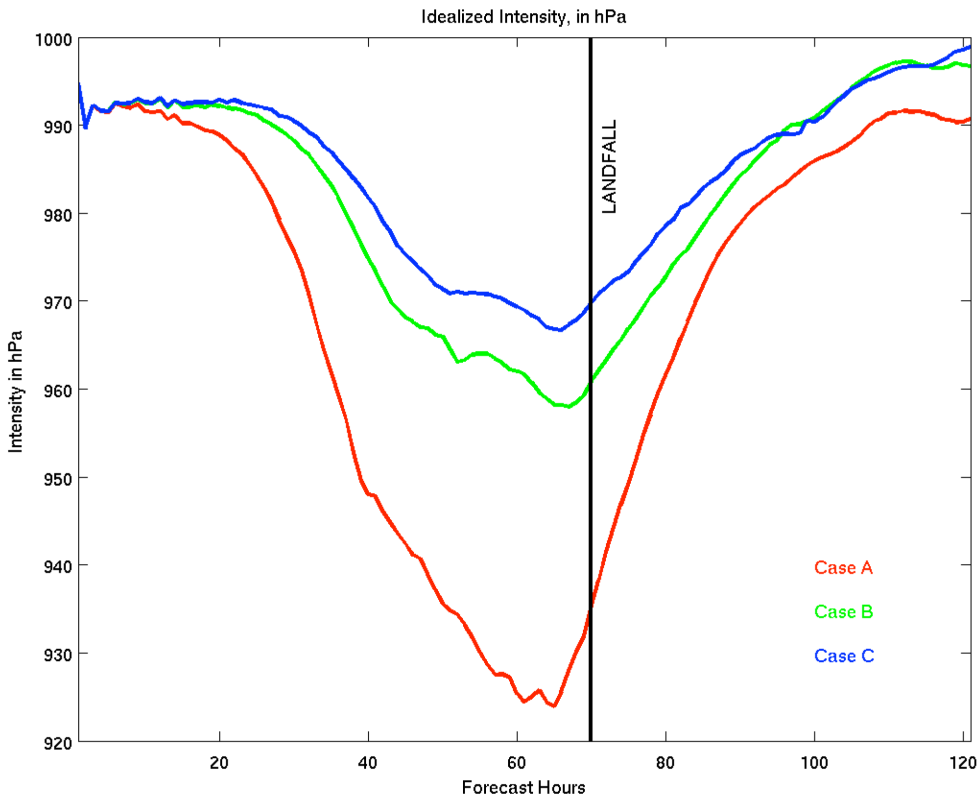

FIG. 3.13. Comparison of intensity for idealized TCs, three experiments: Case A (red), Case B (green), Case C (blue).

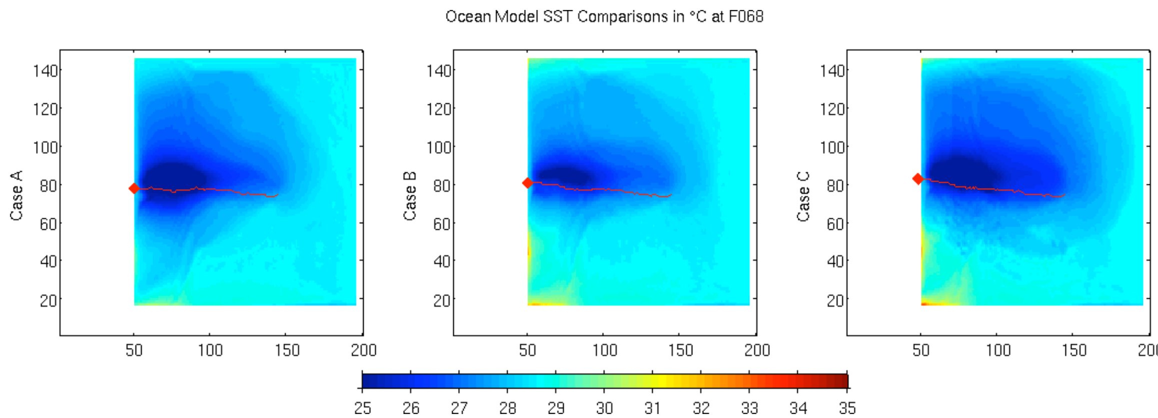

FIG. 3.14. SST condition as demonstrated by ocean model at F068 with individual tracks as red lines, three experiments: Case A (left), Case B (middle), Case C (right).

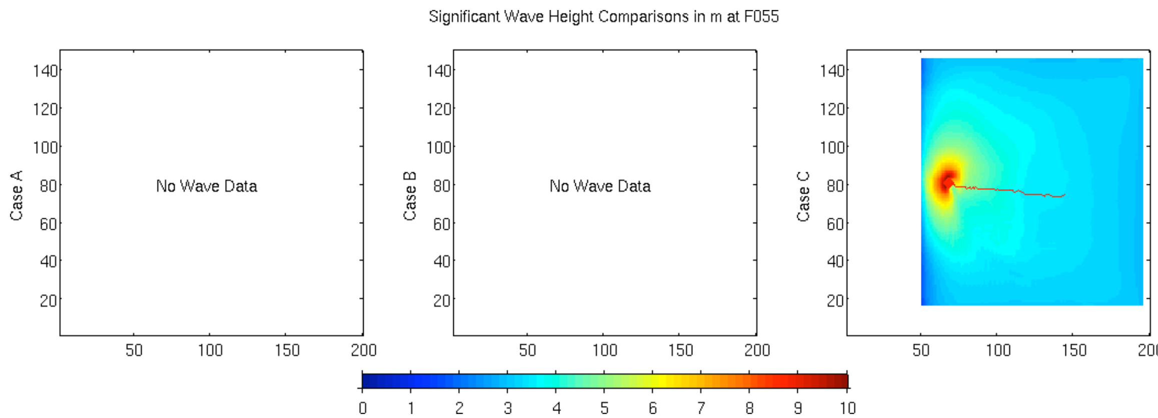

FIG. 3.15. Significant wave height as demonstrated by wave model at F055 with individual tracks as red line, one experiment with wave data: Case C (right).

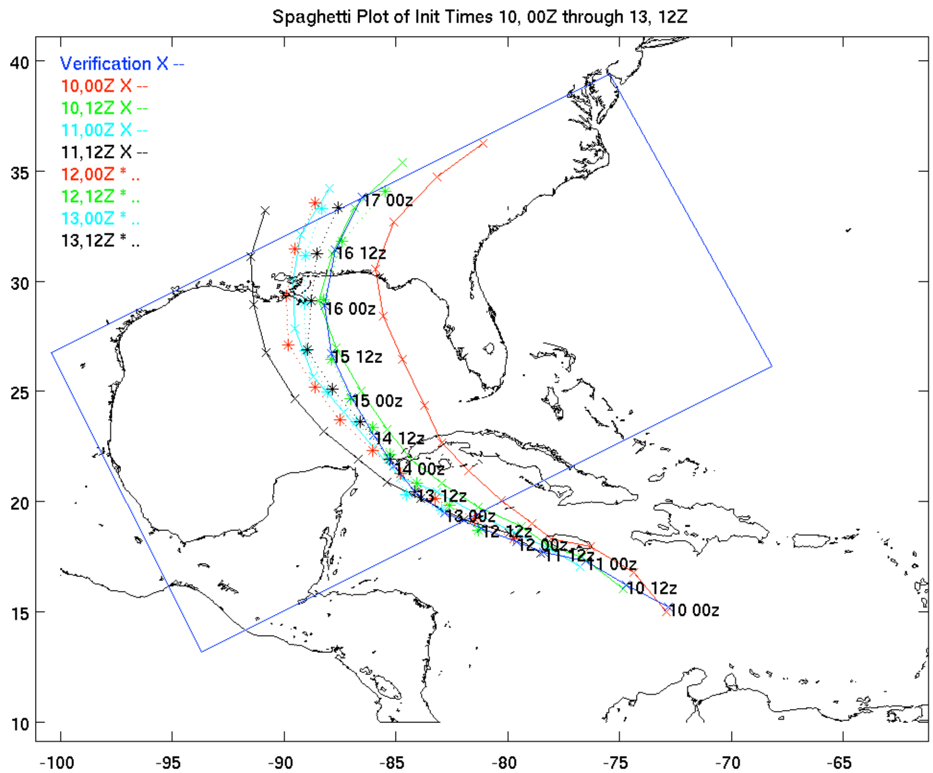

FIG. 4.1. Spatial domain configuration and sensitivity of track to initialization times every 12 hours between 00 UTC 10 September 2004 and 12 UTC 13 September 2004: 00 UTC 10 September 2004 (red, solid line marked with x's), 12 UTC 10 September 2004 (green, solid line marked with x's), 00 UTC 11 September 2004 (cyan, solid line marked with x's), 12 UTC 11 September 2004 (black, solid line marked with x's), 00 UTC 12 September 2004 (red, dotted line marked with *'s), 12 UTC 12 September 2004 (green, dotted line marked with *'s), 00 UTC 13 September 2004 (cyan, dotted line marked with *'s), 12 UTC 13 September 2004 (black, dotted line marked with *'s), and NHC best track verification (blue, solid line marked with *'s).

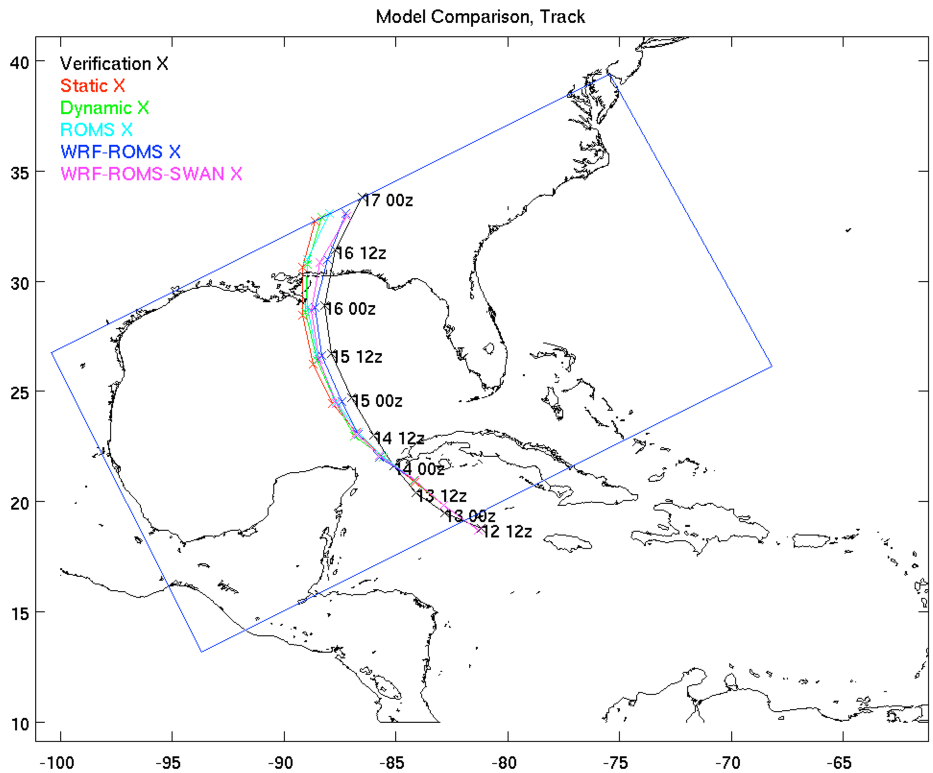

FIG. 4.2. Comparison of forecast track, 5 experiments: Static Case (red), Dynamic Case (green), ROMS Case (cyan), WRF-ROMS Case (blue), WRF-ROMS-SWAN (magenta). NHC best track verification (black).

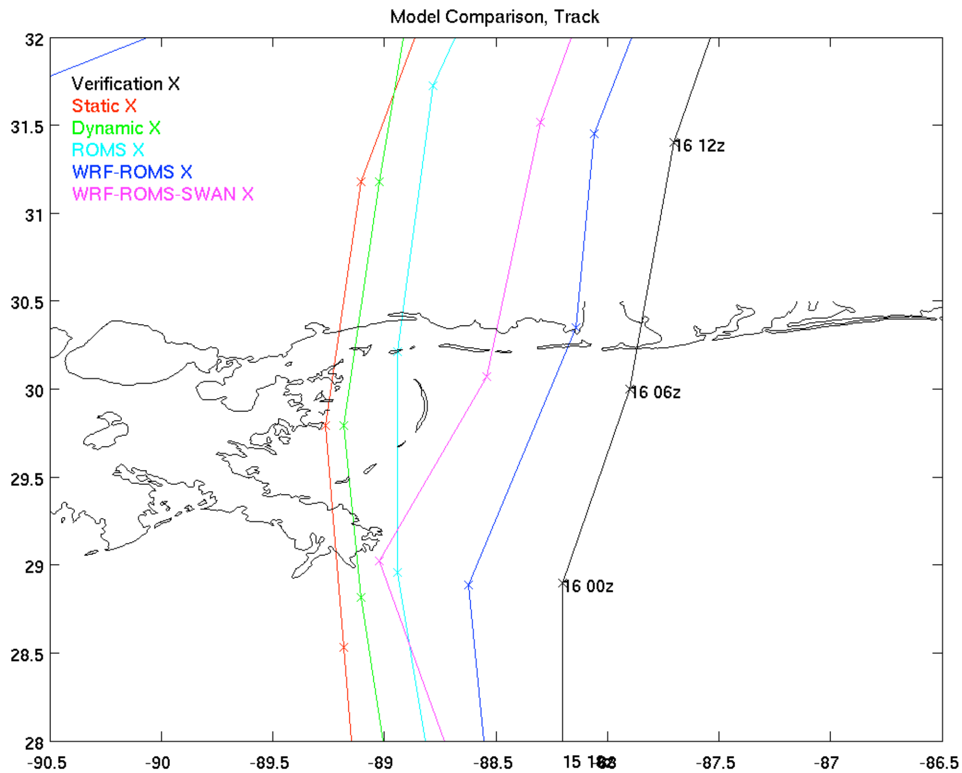

FIG. 4.3. Comparison of forecast track, zoomed into area of landfall, 5 experiments: Static Case (red), Dynamic Case (green), ROMS Case (cyan), WRF-ROMS Case (blue), WRF-ROMS-SWAN (magenta). NHC best track verification (black).

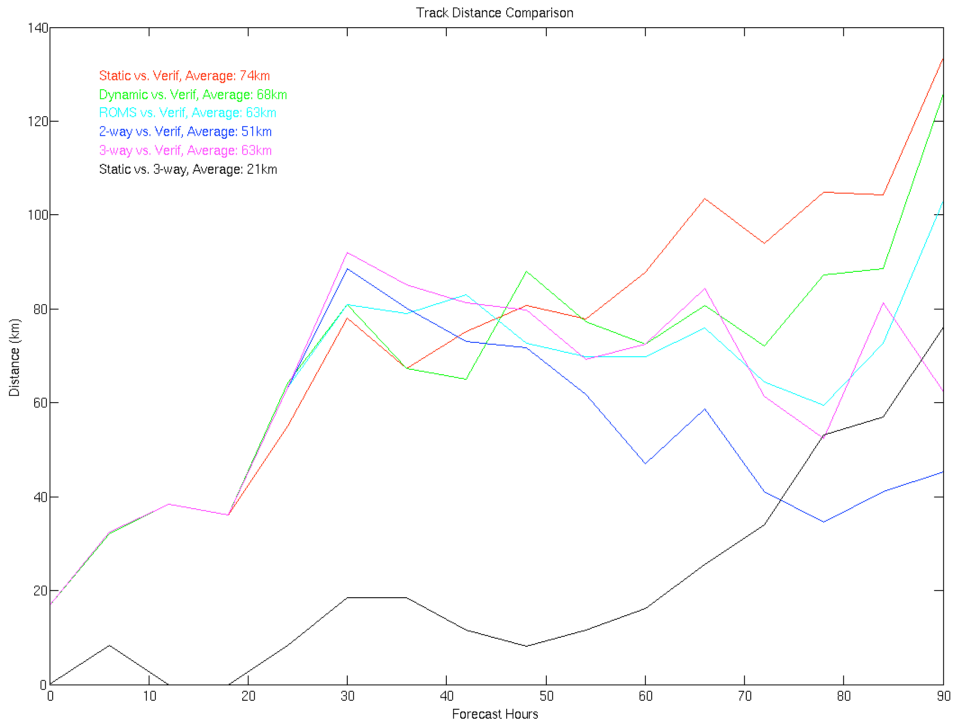

FIG. 4.4. Track differences through landfall at F090 and respective averages. Five comparisons to verification: Static Case (red), Dynamic Case (green), ROMS Case (cyan), WRF-ROMS Case (blue), WRF-ROMS-SWAN Case (magenta). Static Case and WRF-ROMS-SWAN Case difference (black).

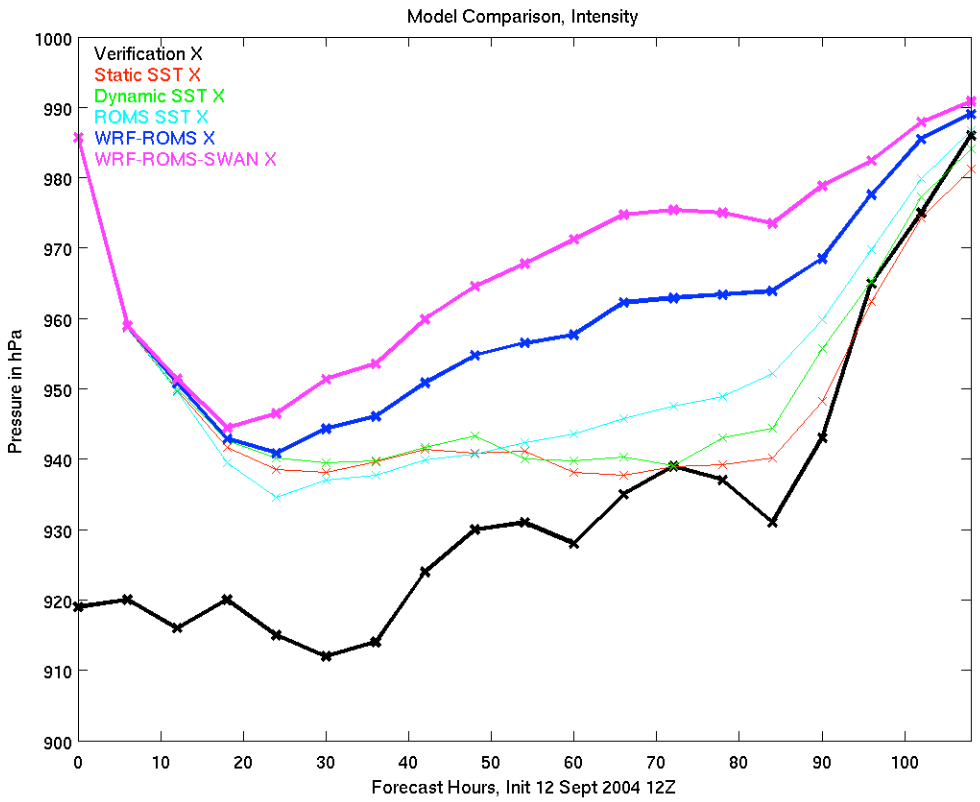

FIG. 4.5. Simulated TC intensity from initialization (12 UTC 12 September 2004) through termination (00 UTC 17 September 2004), 5 experiments: Static Case (red), Dynamic Case (green), ROMS Case (cyan), WRF-ROMS Case (blue), WRF-ROMS-SWAN (magenta). NHC best track verification (black).

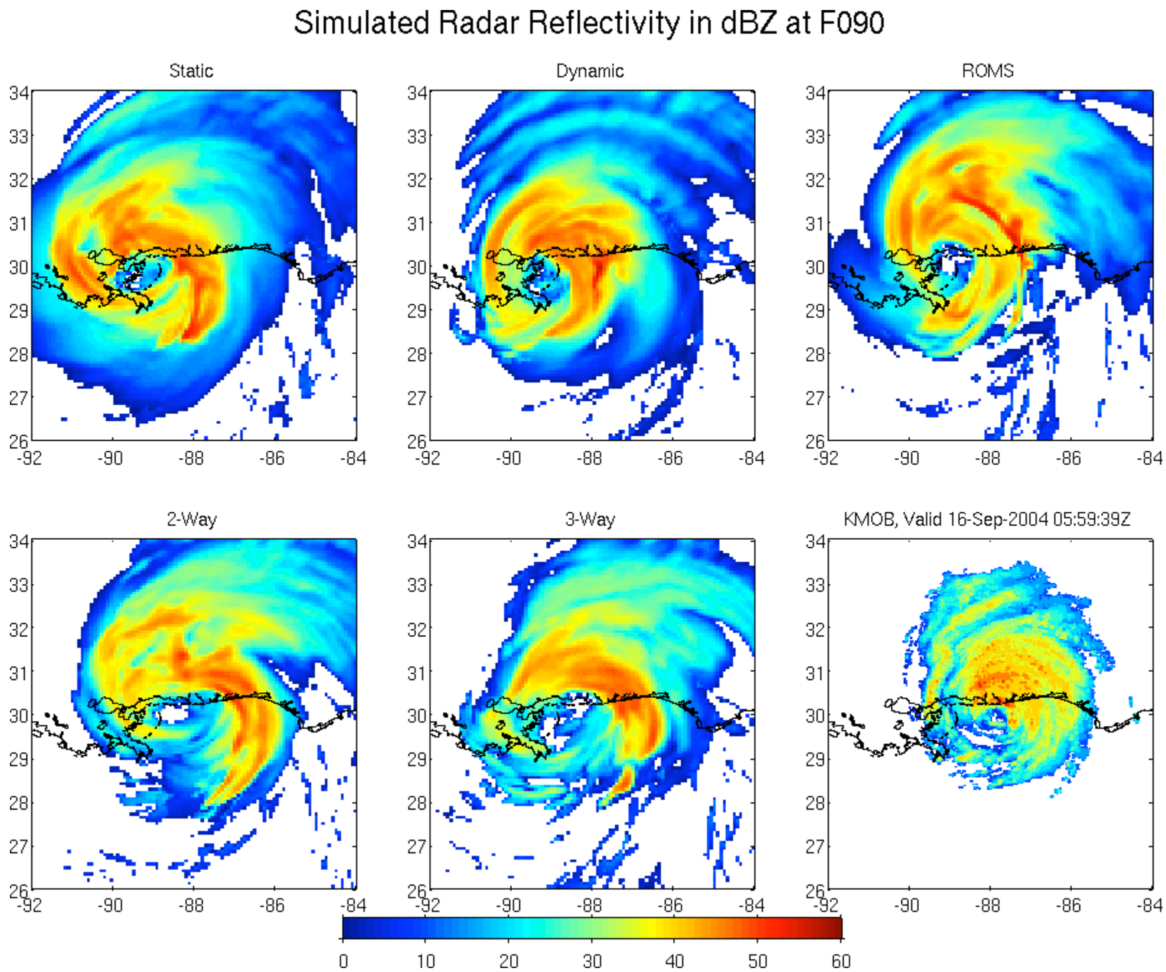

FIG. 4.6. Model simulated radar reflectivity at landfall, 5 experiments: Static Case (upper left), Dynamic Case (upper middle), ROMS Case (upper right), WRF-ROMS Case (lower left), WRF-ROMS-SWAN (lower middle). Verification radar reflectivity taken at landfall from radar station at KMOB in Mobile, AL (lower right). Taken at F090, valid 06 UTC 16 September 2004.

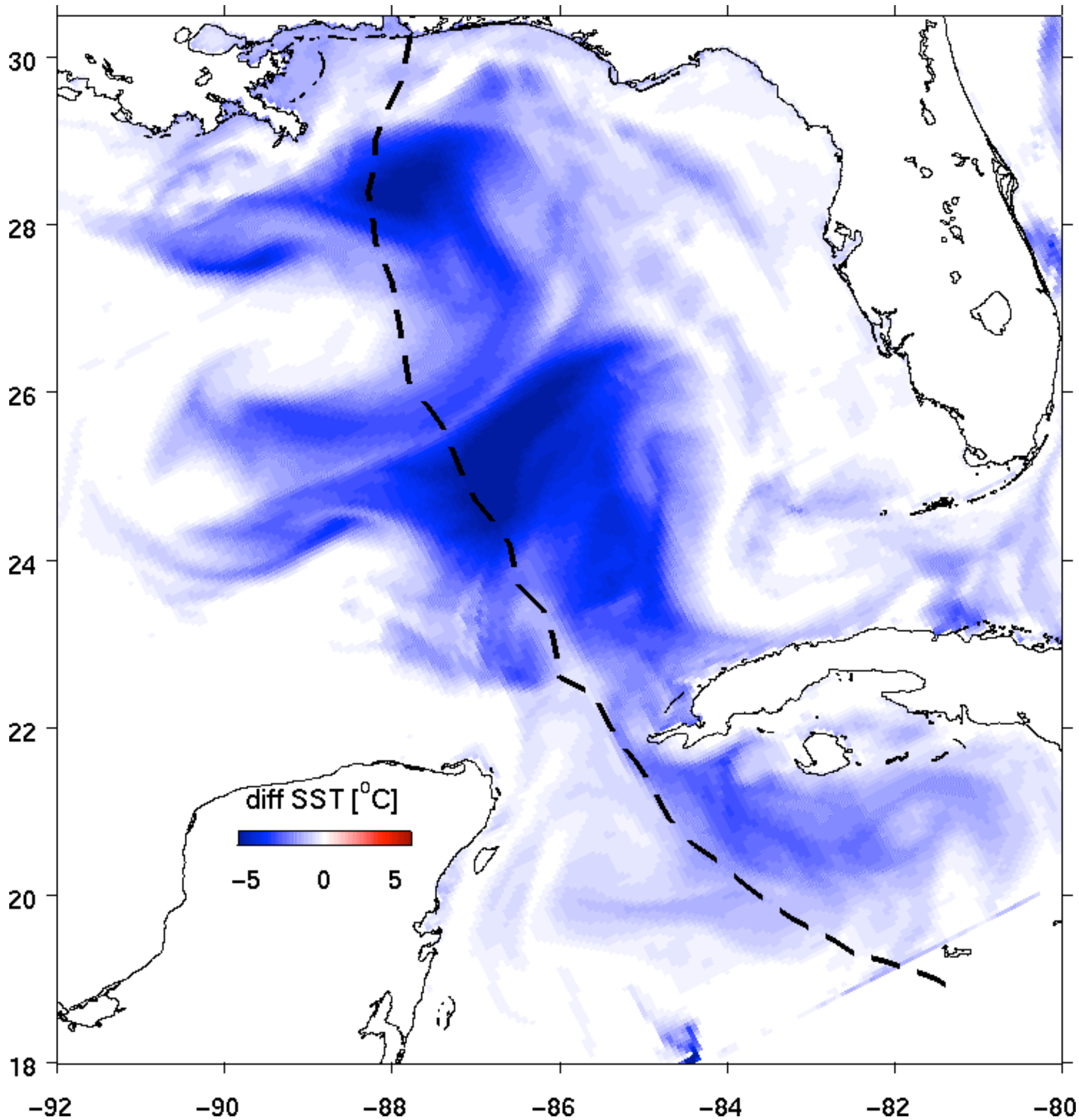

FIG. 4.7. SST difference from initialization (12 UTC 12 September 2004) through termination (00 UTC 17 September 2004) for WRF-ROMS Case.

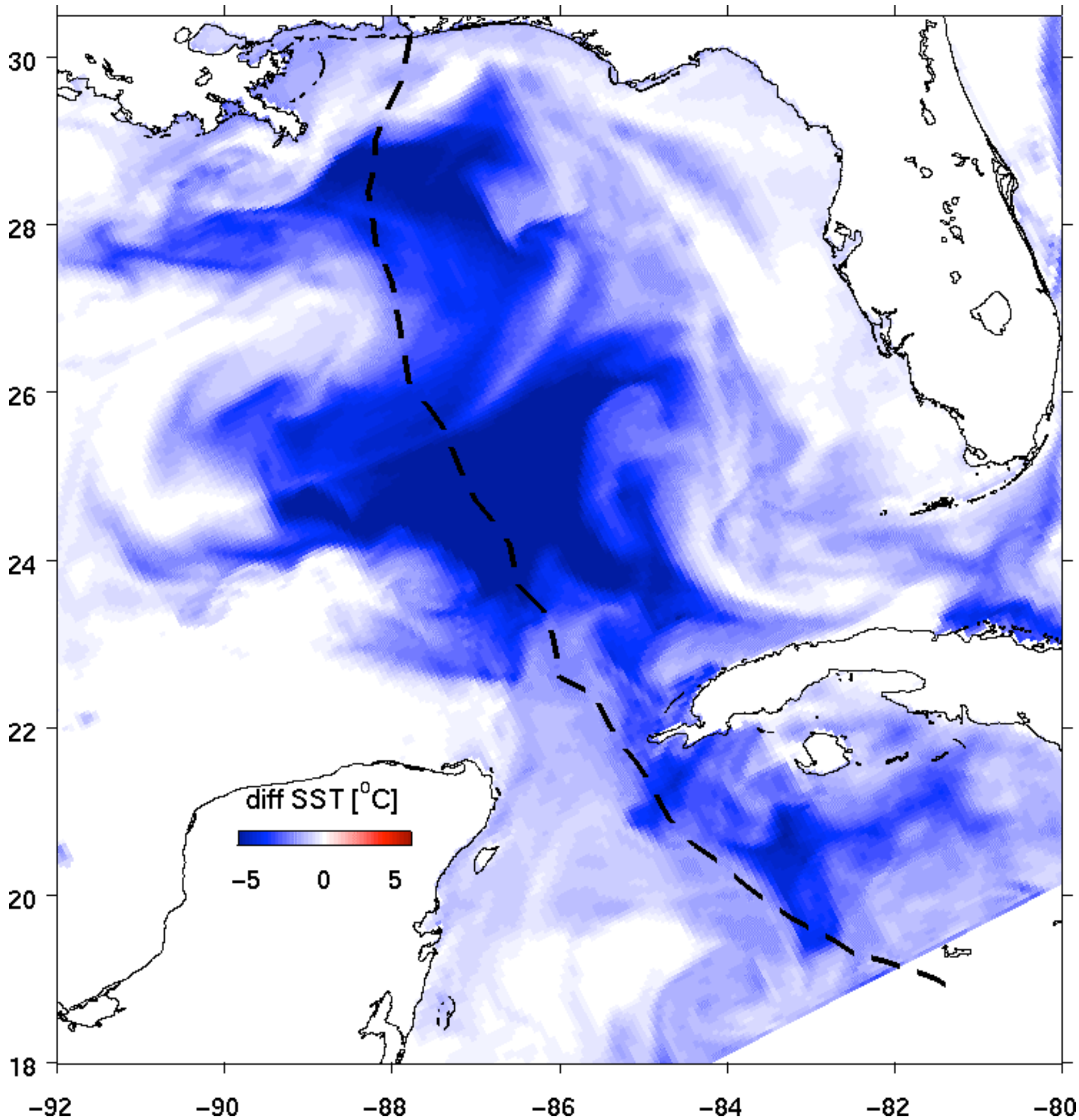

FIG. 4.8. SST difference from initialization (12 UTC 12 September 2004) through termination (00 UTC 17 September 2004) for WRF-ROMS-SWAN Case.

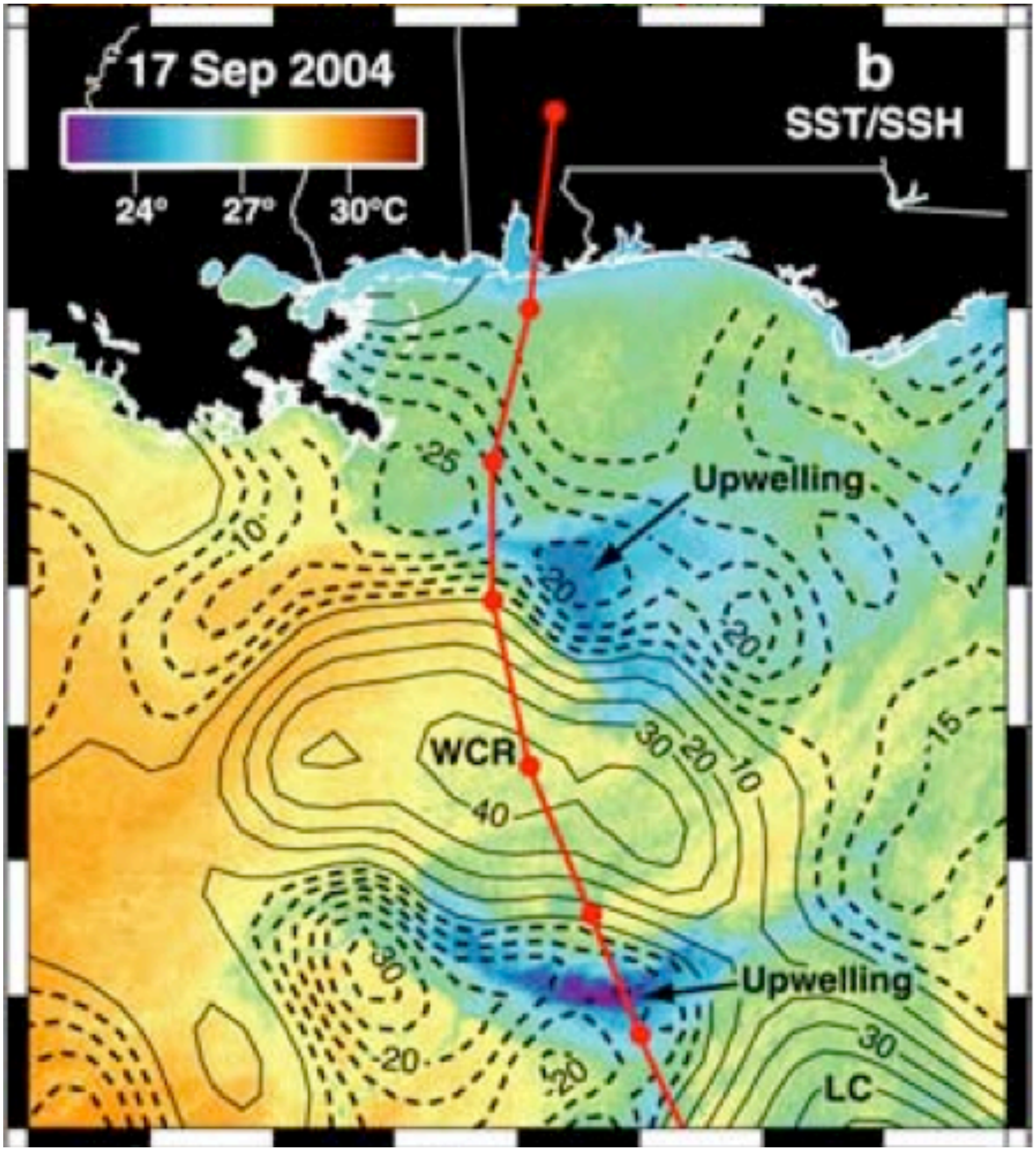

FIG. 4.9. SST Analysis of the Gulf of Mexico demonstrating two distinct cooling features after the passage of Hurricane Ivan, 17 September 2004 (From Walker et al., 2005).

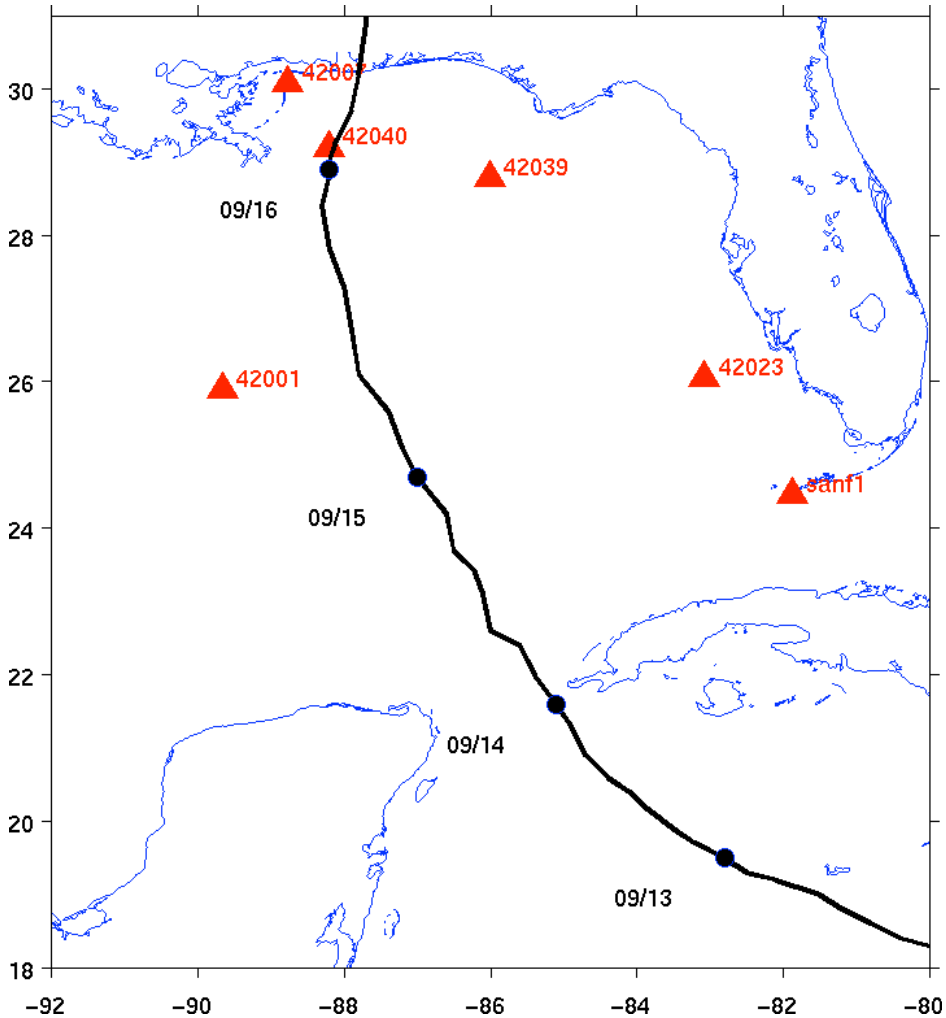

FIG. 4.10. Buoy locations in Gulf of Mexico used for SST analysis in Fig. 4.11 and significant wave height analysis in Fig. 4.17.

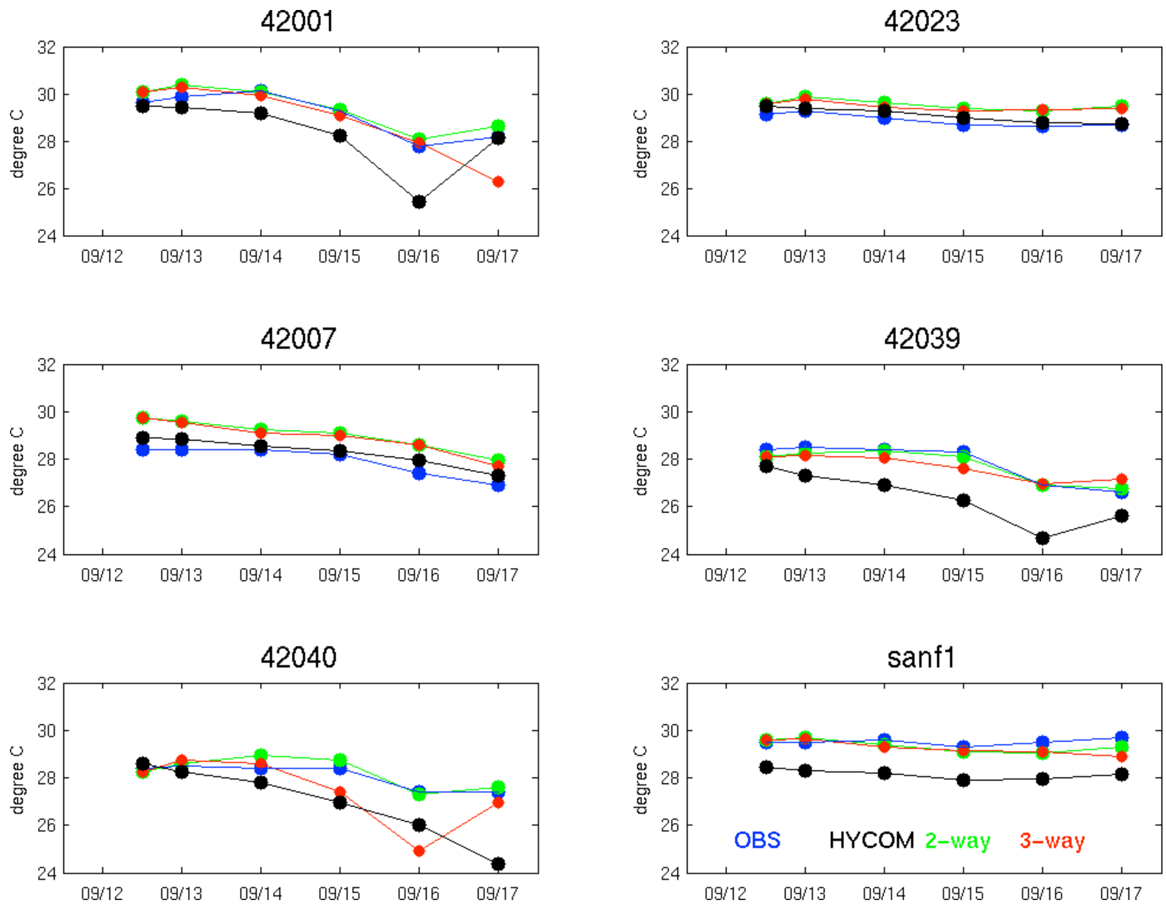

FIG. 4.11. SST analysis at buoy locations in Fig 4.10 from initialization (12 UTC 12 September 2004) through termination (00 UTC 17 September 2004). Four line colors: Observation (blue), HYCOM model SST (black), WRF-ROMS Case (green), WRF-ROMS-SWAN Case (red). Six panels: Buoy 42001 (upper left), Buoy 42023 (upper right), Buoy 42007 (middle left), Buoy 42039 (middle right), Buoy 42040 (lower left), Buoy sanf1 (lower right).

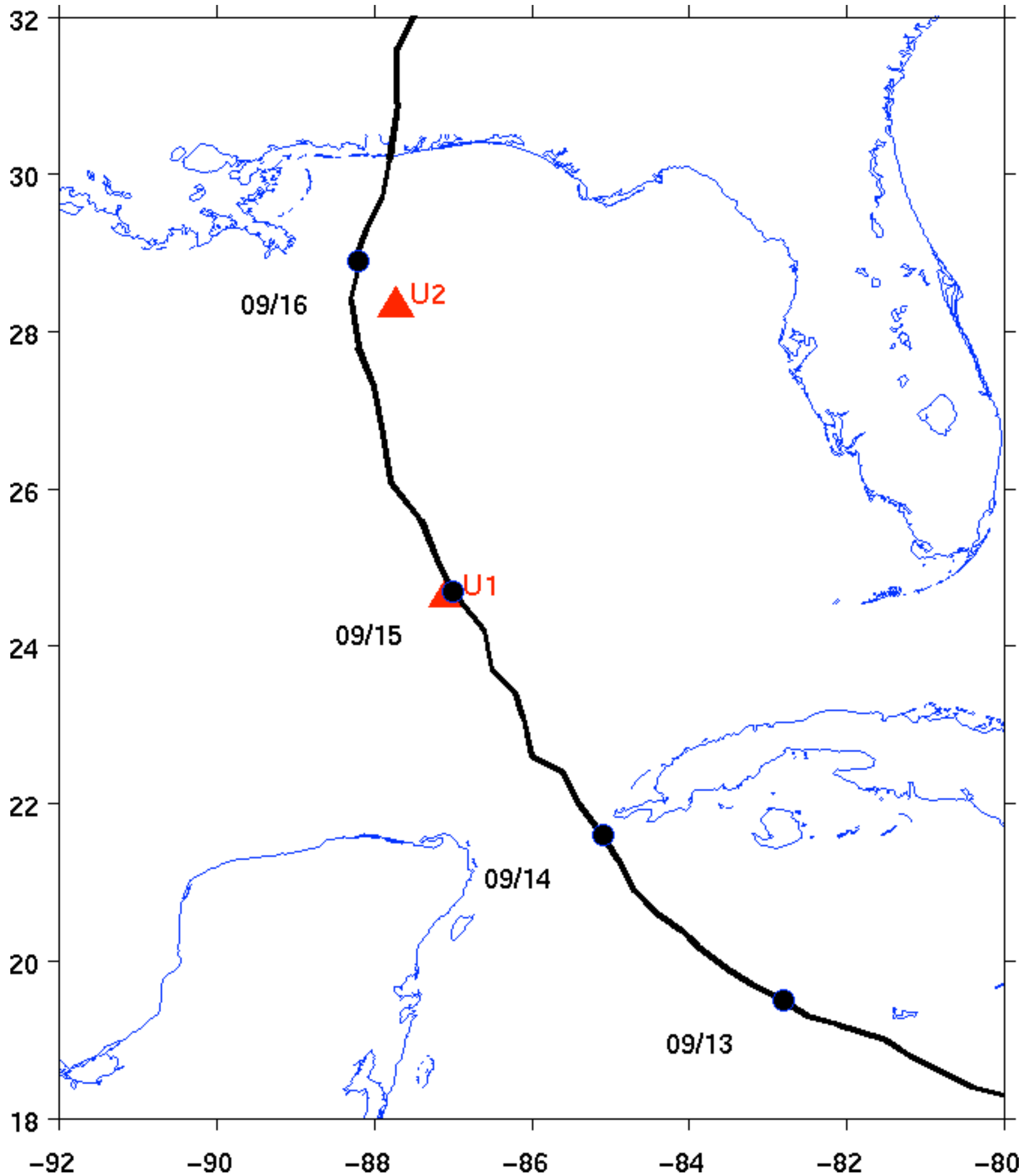

FIG. 4.12. Location of two grid points used for analysis in Figs. 4.13-4.16.

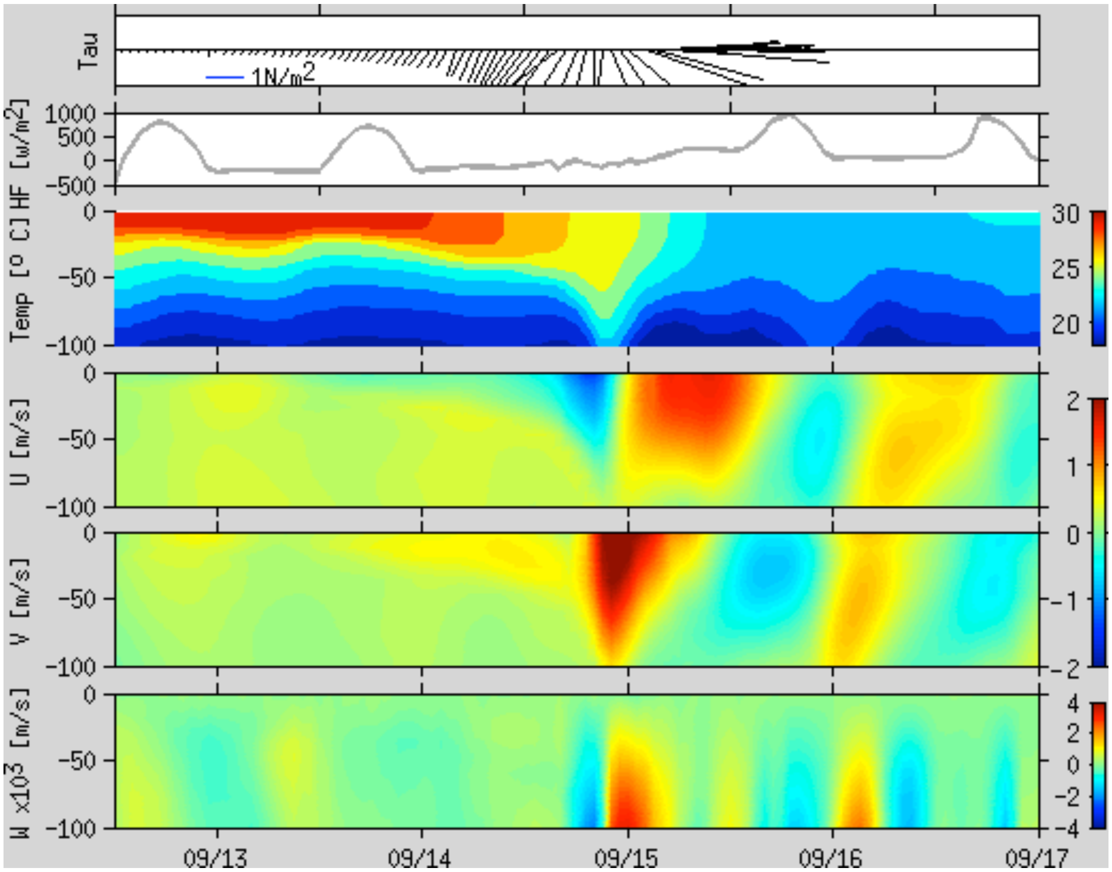

FIG. 4.13. Analysis at point U1 in Fig. 4.12 from initialization (12 UTC 12 September 2004) through termination (00 UTC 17 September 2004), 6 panels from top to bottom: wind stress in Nm^{-2}, heat flux in Wm^{-2}, temperature from surface through 100m depth in °C, U velocity from surface through 100m depth in ms^{-1}, V velocity from surface through 100m depth in ms^{-1}, W velocity from surface through 100m depth in ms^{-1}.

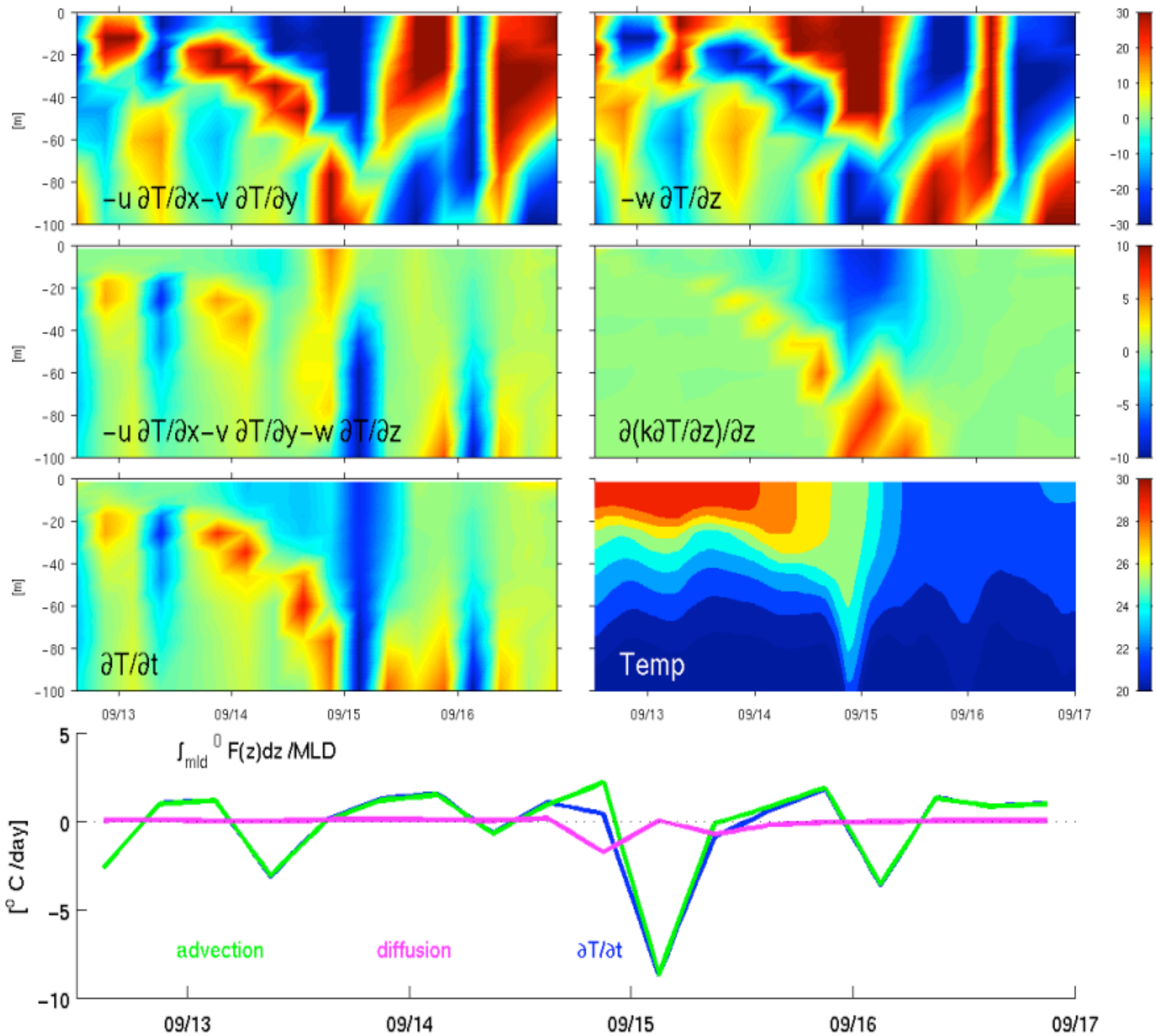

FIG. 4.14. Analysis of heat budget at point U1 from initialization (12 UTC 12 September 2004) through termination (00 UTC 17 September 2004), panels from top to bottom: horizontal advection term in °C day^{-1} (left), vertical advection term in °C day^{-1} (right), total advection term in °C day^{-1} (left), vertical diffusion term in °C day^{-1} (right), total local rate of change term in °C day^{-1} (left), temperature in °C (right), comparison of contributions of advection and diffusion to local change in temperature integrated through 100m.

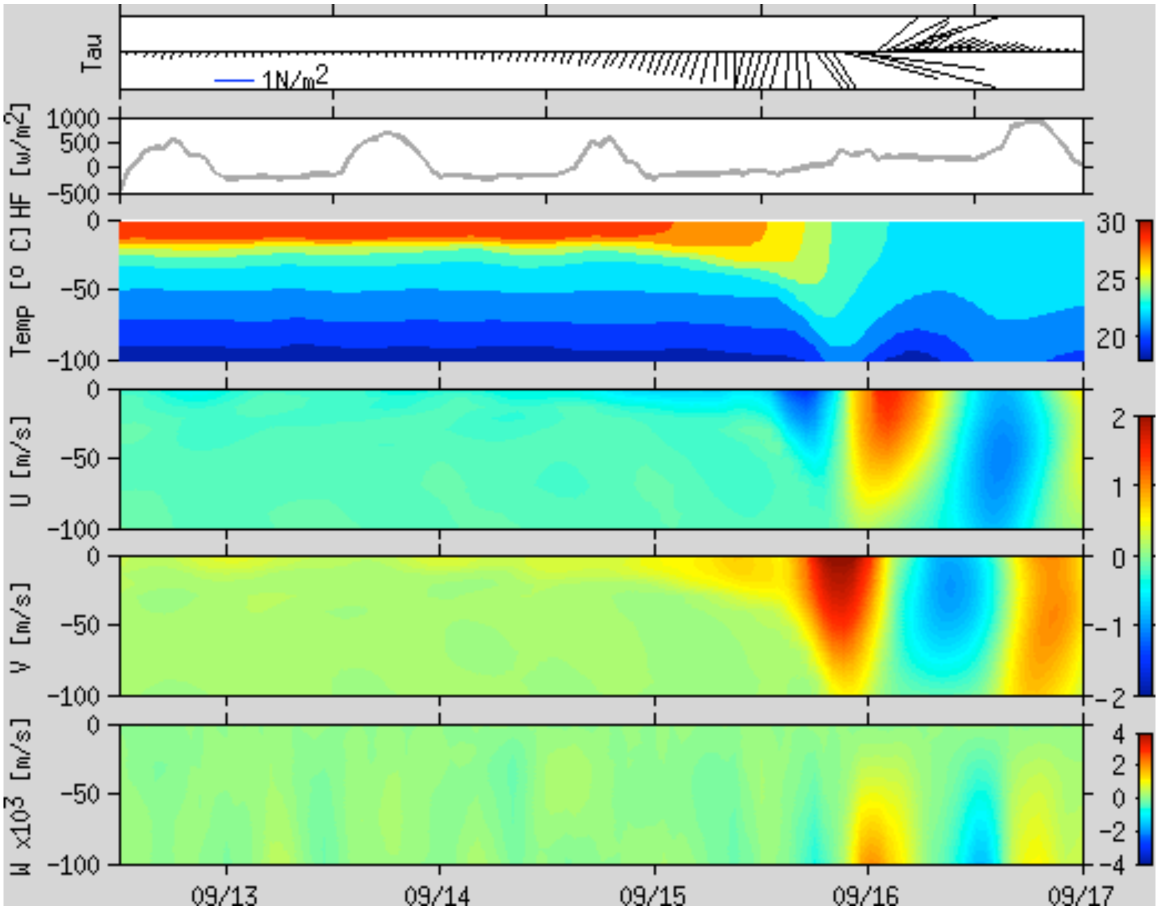

FIG. 4.15. Analysis at point U2 in Fig. 4.12 from initialization (12 UTC 12 September 2004) through termination (00 UTC 17 September 2004), 6 panels from top to bottom: wind stress in Nm^{-2}, heat flux in Wm^{-2}, temperature from surface through 100m depth in °C, U velocity from surface through 100m depth in ms^{-1}, V velocity from surface through 100m depth in ms^{-1}, W velocity from surface through 100m depth in ms^{-1}.

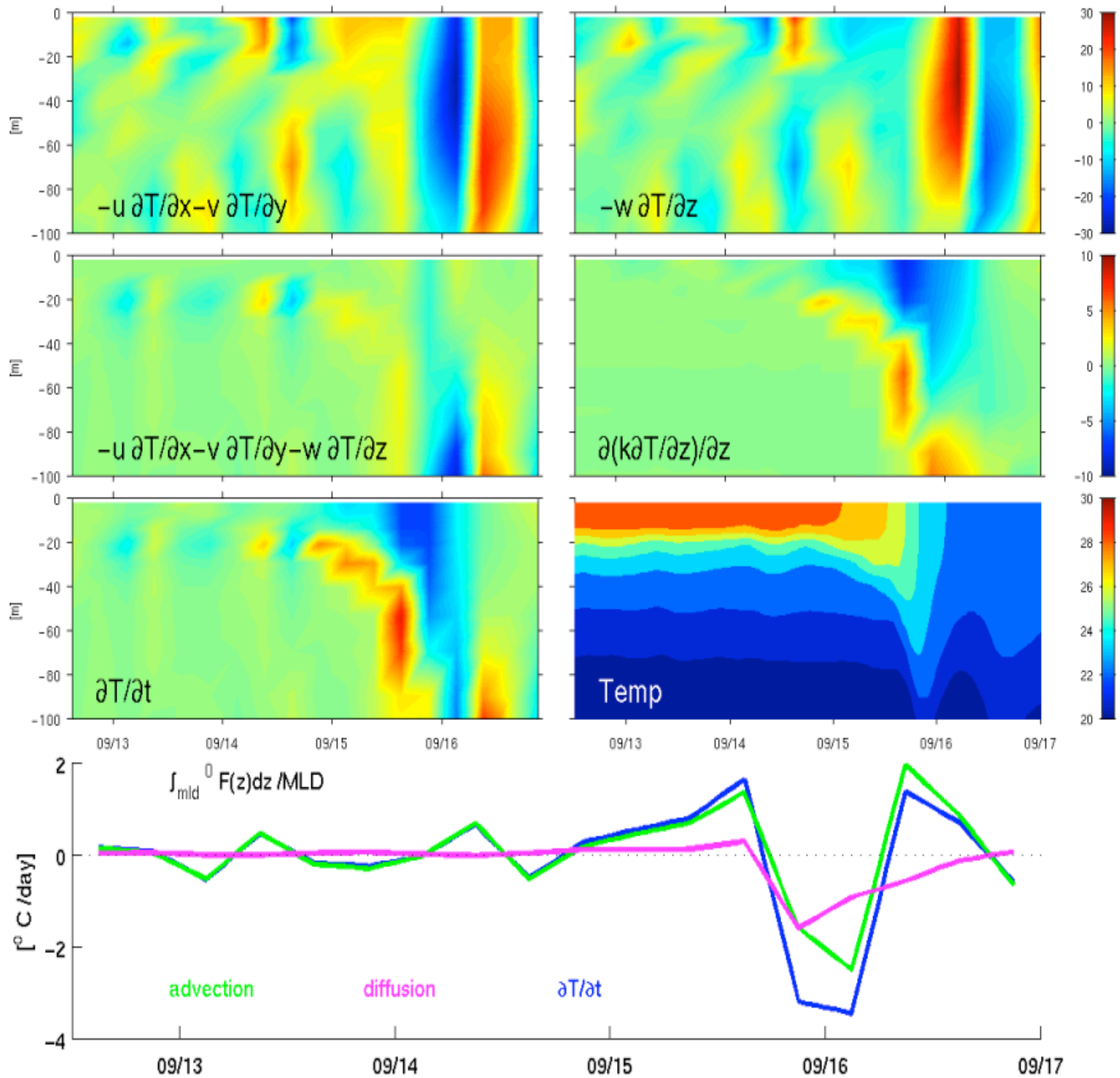

FIG. 4.16. Analysis of heat budget at point U2 from initialization (12 UTC 12 September 2004) through termination (00 UTC 17 September 2004), panels from top to bottom: horizontal advection term in °C day^{-1} (left), vertical advection term in °C day^{-1} (right), total advection term in °C day^{-1} (left), vertical diffusion term in °C day^{-1} (right), total local rate of change term in °C day^{-1} (left), temperature in °C (right), comparison of contributions of advection and diffusion to local change in temperature integrated through 100m.

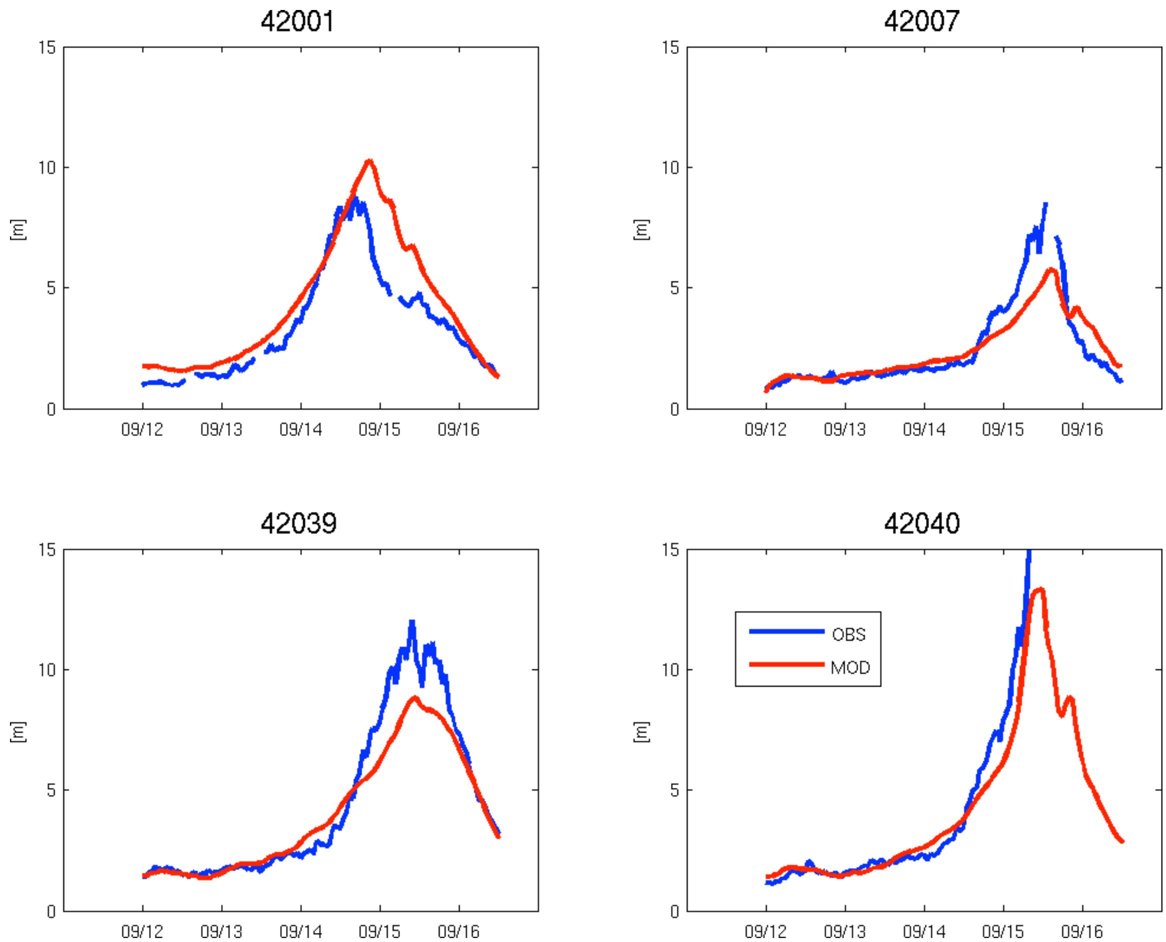

FIG. 4.17. Comparison of observed (blue) and modeled (red) significant wave heights at 4 buoy locations noted in Fig. 4.10: 42001 (upper left), 42007 (upper right), 42039 (lower left), 42040 (lower right). Taken from model initialization (12 UTC 12 September 2004) through termination (00 UTC 17 September 2004), with exceptions to when observations were not available due to extreme waves (as noted in Teague et al., 2007).

REFERENCES

Bao, J. W., J. M. Wilczak, and J. K. Choi, 2000: Numerical simulations of air-sea interaction under high wind conditions using a coupled model: A study of hurricane development. *Mon. Wea. Rev.,* **128,** 2190–2210.

Bao, S., S. Raman, L. Xie, 2003: Numerical simulation of the response of the ocean surface layer to precipitation. *Pure Appl. Geophys.*, **160,** 2419–2446.

Bender, M. A., and I. Ginis, 2000: Real-case simulations of hurricane-ocean interaction using a high-resolution coupled model: effects on hurricane intensity. *Mon. Wea. Rev.*, **128,** 917–946.

Bender, M. A., 2005: A proposal for transition of research to operations: Upgrades to the operational GFDL hurricane prediction system. Joint Hurricane Testbed Final Report [Available online at http://www.nhc.noaa.gov/jht/2003-2005reports/GFDLbender_JHTfinalreport.pdf .]

Bender, M. A., I. Ginis, R. Tuleya, B. Thomas, and T. Marchok, 2007. The Operational GFDL coupled hurricane-ocean prediction system and a summary of its performance. *Mon. Wea. Rev.,* **135,** 3965–3989.

Beven, J. and H. Cobb, 2004: Tropical cyclone report: Hurricane Isabel. National Hurricane Center. [Available online at http://www.nhc.noaa.gov/2003isabel.shtml .]

Bourassa, M. A., D. G. Vincent, W. L. Wood, 1999: A flux parameterization including the effects of capillary waves and sea. *J. Atmos. Sci.,* **56,** 1136–1142.

Brink, K. H., 1989: Observations of the response of thermocline currents to a hurricane. *J. Phys. Oceanogr.*, **19,** 1017–1022.

Blumberg, A. F., G. L. Mellor, 1987: A description of a three-dimensional coastal ocean circulation model. *Three-dimensional Coastal Ocean Models,* **4,** 1–16.

Bye, J. A., A. D. Jenkins, 2006: Drag coefficient reduction at very high wind speeds. *J. Geophys. Res.*, **111,** C03024.

Chassignet, E. P., H. E. Hurlburt, O.M. Smedstad, G. R. Halliwell, P. J. Hogan, A. J. Wallcraft, R. Baraille, and R. Bleck, 2006: The HYCOM (Hybrid Coordinate Ocean Model) data assimilative system. *J. of Marine Systems*, **65,** 60–83.

Chen, S. Y. S., J. F. Price, W. Zhao, M. A. Donelan, and E. J. Walsh, 2007: The CBLAST-hurricane program and the next-generation fully coupled atmosphere-wave-ocean. Models for hurricane research and prediction. *Bull. of the Amer. Met. Soc.* **88,** 311–317.

Church, J. A., T. M. Joyce, J. F. Price, 1989: Current and density observations across the wake of Hurricane Gay. *J. Phys. Oceanogr.,* **19,** 259–265.

Cione, J. J., and E. W. Uhlhorn, 2003: Sea surface temperature variability in hurricanes: implications with respect to intensity change. *Mon. Wea. Rev.,* **131,** 1783–1796.

Cornillion, P., L. Stramma, J. F. Price, 1987: Satellite measurements of sea-surface cooling during Hurricane Gloria. *Nature*, **326,** 373–375.

Davis, C., W. Wang, S. S. Chen, Y. Chen, K. Corbosiero, M. DeMaria, J. Dudhia, G. Holland, J. Klemp, J. Michalakes, H. Reeves, R. Rotunno, C. Snyder, Q. Xiao, 2008: Prediction of landfalling hurricanes with the Advanced Hurricane WRF model. *Mon. Wea. Rev*, **136,** 1990–2005.

Done, J., B. K. Haus, N. Reul, W. J. Plant, M. Stiassnie, H. C. Graber, O. B. Brown, E. S. Saltzman, 2004: The next generation of NWP: Explicit forecasts of convection using the Weather Research and Forecast (WRF) Model. *Atmos. Sci. Lett.,* **5,** 110–117.

Donelan, M. A., B. K. Haus, N. Reul, W. J. Plant, M. Stiassnie, H. C. Graber, O. B. Brown, and E. S. Saltzman, 2004: On the limiting aerodynamic roughness of the ocean in very strong winds. *Geophys. Res. Let.*, **31,** L18306.

Doyle, J. D., 2002: Coupled atmosphere-ocean wave simulations under high-wind conditions. *Mon. Wea. Rev.,* **130,** 3087–3099.

Emanuel, K., 1986: An air-sea interaction theory for tropical cyclones, Part I: Steady-state maintenance. *J. Atmos. Sci.*, **43,** 585–604.

Emanuel, K., 1995: Sensitivity of tropical cyclones to surface exchange coefficients and a revised steady-state model incorporating eye dynamics. *J. Atmos. Sci.*, **52,** 3969–3976.

Emanuel, K., C. DesAutels, C. Holloway, and R. Korty, 2004: Environmental control of tropical cyclone intensity. *J. Atmos. Sci.,* **61,** 843–858.

Emanuel, K., 2005: *Divine Wind-The History and Science of Hurricanes.* Oxford University Press, New York. Environmental Modeling Center, cited 2009: HWRF Homepage. [Available online at http://www.emc.ncep.noaa.gov/HWRF/index.html.]

Fairall, C. W., E. F. Bradley, J. S. Godfrey, G. A. Wick, J. B. Edson, and G. S. Young, 1996: Cool-skin and warm-layer effects on sea surface temperature. *J. Geophys. Res.*, **101,** 1295–1308.

Fairall, C. W., E. F. Bradley, D. P. Rogers, J. B. Edson and G. S. Young, 1996: Bulk parameterization of air-sea fluxes for tropical ocean-global atmosphere Coupled-Ocean Atmosphere Response Experiment. *J. Geophys. Res.,* **101,** 3747–3764.

Fairall, C. W., E. F. Bradley, J. E. Hare, and A. A. Grachev, 2003: Bulk parameterization of air–sea fluxes: Updates and verification for the COARE algorithm. *J. Clim.*, **16,** 571–591.

Flather, R. A., 1976: A tidal model of the northwest European continental shelf. *Mem. Soc. R. Sci. Liege,* **6,** 141–164.

Geist, E. L., V. V. Titov, C. E. Synolakis, 2006: Tsunami: wave of change. *Scientific American*, **294,** 56–63.

Gemmill, W., B. Katz, X. Li, 2007: Daily real-time global sea surface temperature - high resolution analysis at NOAA/NCEP. NOAA / NWS / NCEP / MMAB Office Note Nr. **260,** 39 pp [Available online at http://polar.ncep.noaa.gov/mmab/papers/on260/sst_office_note.pdf .]

Geophysical Fluid Dynamics Laboratory, cited 2009: Geophysical Fluid Dynamics Laboratory - Operational Hurricane Forecasting - Main Page. [Available online at: http://www.gfdl.noaa.gov/operational-hurricane-forecasting.]

Goldenberg, S. B., C. W. Landsea, A. M. Mestas-Nunez, W. M. Gray, 2001. The Recent Increase in Atlantic Hurricane Activity: Causes and Implications. *Science,* **293,** 474–479.

He, R. and J. L. Wilkin, 2006: Barotropic tides on the southeast New England shelf: A view from a hybrid data assimilative modeling approach. *J. of Geophys. Res.*, **111,** C08002, doi:10.1029/2005JC003254.

He, R., D. J. McGillicuddy, Jr., B. A. Keafer and D. M. Anderson, 2008: Historic 2005 toxic bloom of Alexandrium fundyense in the western Gulf of Maine: 2. Coupled biological numerical modeling. *J. of Geophys. Res.,* **113,** C07040, doi:10.1029/2007JC004602.

Hill, K. A., 2006: The Sensitivity of Tropical Cyclone Simulations in the WRF Model to Surface Layer and Planetary Boundary Layer Parameterization. Department of Marine, Earth and Atmospheric Sciences at North Carolina State University, 254 pp.

Hong, S.-Y., J.-O. J. Lim, 2006: The WRF single-moment 6-class microphysics scheme (WSM6). *J. of the Korean Met. Soc.*, **42,** 129–151.

Komen, G. J., S. Hasselmann, K. and Hasselmann, 1984: On the existence of a fully developed wind-sea spectrum. *J. Phys. Oceanogr.,* **14,** 1271–1285.

Kurihara, Y., 1973: A scheme of moist convective adjustment. *Mon. Wea. Rev.*, **101,** 547–553.

Kurihara, Y., M. A. and Bender, 1980: Use of a movable nested mesh model for tracking a small vortex. *Mon. Wea. Rev.*, **108,** 1792–1809.

Kurihara, Y., M. A. Bender, R. E. Tuleya, R. J. Ross, 1995: Improvements in the GFDL hurricane prediction system. *Mon. Wea. Rev.*, **123,** 2791–2801.

Kurihara, Y., R. E. Tuleya, and R. J. Ross, 1998: The GFDL hurricane prediction system and its performance in the 1995 hurricane season. *Mon. Wea. Rev.*, **126,** 1306–1322.

Kwok, J. H. Y., and J. C. L. Chan, 2005: The influence of uniform flow on tropical cyclone intensity change. *J. Atmos. Sci.,* **62,** 3193–3212.

Leben, R. R., G. H. Born, B. R. Engebreth, 2002: Operation altimeter data processing for mesoscale monitoring. *Mar. Geod.,* **25,** 3–18.

Leipper, D. F., and D. Volgenau, 1972: Hurricane heat potential of the Gulf of Mexico. *J. Phys. Oceanogr.,* **2,** 218–224.

Lin, I.-I., C.-C. Wu, I.-F. Pun, D.-S. Ko, 2008: Upper-ocean thermal structure and the western north Pacific category 5 typhoons. Part I: ocean features and the category 5 typhoons' intensification. *Mon. Wea. Rev.,* **136,** 3288–3306.

Lin, Y-L, R. D. Farley, H. D. Orville, 1983: Bulk parameterization of the snow field in a cloud model. *J. Clim. Appl. Meteor*., **22,** 1065–1092.

Liu, W. T., K. B. Katsaros, and J. A. Businger, 1979: Bulk parameterization of the air-sea exchange of heat and water vapor including the molecular constraints at the interface. *J. Atmos. Sci.,* **36,** 1722–1735.

Marchesiello, P., J. C. McWilliams, and A. F. Shchepetkin, 2001: Open boundary conditions for long-term integration of regional oceanic models. *Ocean Modeling*, **3,** 1–20.

Marchesiello, P. J. C. McWilliams, and A. Shchepetkin, 2003: Equilibrium structure and dynamics of the California current system. *J. Phys. Oceanogr.*, **33,** 753–783.

Marks, F. D., and L. K. Shay, 1998: Landfalling tropical cyclones: Forecast problems and associated research opportunities. *Bull. Amer. Meteor. Soc.,* **79,** 305–323.

Mellor, G. L., 1998: User's guide for a three-dimensional, primitive equation, numerical ocean model. Program in Atmospheric and Oceanic Sciences, Princeton University, 35 pp. [Available online at http://www.aos.princeton.edu/WWWPUBLIC/htdocs.pom/ .]
Mellor, G. L., and T. Yamada, 1974: A hierarchy of turbulence closure models for planetary boundary layers. *J. Phys. Oceanogr.,* **17,** 565–583.

Mellor, G. L., and T. Yamada, 1982. Development of a turbulence closure model for geophysical fluid problems. *Rev. Geophys. Space Phys.,* **20,** 851–875.

Mitchell, D. A., W. J. Teague, E. Jarosz, and D. W. Wang, 2007: Observed currents over the outer continental shelf during Hurricane Ivan. *Geophys. Res. Let.,* **32,** L11610.

Moon, I. J., I. Ginis, T. Hara, 2004: Effects of surface waves on Charnock coefficient under tropical cyclones. *Geophys. Res. Let.*, **31,** L20302.

Morey, S. L., M. A. Bourassa, X. J. Davis, J. J. O'Brien, J. Zavala-Hidalgo, 2005: Remotely sensed winds for episodic forcing of ocean models. *J. Geophys. Research,* **110,** Art. No. C10024.

Morey, S. L., M. A. Bourassa, D. S. Dukhovskoy, and J. J. O'Brien, 2006: Modeling studies of the upper ocean response to a tropical cyclone. *Ocean Dyn.*, **56,** 594–606.

Oey, L.-Y., T. Ezer, D.-P. Wang, X.-Q. Yin, S.-J. Fan, 2007: Hurricane-induced motions and interaction with ocean currents. *Cont. Shelf Res.,* **27,** 1249–1263.

Oey, L.-Y., T. Ezer, D.-P. Wang, X.-Q. Yin, S.-J. Fan, 2006: Loop Current warming by Hurricane Wilma. *Geophys. Res. Let.,* **33**, Art. No. L08613.

Oost, W. A., G. J. Komen, C. M. J. Jacobs, C. van Oort, 2002: New evidence for a relation between wind stress and wave age from measurements during ASGAMAGE. *Bound.-Layer Meteor.,* **103,** 409–438.

Ooyama, K., 1969: Numerical simulation of the life cycle of tropical cyclones, *J. Atmos. Sci.* **26,** 3–40.

Pollard, R. T., P. B. Rhines, R. O. R. Y. Thompson, 1973: The deepening of the wind-mixed layer. *Geophys. Fluid Dyn.*, **3,** 381–404.

Price, J.F., 1979: Observations of a Rain-Formed Mixed Layer. *J. Phys. Oceanogr.,* **9,** 643–649.

Price, J. F., 1981: Upper ocean response to a hurricane. *J. Phys. Oceanogr.*, **11,** 153–175.

Price, J. F., T. B. Sanford, G. Z. Forristall, 1994: Forced stage response to a moving hurricane. *J. Phys. Oceanogr.*, **24,** 233–260.

Riehl, H., 1954: *Tropical Meteorology*. McGraw-Hill, 392 pp.

Rosenthal, S. L., 1979: The sensitivity of simulated hurricane development to cumulus parameterization details. *Mon. Wea. Rev.,* **107,** 193–197.

Sanford, T. B., P. G. Black, J. W. Haustein, 1987: Ocean response to a hurricane. Part I: Observations. *J. Phys. Oceanogr.*, **17,** 2065–2083.

Scharroo ,R,. W. H. F. Smith, J. L. Lillibridge, 2005: Satellite altimetry and the intensification of hurricane Katrina. *EOS, Trans. Amer. Geophys. Union,* **86,** 366–367.

Shay, L. K., G. J. Goni, P. G. Black, 2000: Effects of a warm oceanic feature on Hurricane Opal. *Mon. Wea. Rev.,* **128,** 1366–1383.

Shchepetkin, A. F., and J. C. McWilliams 2005: The regional oceanic modeling system (ROMS): a split-explicit, free-surface, topography-following-coordinate oceanic model. *Ocean Modeling*, **9,** 347–404.

Shen, W., and I. Ginis, 2003: Effects of surface flux-induced sea surface temperature changes on tropical cyclone intensity. *Geophys. Res. Let.*, **30,** DOI 10.1029/2003GL017878

Singh, R., P. K. Pal, C. M. Kishtawal, P. C. Joshi, 2005: Impact of bogus vortex for track and intensity prediction of tropical cyclone. *J. Earth Syst. Sci.,* **114,** 427–436.

Stewart, S., 2005: Tropical cyclone report: Hurricane Ivan 2-24 September 2004. National Hurricane Center. [Available Online at: http://www.nhc.noaa.gov/2004ivan.shtml.]

Taylor, P. K., and M. A. Yelland, 2001: The dependence of sea surface roughness on the height and steepness of the waves. *J. Phys. Oceanogr.,* **31,** 572–590.

Teague, W. J., E. Jarosz, D. W. Wang, and D. A. Mitchell, 2007: Observed oceanic response over the upper continental slope and outer shelf during Hurricane Ivan. *J. Phys. Oceanogr.,* **37,** 2181–2206.

Vaccaro, Chris, 2006: Noteworthy Records of the 2005 Atlantic Hurricane Season. National Oceanographic and Atmospheric Administration. [Available online at: http://www.noaanews.noaa.gov/stories2005/s2540b.htm .]

Walker, N. D., R. R. Leben, S. Balasubramanian, 2005: Hurricane-forced upwelling and chlorophyll *a* enhancement within cold-core cyclones in the Gulf of Mexico. *Geophys. Res. Let.*, **32,** Art. No. L18610.